**FEDERAL UNIVERSITY OF TECHNOLOGY - PARANA**

**POSTGRADUATE PROGRAM IN MECHANICAL ENGINEERING**

**DEPARTMENT OF MECHANICAL ENGINEERING**

**WAGNER BARTH LENZ**

# NEURO-FUZZY CONTROL AND PARTICLE SWARM OPTIMIZATION ON HORIZONTAL AXIS WIND TURBINE

**THESIS**

**PONTA GROSSA**

**2019**

**WAGNER BARTH LENZ**

# NEURO-FUZZY CONTROL AND PARTICLE SWARM OPTIMIZATION ON HORIZONTAL AXIS WIND TURBINE

Master thesis presented as partial requirement to obtain a Master Degree in Mechanical Engineering from the department of Mechanical Engineering at Federal University of Technology - Parana - UTFPR

Advisor: Prof. Dr. Ângelo Marcelo Tusset
Advisor: Prof. Dr. José Manoel Balthazar

**PONTA GROSSA**

**2019**

**FOLHA DE APROVAÇÃO**

Título da Tese Nº 29/2019

NEURO-FUZZY CONTROL AND PARTICLE SWARM OPTIMIZATIONON
HORIZONTAL AXIS WIND TURBINE

por

WAGNER BARTH LENZ

Esta Tese foi apresentada às **09:00** de **11 de Junho** de 2019 como requisito parcial para a obtenção do título de Mestre em Engenharia Mecânica, na área de concentração em Térmica e Fluídos, do Programa de Pós-Graduação em Engenharia Mecânica. O candidato foi arguido pela Banca Examinadora composta pelos professores abaixo citados. Após deliberação, a Banca Examinadora considerou o trabalho **aprovado**.

**Prof. Dr. Ângelo Marcelo Tusset**
Orientador(a)

Prof. Dr. Maurício Aparecido Ribeiro
UTFPR

Profa. Dra.  Yara de Souza Tadano
UTFPR

Prof. Dr. Paulo José Paupitz Gonçalves
UNESP

Prof. Dr. Gerson Henrique dos Santos
Coordenador do PPGEM

A Folha de Aprovação assinada encontra-se no
Departamento de Registros Acadêmicos da UTFPR – Câmpus Ponta Grossa

To my parents and siblings

## ACKNOWLEDGEMENTS

# ABSTRACT

LENZ, Wagner Barth. **Neuro-Fuzzy control and particle swarm optimization on horizontal axis wind turbine**. 2019. 100 p. Dissertation (Master's Degree in Mechanical Engineer) – Federal University of Technology – Paraná. Ponta Grossa, 2019.

The consumption of electric energy is increasing. This growth stimulates production that is entirely based on fossil fuels. However, for social, political or environmental reasons there is a need to change the energy source. Large, medium and low-scale generation by means of wind turbines is a viable solution. Similar to other generation methods, the wind turbine needs to be optimized and controlled to function as efficiently as possible. In this work a particle swarm optimization process optimized a profile of a wind turbine based on two stretching equations that had as objective the best coefficient of power for the average speed. We also used a fuzzy neuro controller based on the maximum for each ratio between speeds ($T_{SR}$). Three wind speed profiles were used to analyze the dynamics of the wind turbine. The controller was efficient and kept the rotation within the expected range. The results show that the controller prevented the generation above the maximum power, reducing the rotations by up to 12 [rad/s] above the maximum power, in cases of oscillation in the velocity of the view the control remained stable with a low standard deviation and reducing the power in at up to 8 [rad/s] for sine waves and up to 9 [rad/s] for random inputs.

**Keywords:** Wind Turbine. PSO. Neuro-Fuzzy. Optimization. Control.

# RESUMO

O consumo de energia elétrica vem aumentando. Esse crescimento estimula a produção que está inteiramente baseada em combustíveis fósseis. Entretanto, por razoes sociais, politicas ou ambientais há uma necessidade de mudar a fonte energética. A geração em larga, média e baixa escala por meio de turbinas eólicas é uma solução viável. Similar a outros métodos de geração, a turbina eólica precisa ser otimizada e controlada para funcionar da forma mais eficiente possível. Nesse trabalho um processo de otimização por enxame de partículas otimizou um perfil de uma turbina eólica baseado em duas equações de esticão que tinha como objetivo o melhor coeficiente de potência para a velocidade média. Também utilizou um controlador neuro fuzzy com base nos máximos para cada razão entre velocidades ($T_{SR}$). Três perfis de velocidade de vento foram usados para analisar a dinâmica da turbina eólica. O controlador se mostrou eficiente e manteve a rotação dentro da faixa esperada. Os resultados mostram que o controlador preveniu a geração acima da potência máxima, reduzindo as rotação em até 12 [rad/s] acima da potencia máxima, em casos de oscilação na velocidade do vendo o controle se manteve estável com um baixo desvio padrão e reduzindo a potencia em ao em até 8 [rad/s] para ondas senoidal e em até 9 [rad/s] para entradas aleatórias.

**Palavras-chave:** Turbina Eólica. PSO. Neuro-Fuzzy. Otimização. Controle.

# LIST OF FIGURES

# LIST OF GRAPHS

# LIST OF TABLES

# LIST OF ABBREVIATIONS AND ACRONYMS

ABBREVIATIONS

| | |
|---|---|
| HAWT | Horizontal Axis Wind turbine |
| VAWT | Vertical Axis Wind Turbine |
| CFD | Computational fluid dynamics |
| PSO | Particle swarm optimization |
| GA | genetic algorithm |
| AI | Artificial Intelligence |
| PBL | Planetary boundary layer |
| MPPT | Maximum power point tracking |

PSEUDO-ACRONYMS

| | |
|---|---|
| NACA | National Advisory Committee for Aeronautics |
| NASA | National Aeronautics and Space Administration |
| NOAA | National Oceanic and Atmospheric Administration |

# LIST OF SYMBOLS

## LATIN LETTERS

| | | |
|---|---|---|
| $a$ | Axial coefficient | [ ] |
| $a'$ | Radial coefficient | [ ] |
| $B$ | Number of the blades | [ ] |
| $c$ | Chord | [m] |
| $c_P$ | Coefficient of power | [ ] |
| $c(r)$ | Function chord | [m] |
| $C_D$ | Coefficient of drag | [ ] |
| $C_L$ | Coefficient of lift | [ ] |
| $c_P$ | Coefficient of power | [ ] |
| $F_x$ | Force on the axis axial | [N] |
| $F_y$ | Force on the axis radial | [N] |
| $F_D$ | Force of drag | [N] |
| $F_L$ | Force of lift | [N] |
| $P_f$ | Power of fluid | [W] |
| $P(v)$ | Probability of wind | [%] |
| $r$ | Local radius | [m] |
| $r_t$ | Radius of the section | [m] |
| $R$ | Radius of the HAWT | [m] |
| $U_1$ | Axial speed on the $dx$ element | [m/s] |
| $U_2$ | Radial speed on the $dx$ element | [m/s] |
| $U_T$ | Total speed on the $dx$ element | [m/s] |
| $u$ | Average speed at the desired height | [m/s] |
| $u_r$ | Reference wind speed | [m/s] |
| $u_n$ | Variable to be optimized | [ ] |
| $T_{SR}$ | Tip speed Ratio | [ ] |
| $V_{start}$ | Wind speed to start generation | [m/s] |
| $V_{max}$ | Wind speed of maximum generation | [m/s] |
| $V_{cut\ off}$ | Wind speed of stop generation | [m/s] |
| $\overline{v}$ | Average wind speed | [m/s] |
| $V_\infty$ | Instantaneous wind speed | [m/s] |
| $z_r$ | Reference height | [m] |
| $z$ | Desired height | [m] |

## GREEK LETTERS

| | | |
|---|---|---|
| $\alpha$ | Angle of attack | [°] |
| $\beta$ | Control Angle | [°] |
| $\phi$ | Flow angle | [0] |
| $\nu$ | Kinematic Viscosity | [m²/s] |
| $\Omega$ | Rotation speed | [rad/s] |

| | | |
|---|---|---|
| $\theta_p$ | Twist angle of the blade | [°] |
| $\theta(r)$ | Function twist angle | [°] |
| $\rho_{air}$ | Air density | [kg/m$^3$] |
| $\sigma$ | solidity | [ ] |

# CONTENTS

# 1 INTRODUCTION

The global consumption of electric energy has been continuously growing, over the past decade the Earth consumption of electric energy grew 24%, and on the last twenty years it grew 54% (CHEN; WU, 2017). Currently, this system is extremely dependent on fossil fuel, such as coal, petroleum, and natural gas. Consequently, the whole world is eager to an unsustainable energy source.

In addition, fluctuation on supply can be caused by war, political crises and environmental awareness, that are forcing the electric grid to look for a substitute source of fuel (HANSEN, 2008). Recent international treaties set the tone for the decades to come. Some countries are leading the way, such as New Zealand and Germany. New Zealand has a goal to have more than 90% of electric energy produced by renewable sources such as wind, solar and geothermal, by 2025 (WHITE; WAKES, 2014; STEPHENSON et al, 2017; JUNG; SCHINDLER; GRAU, 2018). Germany have one of the most drastic incentives on green energy and energy efficiency, with higher than the average on pay-back for consumers and subsidies for solar and wind (BUNDESVERBAND WINDENERGIE E.V., 2018).

Proposed as an alternative, on the 1950's nuclear energy was considered cheap, safe and endless. Consequently several nuclear power were built. However, it lost momentum since 1960 due to several events such as accidents and concerns regarding safety on the reactors, and since then it has been discredited by government and local population (MURRAY; HOLBERT, 2015). Mainly because of the major loss of land in case of accidents and the lack of option regarding long therm storage of nuclear reactive waste. For instance, Germany already has plans to shut down nuclear power plants, and after the Fukushima incident, it has been accelerating the program. Thus, making nuclear a not viable and desirable long-term solution (AUER, 2016; WEBER; C., 2018; BUNDESVERBAND WINDENERGIE E.V., 2018; JUNG; SCHINDLER; GRAU, 2018).

Solar energy is the most abundant renewable energy on the Earth. Usually, solar panels are installed on the roof in array to increase the voltage to be converted and connected to the grid. This system has no moving parts and has a high reliability. Nevertheless, the solar radiation is heterogeneous through the globe and the system is

sensitive to shades on panels (CHANG; STARCHER, 2019). In addition, the production time is limited by solar time and the respectability of the whole system compose of battery and panels (crystalline silicon) are uncertain (XU et al, 2018b) .

Another option is hydroelectric power. It is a renewable source, without scalability issues to larger production. For example, Brazil produces 76% of its energy from Hydraulic power. Brazil has one of the biggest Hydraulic power plants installed on the planet, the Itaipu Dam. It produced more than 100GWh in 2016 alone, and it has been in operation since 1984. It has accumulated a production of 2.5 billion of MWh, representing roughly 5% of the installed power in the country. Nevertheless, it has drawback as well. The initial cost of installation was immense, around U$17.5 billion in 1984, and it left a vast area of agricultural land useless because of the reservoir size. In addition, as many renewable energy sources it is susceptible to environment changes. In this case, long droughts can lead to higher prices and lower production, for example. The Fig. 1 shows the area affected by the Itaipu dam (RUFFATO-FERREIRA et al, 2017; ANEEL, 2018; SEMSP, 2018).

**Figure 1 – Estimated size of Itaipu dam**
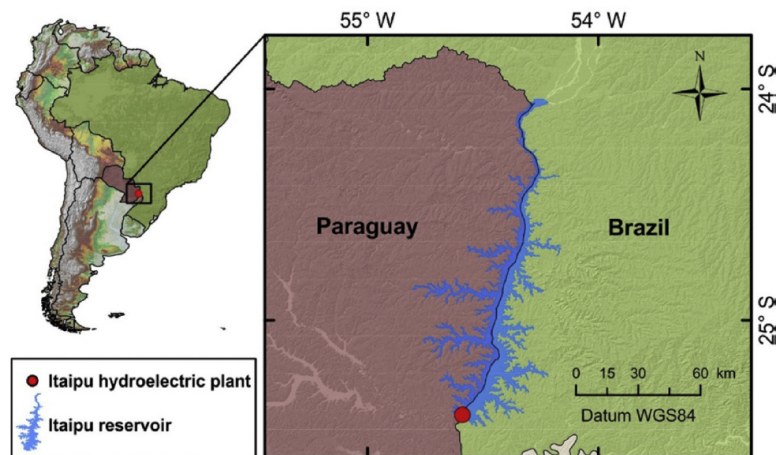


**Source: Lorenzon et al (2017)**

Among the alternative fuel sources, wind is a good option for cleaner and renewable source of energy. First, the carbon emission is zero, because it uses the wind as source of energy. Thus the bulk greenhouse production occurs during the installation and fabrication phase (90%), already accounting with regular maintenance checks and end of life recycling and disposal (WANG; WANG; LIU, 2019). In addition, re-powering is common mechanism to prolong the life of old wind turbines. After the economical requirements are met, old wind turbines are transferred to a new location, and installing a

new and more efficient turbines at that location (ZIEGLER et al, 2018; SIMÓN-MARTÍN et al, 2019). Thus, encouraging the rational and efficient use of resource (sites and materials) and increasing the renewable power installed (LACAL-ARÁNTEGUI, 2019).

Second, the technology involved is similar to many production sources, where shaft spins and the kinetic energy of the shaft is transformed in electric energy by a generator. Effectively, creating an inertia to electric power avoiding resonates in voltages and frequency changes as in solar energy (KARIMI et al, 2016; FREITAS; SANTOS; BRITO, 2018). Wind turbines stand out for being used to more then 2000 years. It was primarily used to grind crops and to pump water. Nowadays, the popular design is the Danish with three blades. In addition, it can produce in large scales from 200W to 12MW (WOOD, 2010; SØRENSEN, 2011; GENERAL ELECTRIC, 2018).

Third, the vast amount of designs can make integrable on public sight, near to the final costumer,such as highways and parks. The main concern of residence are the price and location (HUI; CAIN; DABIRI, 2018). As a result, it has been vastly used and can be a substitute to fossil fuels. Fourth, wind turbines industries are associated with a big portion on the economics.

Wind turbines can be classified by the orientation of the rotate axis, vertical axis wind turbines (VAWT) and Horizontal axis wind turbines (HAWT), and the main features can be compared on Table 1 (RUFFATO-FERREIRA et al, 2017).

**Table 1 – Comparison on wind turbine types**

| Characteristics | VAWT | HAWT |
|---|---|---|
| Power Rate | 50W - 300KW | 200W – 12MW |
| Axis Orientation | Vertical | Horizontal |
| Efficiency | 0.10-0.30 | 0.2-0.58 |
| Public Sight | Easily integrable | Usually it is not use |
| Physical Force | Drag and Lift | Lift |
| Noise Pollution | Lower | Higher |
| $T_{sr}$ (Tip speed ratio) | 0.01 to 0.1 | Until 10 |

**Source: Adapted from Wood (2010), Sørensen (2011), Schaffarczyk (2014)**

As shown in Table 1, the use of VAWT is more adaptable to urban environment and HAWT is used on large production. VAWT can be further divided on rotor types and it is shown in Fig. 2 (SCHAFFARCZYK, 2014).

**Figure 2 – Types of VAWT**



Savonius-Rotor          Darrieus-Rotor          H-Darrieus-Rotor
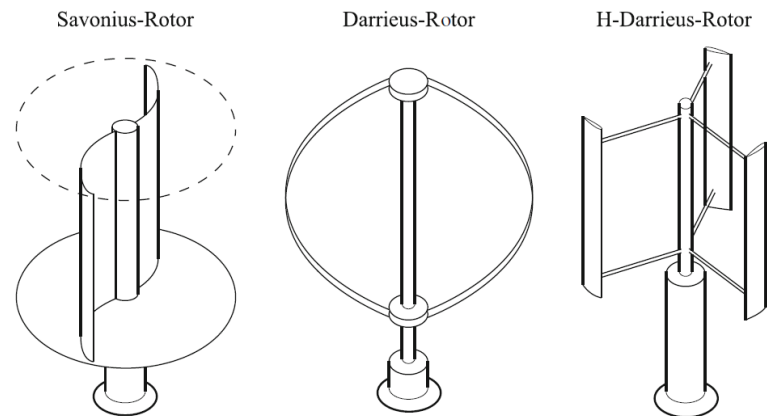
**Source: Schaffarczyk (2014)**

Fig. 2 shows the most common types of VAWT. The oldest model is the Savonius-Rotor, working by Drag, it can be improved using a jet effect (WAHYUDI; SOEPARMAN; HOEIJMAKERS, 2015; TIAN et al, 2018). On the other hand, the Darrieus models work by lift, they are more efficient and faster. The VAWT has a power range from 50W to 300kW, usually the most powerful ones are based on the Darrieus-rotor. One example of VAWT is the wind tree, which is a commercial wind turbine sold by New Word Wind. It is adaptable to be installed in urban environment. Fig. 3 shows the prototype (HEIER, 2014; New World Wind, 2018).

**Figure 3 – VAWT on the tree of wind**
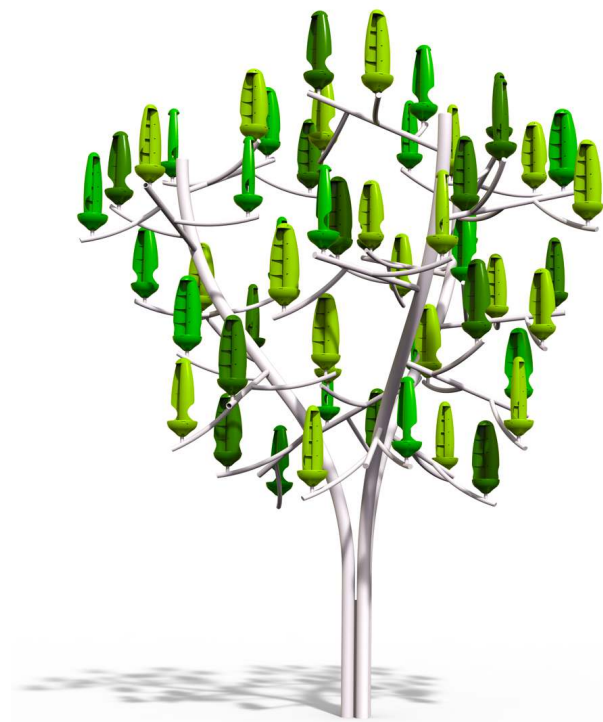


**Source: New World Wind (2018)**

It can produce up to 4.3 kW, this prototype educates about renewable energy and integration of wind energy with the urban environment. However, it requires 63 small wind turbines, and the energy production starts at two meters per second, using an adapted Savonius' rotor. Additionally, many researchers investigated the microgeneration with wind VAWT on rooftop in residential neighborhood, the principal advantages in this location is the local productions, being aesthetic pleasing and low noise production (MITHRARATNE, 2009; HEIER, 2014; BILIR et al, 2015; New World Wind, 2018).

On the other hand, HAWT are almost banned from human sight. The old generation use of high Tip speed Ratio ($T_{sr}$), thus unpleasant and noisy (VAZ; WOOD, 2016; BAKIRCI; YILMAZ, 2018). One strategy to mitigate this issues is using two setting for the $T_{sr}$, one for diurnal and another for night periods to avoid excess noise (WOOD, 2010). Another solution is the substitution for newer generation of wind turbine which uses lower speeds, and noise absorption material will increase the installed power and at the same time reducing the amount of turbine local community. Because production depends heavily on the site, many productions site agglomerates HAWT in farms to extract the most possible power, as can be seen on Fig. 4 (HANSEN, 2008; SCHAFFARCZYK, 2014).

**Figure 4 – HAWT farm**



**Source: BUNDESVERBAND WINDENERGIE E.V. (2018)**

As shown in Fig. 4 , the stack of wind turbines can increase the productivity, maintenance and take advantage of a good location, to commercial turbines, it can range from 10kW to 6MW each turbine, in many cases hundreds of wind turbines can be stack together (WAGNER; MATHUR, 2011; WAGNER, 2013). For example,

Tararua Wind Farm in New Zealand has 134 turbines with an annual output of 620GWh, and power installed of 160MW (ELTAYEB, 2013; ASSOCIATION, 2018). Additionally to impressive power output, it is common to use pitch angle control to avoid over speeding and allow the production in lower speeds, and improve performance (TJIU et al, 2015; WALMSLEY; WALMSLEY; ATKINS, 2017) . Thus, providing steady power supply, with a controller to prevent unnecessary wear and tear at low wind speed. Additionally, the controller reduces the fluctuations on the rotation shaft, caused by wind gust and windstorm.

However, the initial cost is high, and there are many options to control and stabilize the motion, and the selection of the site can lead to low utilization (LUO; VIDAL; ACHO, 2014; AGHBALOU et al, 2018). A few known models of regression and control use variables $K$ on the proportional–integral–derivative controller (PID controller). Other way is to use fuzzy and neuro fuzzy for controlling, where there is a data to support the construction of rules. In addition, hybrid methods based on the optimum angle for each element are available. All the methods smooth the production and allow for bigger turbine. New Zealand and Germany already have big farms with 8MW wind turbines (BIANCHI; MANTZ; BATTISTA, 2007; LUO; VIDAL; ACHO, 2014; ASHRAFI; GHADERI; SEDAGHAT, 2015; GOUPEE; KIMBALL; DAGHER, 2017; JUNG; SCHINDLER; GRAU, 2018).

On the other side of the spectrum, small HAWT can provide self-sufficiency on energy to houses and small towns, especially in remote locations. Working with a passive controller to regulate the power and rotation speed, a constant load that is resistor to transform in heat or a converted to household use or battery storage. This implantation of small wind turbine, with a battery bank can buffer and store energy to low production periods. Thus, removing the necessity of a generator and diminish the demand on fossil fuel generators.

Despite the spread use of wind turbine, the design process of the blade is interactive. The inputs to design are required power, wind speeds and desire tip speed ratio. This variables are going to start the design process to select the twist profile, cord size, selection of airfoil and radius of the rotor. The principal requirements are structural, economical and efficiency. Additionally, there is no defined optimization method or selection on blades airfoils. Thus, many approaches have tried to consolidate on the literature the methods and optimization tools (LUO; VIDAL; ACHO, 2014; LENZ et al,

2018; LENZ et al, 2019)

In addition, one of the drawbacks of all renewable energies is the storage. Because of irregular production, many methods were proposed such as gravity storage, Pumped-storage, hydroelectricity and battery (RICHTER, 2013; REHMAN; AL-HADHRAMI; ALAM, 2015; LOUDIYI; BERRADA, 2017).

Glauret (1947) created a method to design helicopters and airplane propellers. On top of his model, many derivative methods of calculation were created to increase the precision (PRATUMNOPHARAT; LEUNG, 2011; SCHAFFARCZYK, 2014; PINTO; GONÇALVES, 2017). It decomposes the flows in axial and radial and, it compares the inlet and outlet speeds. Thus, providing a good estimate and predictability on the HAWT efficiency (GLAUERT, 1983).

Despite many correction methods, all have a good prediction and fluctuate the error when compared with different experimental cases. This deviation on the trust, changes the produced torque and the design of the structure. Because of that, many optimization for better performance were used and reducing the amount of manufacturing material (PRATUMNOPHARAT; LEUNG, 2011; CHEHOURI et al, 2015) .

The first optimization was evolutionary. Previous wind turbines that performed well were used as a starting point. Optimization on angles on chord bases on airfoils regressions were the second method (WOOD, 2010). In recent times, optimization techniques has been used instead, by far Genetic Algorithm (GA) have been used the most. For example, Yang et al (2016) used GA for selection of blade airfoil, where structural and financial aspects were computed in one cost function to extract the optimum efficiency to a fix pitch angle. Many other optimization can be seen on Diveux et al (2001), Wang, Wang and Luo (2011), Luo, Vidal and Acho (2014), Chehouri et al (2015), Lenz et al (2019).

Working similarly as GA, Particle Swarm Optimization (PSO) is an evolutionary optimization. By random generation particle and swarming in the all-possible options, PSO tends to be quicker than GA. Evolutionary optimization works with HAWT, because it can change and adapt as the particles are zooming in the final solution, regardless of the amount of variables. For example, Endo (2010) used PSO to optimizes the S809 airfoil to chord to fix Reynolds Numbers. Liao, Zhao and Xu (2012) used PSO with FAST® to optimizes structural layers in a HAWT blade.

On energy management, PSO has been used to optimize the scheduling of ap-

pliance and loads on a residential level with Photo-voltaic generation (MA et al, 2018). Jiang et al (2017) compared different types of PSO for wind site assessment. In addition, a PSO version was already used to optimize the site location, where sound was a trade-off with power output (MITTAL; MITRA; KULKARNI, 2017).

Many approaches have been used, for the basic controller until the most advances. As a practical stand point, the control has the function to protect and avoid mechanical shocks and electrical noises (SAQIB; SALEEM, 2015). Thus, avoiding sudden shaft accelerations due to gust, quick deceleration due to demand on the grid, and avoiding electrical noise.

Basic safety controllers use the power output as a threshold, however the production can be stagnated with one gust in period of high wind because of false positive. Other type is the Optimal torque control relies on the torque according to the standard turbo machine equation (MENEZES; ARAÚJO; SILVA, 2018). More advance control is the sliding modes, where the controller tracks the ideal $T_{SR}$ (OUDAH; I.MOHD; HAMEED, 2014).

Another mechanic, is springs use to sense the load on the blade and limiting the production, by changing the pitch angle. Consequently, the blade is self-regulated and can produce on higher winds periods and avoid damages (LUO; VIDAL; ACHO, 2014). Thus, working as collective pitch control. Because all the blades have the same orientation.

More advance strategies relies on sensing each blade position due to length and flexibility of material, providing individual outputs (PETROVIĆ; JELAVIĆ; BAOTIĆ, 2015). This controllers take into account the change in shape of the airfoil and the increase of the speed on the height.

Different types of controller and strategies have been proposed on the electrial side, Bai and Wang (2016) defines a strategy where the Maximum Power Point Tracking (MPPT), associated with any type of control for the turbine and for the generator, to smooth the power and improve efficiency (MENEZES; ARAÚJO; SILVA, 2018).

Luo, Vidal and Acho (2014), Ashrafi, Ghaderi and Sedaghat (2015) regulate the angle by an averaging of the optimum $C_L/C_D$ angle of each infitesimal element. Other types of controllers are based on a simplified function of coefficient of power with the generator to reach the max power output (NAGAI; AMEKU; ROY, 2009).

By far the most common combination is the PID controller with another con-

troller using a dynamic plant to account the non-linearity, or the Gaussian PI. The results with this kind of combination have been satisfactory (JONKMAN S. BUTTERFIELD; SCOT, 2009; LUO; VIDAL; ACHO, 2014).

However, there is a combination with different types of controllers wind farms. This type of controller has multiple inputs, and monitoring wind speed and directions, rotation speed, pitch angle and demand of the grid. Providing efficient use of the installation and extracting most energy possible. One of the challenges is not to produce enough renewable energy, it is in adequate the supply to the oscillating demands.

In addition to further improve the performance, and mitigate vibration effects such as fatigue and flutter. Flutter is an interaction with the torsion and longitudinal vibration mode, due to the long blade interacting with the aeroelastic modes, causing damage to the blade. This phenomena occurs when the load generates a torsion moment. Thus self loading and unloading the blade, combining the flapwise and torsion motions. The values of rotation can be as low as $1[rad/s]$ (ZHANG; CHEN; NIELSEN, 2017). This can be achieved by sensing and changing the shape of the airfoil, or forcing the turbine to accelerate and pass the flutter avoid using controllers on the angle (HAYAT et al, 2016) .

## 1.1 GENERAL OBJECTIVE

The general objective of this thesis is the optimization and control of horizontal axis wind turbine (HAWT), using Particle Optimization Algorithm (PSO) for a wind turbine using neuro fuzzy controller to control energy generation.

## 1.2 SPECIFIC OBJECTIVES

- To optimize the parameters pitch, cord, and blade selection on HAWT using PSO.

- To use the $T_{SR}$, rotation and wind speed to control the power output on HAWT.

- To analyze through numerical simulation the efficiency and efficacy of the controller

## 1.3 JUSTIFICATION

The continuous increase demand for energy is pushing the electric generation system toward the carbon off-set and replacement of carbon base fuels to renewable methods, such as wind. Thus, it is possible to sustain this growing demand without further damage the ecosystem (KOOTEN; VRIES, 2013; OLIVEIRA; VARUM; BOTELHO, 2019).

The current projection appoints that between 2025 and 2030, many countries will change from oil to complete renewable energy. For example, New Zealand expect 90% of electric production from other sources than fossil fuels until 2025 (STEPHEN-SON et al, 2017).

With the transition from fossil fuel to renewable energy sources, there is a necessity to have knowledge in wind turbine on the future. Despite of that, there is no dominated strategy to optimization. Using PSO it is possible to optimize many variable at the same time, reducing cost, material and improving the efficiency overall. Thus, leading to a better HAWT, cheaper, and a more reliable energy source.

In addition, it is a standard procedure to deploy the possible option. Thus, an optimized and controllable wind turbine is a modern requirement. To further improve the efficiency, many recent researches with the different methods on HAWT has being published. Despite of being an ancient technology there is relevancy on the subject, due to complexity and better efficiency (VAZ; PINHO; MESQUITA, 2011; PINTO; GONÇALVES, 2017; TALAVERA; SHU, 2017).

## 1.4 THESIS ORGANIZATION

The Master Thesis was divided in five chapters, where the Chapter 1 one has a brief introduction on energy source, HAWT, how controllers and optimization works on them.

Chapter 2 will present the HAWT models, PSO optimization and Neuro-Fuzzy control. Chapter 3 will present the used methodology, the selected variables, airfoils, the cost function for optimization, and the control technique was expected to behavior. On Chapter 4 the families of solution are shown, and the behavior with and without the controller. On Chapter 5 the discussions of the results and future researches.

## 2  LITERATURE REVIEW

In this chapter, the literature review will be presented along with mathematical models to HAWT, the optimization technique PSO and the neuro fuzzy logic to be used as a controller.

### 2.1   WIND CHARACTERISTICS

The wind analysis involves two main factors: the high frequency of sampling and the planetary boundary layer. Because of the elevated frequency, around 100Hz, the amount of available data introduces noise. Thus, fluctuating the average. To overcome this problem, it is commonly used a 10 minutes span to average out the peaks. (WOOD, 2010).

The planetary boundary layer (PBL) is the layer between the earth and the free flow of air, it is the livable region of the atmosphere and where the wind turbines are installed. In the PBL the heterogeneous heating and cooling cycles occurs, on soil and water, thus creating convection currents, and evaporation. This is the engine to all the meteorologic effect, in the globe. In other words, it is a larger scale of the laminar boundary layer flow. PBL depends on geographical location, temperature, evaporation height and many other variables (HOLTON; HAKIM, 2012). The Fig. 5 shows an example of the planetary boundary layer.

**Figure 5 – Example of Planetary Boundary Layer**
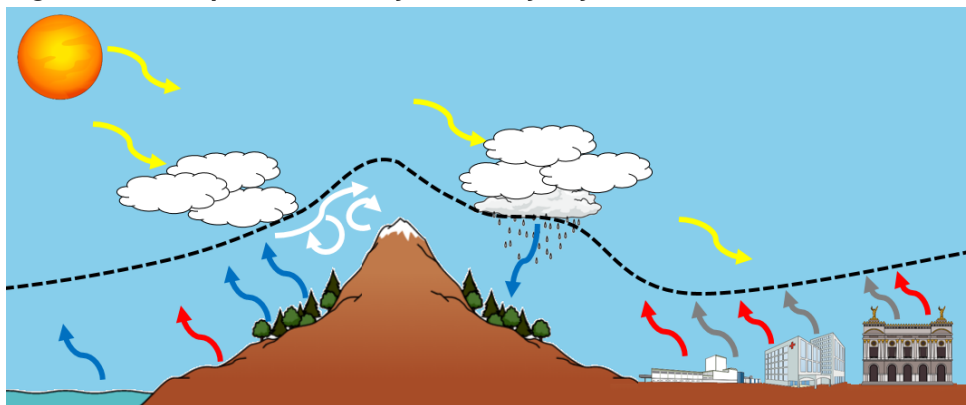


Source: Adapted from National Oceanic and Atmospheric Administration (2018)

where: dashed black line is the top of PBL, yellow arrows are the radiation from sun,

blue arrows are the direction of humidity, the red arrows are the raising heat waves, gray arrows are the change of air composition due to pollution, white arrows are the cold masses.

As shown in Fig.5, the PBL can affect the meteorology, air transport, agriculture and many other fields. The density, humidity and air speed change with the landscape, and it is influenced by cloud formation and rain, heat absorption, creating an unpredictable behavior. Despite of the complex and random behavior there are distributions that relate the wind behavior.

## 2.1.1  Rayleigh Distribution

The most used mathematical model to describe wind behavior is Rayleigh distribution. The Rayleigh distribution is a random distribution with scatter values and with the average almost on the middle. It has been used for predicting the average life on products and it is one of the most reliable wind predictions (WOOD, 2010; LUO; VIDAL; ACHO, 2014). The probability function is shown on Eq. 1 :

$$\begin{cases} P(v) = \frac{v}{\sigma^2} e^{\zeta} \\ \zeta = \frac{-v^2}{2\sigma^2} \end{cases} \tag{1}$$

where $P(v)$ is the probability of that specific speed, $v$ is the wind speed, $\sigma$ is the shape parameter. The shape format can be calculated using the average speed in Eq. 2:

$$\sigma = \overline{v}\sqrt{\frac{\pi}{2}} \tag{2}$$

where: $\overline{v}$ is the average speed. This average speed is an important factor on the beginning of the design. Because it will determine the available energy on the air. The amount of energy is going to estimate the feasibility of the wind turbine site. The available power on any fluid ($P_f$), on a circle section, can be obtained by Eq. 3 (HANSEN, 2008; CHEHOURI et al, 2015).

$$P_f = \frac{\pi r_t^2 \rho_{air} V_\infty^3}{4} \tag{3}$$

where $r_t$ is the radius of the section, $\rho_{air}$ is the density of the air, $V_\infty$ is the instantaneous wind speed. Because the energy grows at third power, a small increase on wind speed

causes a significant increase on the available power. To better asses the available power, it is necessary to plot the wind and its probability for two sites as in Fig. 1 .

**Graph 1 – Rayleigh probability distribution on different sites, (A) the wind speed, (B) the energy**



(A)

(B)
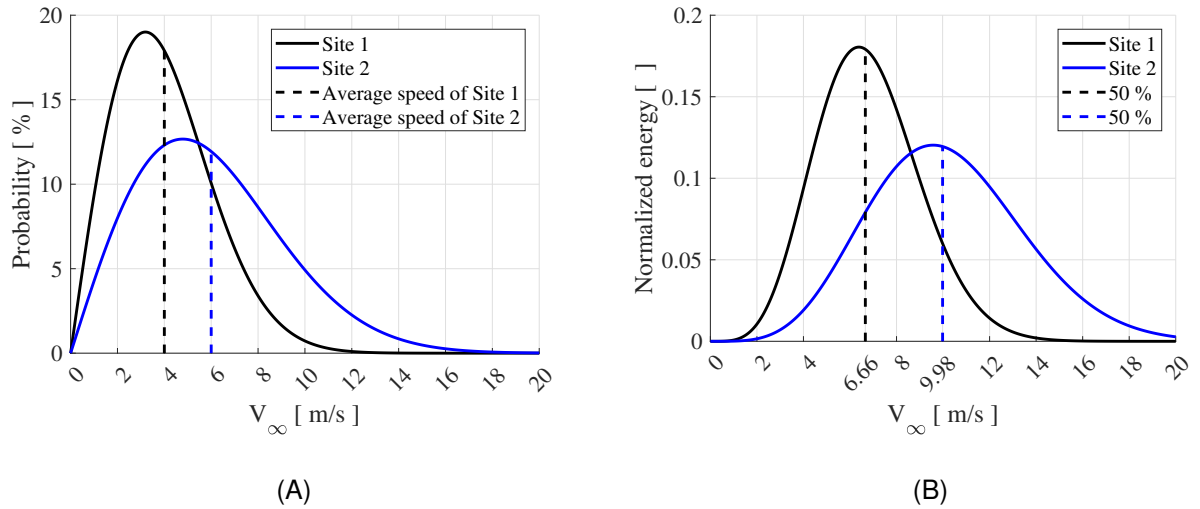
**Source: Self-Authorship**

As seen on the Graph 1, site 1 has an average of 4 [m/s] and a very concise distribution. On the other hand, site 2 has a higher average than site 1, of 6 [m/s], but it is diluted over the wind speed spectrum. Comparing only the amount of energy available using Eq. 3, site 2 has more energy available. But it is more spread during the spectrum, thus one of the drawbacks of wind energy. It can pass many days without producing energy, but it can produce a higher quantity in a short period of time (WOOD, 2010).

To estimate the average wind speed at different heights the power law is used to estimate the average wind speed, in Eq. 4.

$$u = u_r \left( \frac{z}{z_r} \right)^p \tag{4}$$

where $u$ is the average speed at the desired height, $u_r$ is the reference speed, $z_r$ is the reference height, $z$ is the desired height, and $p$ is a landscape factor and usually can be used as $p = \frac{1}{7}$ (HSU; MEINDL; GILHOUSEN, 1994; HOLTON; HAKIM, 2012).

The $p$ factor is related with the surface roughness and the stability of the site. Because the site can influence in different forms such as, evaporation, mountains and pollution from cities. To cities the value increase to $p = \frac{1}{4}$ (COUNIHAN, 1975; KIKU-MOTO et al, 2017).

Another factor to consider is physical limitation of the power plant. A typical wind turbine works supplying energy to the grid, thus it has to maintain the same standards of frequency and voltage to supply the power. In addition, the wind power curve is at third power, and it can easily overcome the power production of a given generator. Thus, a balance between instant power and available energy must be balanced, for that some parameter of the wind turbine must be set to avoid overloading and yielding energy at a reasonable cost (BIANCHI; MANTZ; BATTISTA, 2007; MA, 2015).

**Graph 2 – Difference between controlled and uncontrolled HAWT**
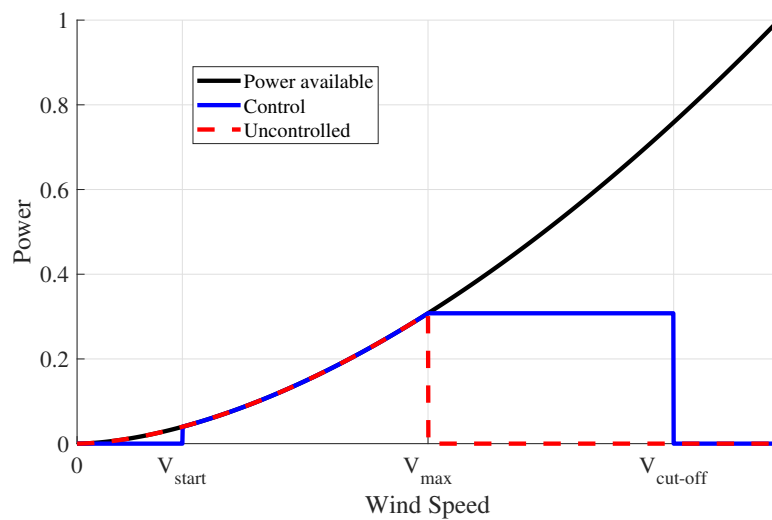


**Source: Self-Authorship**

As presented in Graph 2, the available power at the blade is on black, and it grows at a third power according to Eq. 3. The uncontrolled turbine is passive to wind speed. Thus, it relies on the optimization, to breaks the inertial quickly and maintain the correct rotation speed (WOOD, 2010; YANG et al, 2016; PINTO; GONÇALVES, 2017). As wind speed increases, the amount of power that can be extracted grows significantly until it satures the generator capability of production. It must be regulated, a common way is shorting the generator to break and avoid over speeding the blades.

Comparing Graph 1 (A), with (B) it is possible to design a wind turbine where most energy can be between $V_{start}$ and $V_{max}$. Thus, extracting the most energy possible using an unregulated turbine, nevertheless it must be oversized to avoid damage (HEIER, 2014; MA, 2015).

On the other hand, with control in Graph 2 on blue, the wind turbine has breaks, and do not start to spin until the wind speed crosses a threshold. Thus, avoiding pre-

mature wear and tear when it can spin fast enough to produce significant energy. The active control also will keep the angle of attack to have the most efficient regime. When the control wind turbine reaches the $V_{max}$, the control has the task of not overloading the generator. Thus, it keeps the angle of attack so the power extracted matches the maximum of the generator. The last threshold is the $V_{cut\ off}$, at this wind speed it is not safe to operate, the aerodynamics loads are greater than the design. Thus, the controller changes the angles of attack or applies the breaks to stop all the rotation to secure the HAWT.

## 2.2  HAWT CHARACTERISTICS

Working as an airplane wing, the blades of HAWT produce lift and drag based on the amount of air that passes through the blade. First, mathematically modeled by Glauret (1947), describes the relationship between the axial and radial flow (GLAUERT, 1983). His model was used to design helicopter and airplane rotors. Investigating his design, it is possible to find the maximum coefficient of power ($c_P$), and it can be 16/25 or 59.3%, this values is known as the Beltz limit. Because at an energy level, the turbine can be simplified and to be consider as a disk, and the efficiency is only related with the deceleration of wind speed, Fig. 8 shows macro and micro interaction relate through $U_T$ (HANSEN, 2008).

**Figure 6 – Analyses of HAWT, in (A) the Macro, in (B) the Micro**
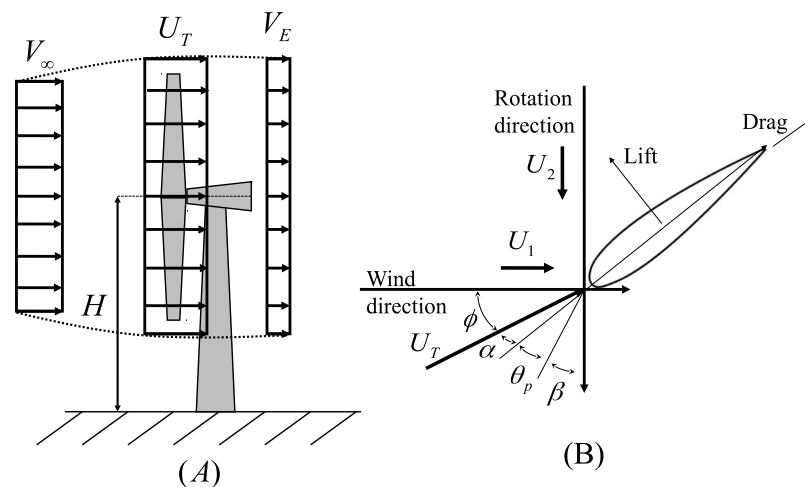


**Source: Adapted from Wood (2011)**

where $V_\infty$ is the wind speed, $U_T$ is the resulting speed and $V_E$ is the outlet speed. As

shown in Fig. 6 (A) at a macro level, at the intake the speed is higher than at the output. Passing through the rotor shaft, some energy is extracted, by conserving the mass, the area must grow to maintain the same speed. To keep operating, the fluid must pass by the blades and flow. If all the energy on the fluid could be extracted, the outlet speed would be zero. Thus, having no flow.

The maximum feasible efficiency is on the maximum that the fluid can retard without stagnating the flow. This speed is determined by the ratio between $V_E$ and $V_\infty$ is a third. However, it is hardly possible, for the most of commercial turbine, the maximum $c_P$ that can reach is 90% of the Beltz limit (HANSEN, 2008; WOOD, 2010).

Looking to the flow at the micro level at Fig. 6 (B) , where the blade can be break down on dx elements. The axial flow and radial flow can be studied at infinitesimal and after extrapolated to the whole blade. The important angles are on Fig. 6 (B) are obtained by the Eq. 5.

$$\phi = \alpha + \theta_P + \beta \tag{5}$$

where $\phi$ is the angle of flow, $\alpha$ is the angle of attack, $\theta_p$ is the blade twist angle, and $\beta$ is the angle of control. As a consequence of Fig. 6, the net force can be break down on axis as follows in Eq. 6.

$$\begin{cases} F_x = F_L cos(\phi) + F_D sin(\phi) \\ F_y = F_L sin(\phi) - F_D cos(\phi) \end{cases} \tag{6}$$

where, $F_L$ is the lift force, $F_D$ is the drag force, $F_x$ is the force on the axial direction and $F_y$ is the force on the radial direction. To overcome the inertial, the force on lift must be many magnitudes higher than the drag to start the rotation. Also, it is possible to define the speeds Fig. 6 (B) as Eq. 7.

$$\begin{cases} U_1 = (1 - a)U_0 \\ U_2 = (1 + a')r\Omega \\ U_T^2 = U_1^2 + U_2^2 \end{cases} \tag{7}$$

where: $a$ is the axial coefficient, $a'$ is the radial coefficient, $U_1$ is the axial speed, $U_2$ is the radial speed, $r$ is the local radius, $\Omega$ is the rotation speed. The flow angle can be

determined by Eq. 8

$$\phi = tan^{-1}\left(\frac{U_1}{U_2}\right) \tag{8}$$

Defining the tip speed ration ($T_{SR}$) in Eq. 9, a parameter of efficiency used to determined the optimization speeds, and the Number of Reynolds ($R_E$) on the following equations. The $T_{SR}$ is an important parameter because it is directly related to the efficiency and the orientation of the angles. At lower $T_{SR}$ the airfoil does not have the correct orientation of $\alpha$ and high $U_T$ to produce lift. Usually, for commercial turbine it is used between 7 and 10 for HAWT so the airfoil can have enough flow , values higher are not aesthetics pleasing and generate excisive noise (WOOD, 2010).

$$\begin{cases} T_{sr} = \frac{r\Omega}{V_\infty} \\ Re = \nu U_T c \\ \sigma = \frac{Bc}{2\pi r} \end{cases} \tag{9}$$

where: $\sigma$ is the solidity, $B$ is number of the blades, $c$ is the chord, $r$ is the local radius, $\nu$ is the kinematic viscosity. Because of the discontinuity of the wing, the wing tip generates a vortexes and it works as a brake. It will be considered the Prant model to infinitesimal element presented in Eq. 10:

$$\begin{cases} F = \frac{2}{\pi}arcos\left(-e^T\right), \\ T = \frac{-B(R-r)}{2Rsin(\phi)} \end{cases} \tag{10}$$

where, $B$ is the number of blades, $R$ is length of the blade, $r$ is the local radius. The $F$ is an efficiency parameter due to the wind tip vortex of the blade. The axial and the radial coefficients are defined in Eq. 11:

$$\begin{cases} C_x = C_L cos(\phi) + C_D sin(\phi) \\ C_y = C_L sin(\phi) - C_D cos(\phi) \end{cases} \tag{11}$$

where, $C_x$ is the axial coefficient, $C_y$ is the radial coefficient, $C_L$ is the lift coefficient, $C_D$ is the coefficient of drag of the airfoil based on the angle of attack and the Reynold

Number presented on the Eq.7 and Eq. 9. The $a$ and $a'$, can be calculated as Eq. 12:

$$\begin{cases} a = \frac{\sigma C_x}{4F sin^2(\phi)+C_x\sigma} \\ a' = \frac{\sigma C_x}{4F sin(\phi)cos(\phi)-C_y\sigma} \end{cases}$$

(12)

if $a > 0.4$, then:

$$\begin{cases} a = \frac{0.5(18\sigma C_x+36F^2 sin^2(\phi)-40F sin^2(\phi)-6\sqrt{C_1})}{C_2} \\ C_1 = 18F sin^2(\phi)\sigma C_x + 36F^4 sin^4(\phi) - 48F^3 sin^4(\phi) \\ C_2 = 9\sigma C_x - 50F sin^2(\phi) + 36F^2 sin^2(\phi) \end{cases}$$

(13)

This method is iterative, meaning the initial guess as recommend by the author as $a = 0.3$, and $a' = 0.001$. If the $a$ and $a'$ used in Eq. 7 are different from those obtained in Eq. 12 or 13, this method should be repeated until they converge to an admissible error ,as recomend, of $10^{-3}$. A comparison between model can be seen at Pratumnopharat and Leung (2011). After that, the torque and power on each element can be calculated by Eq. 14 :

$$\begin{cases} dT_m = 4a'(1 - a)\rho_{air}V_\infty \pi r^3\Omega dr \\ P_t = T_m\Omega \end{cases}$$

(14)

where, $dT_m$ is the torque, $\rho_{air}$ is the density of the air, $P_t$ is the power of the turbine. Thus, it is possible to establish the coefficient of power ($c_P$) to the turbine, in Eq. 15:

$$c_P = \frac{4P_t}{\pi R^2\rho_{air}V_\infty^3}$$

(15)

The $c_P$ is a function of several factors. Thus, it can be expressed as $c_P(T_{SR},V_\infty, \text{Airfoil},\beta)$. The $\beta$ effect can be describe as delay angle on the $c_P$ and it is described on Wood (2010), Golnary and Moradi (2019). The airfoil selection and the $T_{SR}$ are shown on the Graph 3.

**Graph 3 – Efficiency for different NACA profiles**
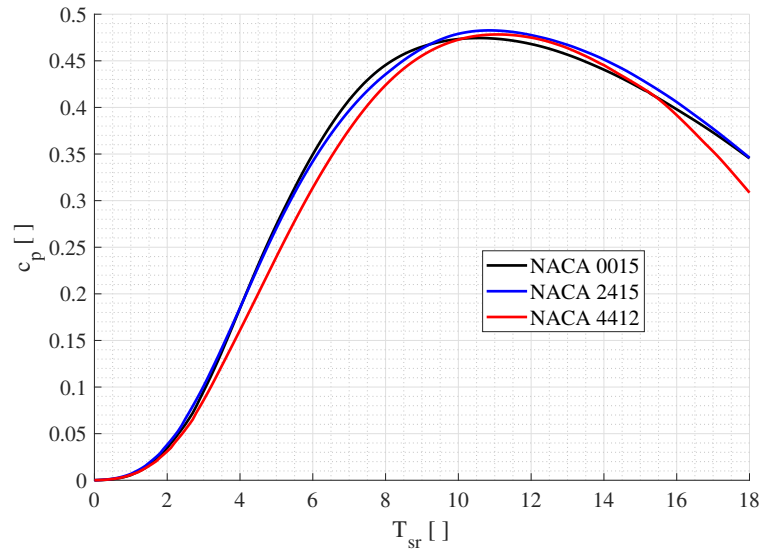
where NACA 0015,NACA 2415 and NACA 4412 are different types of airfoils. As shown on Graph 3, for different types of airfoils, each airfoil increase differently, the $c_P$ increases quickly from zero, because the angles start to get closer to the desires, after the optimum $T_{SR}$ the $c_P$ decreases, because the rotor starts to work as a motor.

2.2.1   NACA Profiles

As an initiative to improve access to airfoil data they were standardized in 1958 by the National Advisory Committee for Aeronautics(NACA). NACA was the former agency that gave rise to National Aeronautics and Space Administration (NASA). This agency made a compilation, with known and reliable data. Because of the complex shape, many profiles are dimensionless and the equation that describes the boundary are in relation with the chord length.

**Figure 7 – Shape of NACA airfoils**
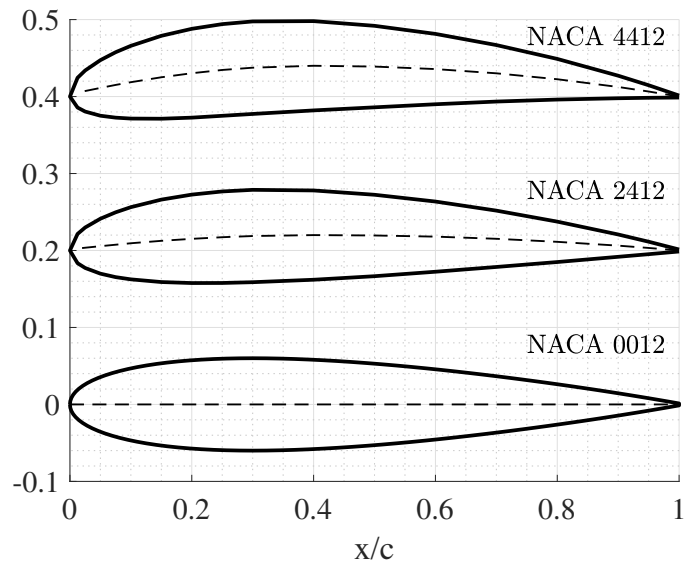


**Source: Adapted from Wood (2010)**

As shown in Fig. 7, the tear drop is the shape of the $4^{th}$ series. This shape is bend to achieve the desired output in therms of $C_L$ and $C_D$. The dashed line is the center line. The advantage was the standardization enabled all important information features and geometry were referenced in the name of the airfoil, such as thickness, camber angle and location, are on the name of the Airfoil (AERONAUTICS; NASA, 2018). The selection of NACA $4^{th}$ series has been investigated by Michos, Bergeles and Athanassiadis (1983), Ostowari and Naik (1984). The thickness remained the same through out 0012, 2412, 4412. The only changed variable was the location of the camber. The standardization can be explained as NACA XYZZ generic airfoil. Where ZZ means the thickness of the airfoil in relation to the cord, X is the rotation of the camber angle divided by 100, Y is the location of the camber divided by 10 (WOOD, 2011; AERONAUTICS; NASA, 2018).

## 2.2.2 S Airfoil

The S profiles are a selection of airfoil design and used on by HAWT. Despite of having a similar performance of the NACA $4^{th}$ series, the S series is quitter than the NACA $4^{th}$ series. Thus, alleviating the noise pollution that causes harm to animals and the acceptability on the urban site.

**Figure 8 – Shape of S airfoil**
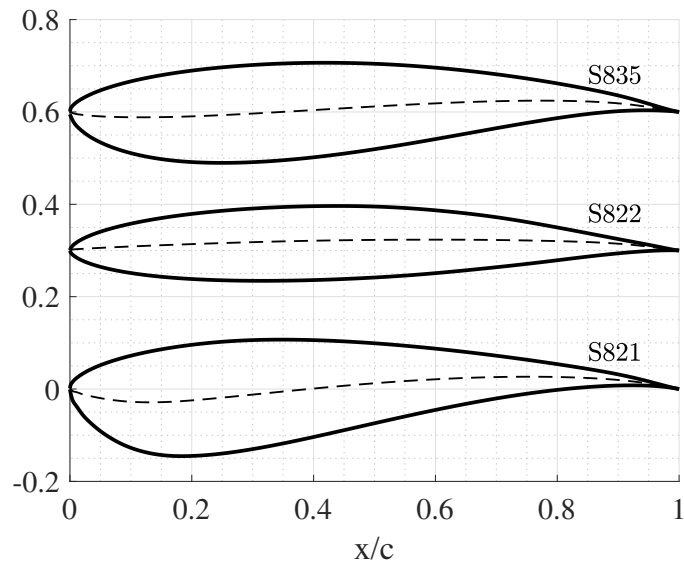
Comparing Fig. 7 with Fig. 8, it is clear that NACA airfoils are thinner than S airfoils. In addition, the S series is thoroughly studied by the National renewable energy laboratory (NREL). The NREL is a national laboratory of the U.S. Department of Energy, Office of Energy Efficiency & Renewable Energy, providing airfoil licensing and data information, to popularize this airfoils and raise awareness on wind and water power technologies (TANGLER; SOMERS, 1995; GRIFFIN, 2000; SELIG; MCGRANAHAN, 2004; SOMMERS, 2005; GHASEMIAN; ASHRAFI; SEDAGHAT, 2017).

### 2.2.3 Aerodynamics of Airfoils

An airfoil on a flow generates two forces, as shown on the Fig. 6. The lift ($F_L$) and the drag ($F_D$) forces are quantified in Eq. 16 (PRITCHARD, 2011; ANDERSON, 2011; GERHART, 2016).

$$\begin{cases} F_L = \frac{C_L c \rho U_T^2}{2} \\ F_D = \frac{C_D c \rho U_T^2}{2} \end{cases} \tag{16}$$

where $C_L$ is the lift coefficient, $C_D$ is the drag coefficient, $\rho$ is the density of the fluid, $U_T$ is the resultant speed over the airfoil. Because of the complexity of the $C_L$ and $C_D$ are functions of the shape of the airfoil, angle of attack and Reynolds number. It can be rewritten as $C_L(\text{type}, R_E, \alpha)$ and $C_D(\text{type}, R_E, \alpha)$. Thus, the use of Computational

fluid dynamics (CFD) is a very common strategy, instead of wind tunel experiments (KUMAR; ALI; AROCKIARAJAN, 2018; SURESH; RAMESH; PARAMAGURU, 2015).

**Graph 4 – Characteristic of an airfoil, on A the Lift, on B the Drag and C the relation between Lift and Drag Coefficient**
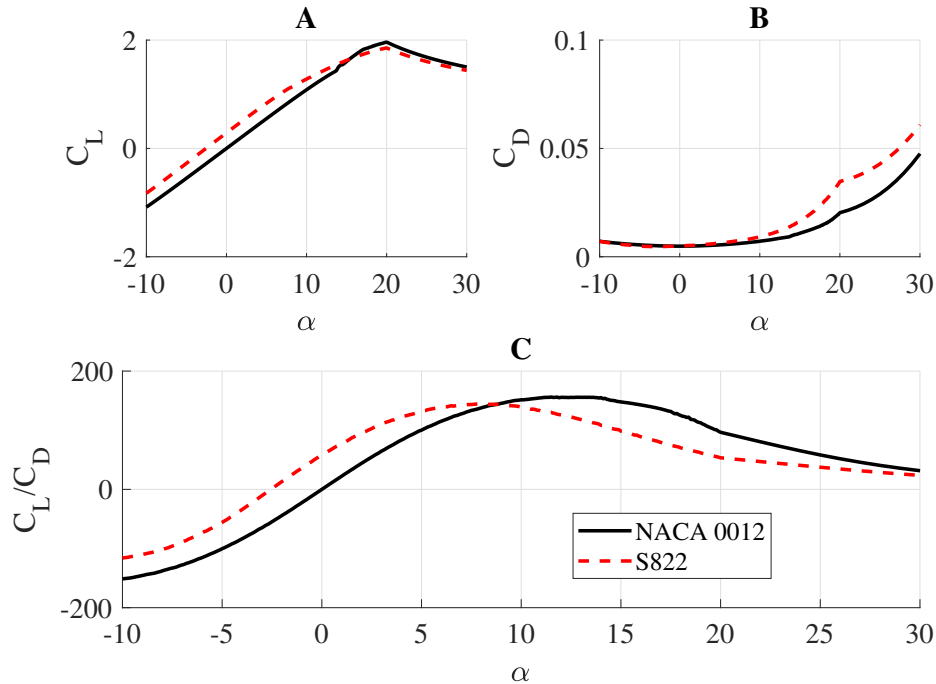


Source: Self-Authorship

Comparing the two airfoils in Fig. 4 (A) and (B) between NACA 0012 and S822, it shows similar performance. However, when analyzing the $C_L/C_D$ in Fig. 4 (C), it shows different maximun at different angles. This optimum angles are important because they need to be aligned with the flow, so the HAWT can be efficient. Additionally, higher $C_L/C_D$ leads to more efficient airfoils, *i.e.* $C_L/C_D$ is the ratio of energy to generate torque and the energy to slow the airfoil. HAWT usually have higher $C_L/C_D$ than airplanes, because airplanes are designed to have lower drag, where as HAWT to produce torque (WOOD, 2011; SURESH; RAMESH; PARAMAGURU, 2015).

2.2.4  Viterna Lift and Drag Extrapolation

In order to compute the whole range of angles of attack ($\alpha$) in wind turbine, an extrapolation from the simulated or wind tunnel data is required. This is necessary, because the range of angle of attack starts at 90° as the wind direction is perpendicular to the airfoil. As rotational speed increases the angle reduces. Thus, the airfoil is

in a stall, then the $C_l$ and $C_d$ can be approximated by the Eq. 17 (GLAUERT, 1983; MAHMUDDIN et al, 2017).

$$
\begin{aligned}
C_L &= D_1 sin(2\alpha) + D_2 \frac{cos^2(\alpha)}{sin(\alpha)} \\
C_D &= E_1 sin^2(\alpha) + E_2 cos(\alpha)
\end{aligned}
\tag{17}
$$

where $C_{D_{max}} = 1.11 + 0.018AR$, $AR = \frac{c}{R}$ is the aspect ratio, $D_1 = \frac{C_{D_{max}}}{2}$, $E_1 = C_{D_{max}}$, $D_2 = (C_{L_{stall}} - E_1 sin(\alpha_{stall})cos(\alpha_{stall}))\frac{sin(\alpha_{stall})}{cos^2(\alpha_{stall})}$, $E_2 = \frac{E_1(1-sin^2(\alpha_{stall}))}{cos(\alpha_{stall})}$. Thus, it is possible to establish the whole range required to simulation, only using the range where the CFD are precise.

## 2.2.5 Blade of HAWT

The blade is responsible for transferring the wind energy to the shaft. Subjected to bending and torsion forces due to aerodynamic forces. In a simplified way, a blade works like a wing on an airplane. The net torque between the lift and drag generates the torque.

The primitive wind turbine had blade built from wood and shape by hand. More recent models use material developed for this purpose, such as aluminum and carbon fiber. This materials are low friction and not adherent to moss, light and resistance, thus with lower inertia and good air flow (SHAKYA; SUNNY; MAITI, 2019).

Some airfoils are sensitive to variation of roughness on the blade, changing drastically the optimum angle and the behaviour present in Fig. 4. Depending on the location, dirty can bond to surface and disturb the flow and reduce the efficiency, such as salt, pollen and dust. On bigger HAWT, there is scheduled wash of the blades and sometimes it can be mitigated with heavy rain (SCHAFFARCZYK, 2014).

The non-linearity is intrinsic to the movement. The root of the blade has a lower speed and high angle of attack. On the other hand, the tip is a high speed and low angle of attack. Thus, a twist on the blade is used to compensate this rotation of the angles (MAHMUDDIN et al, 2017).

The optimized blade is corrected to this. Where, slow airfoils are used at the base to avoid drag and usually big chord to be structure sound. At the tip there is the

opposite situation, the angle is lower than the root and the Reynolds is high, so fast airfoils could be selected for that. The Figure 9 show an example of selected airfoils and the change the on the chord.

**Figure 9 – Modern blade characteristics (A) Top View (B) Airfoils used on A**



(A)    (B)
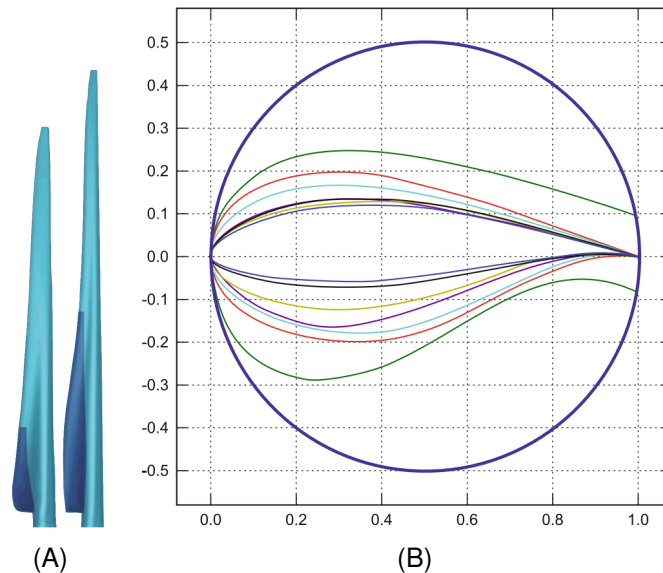
**Source: Adapted from Schaffarczyk (2014)**

Another important fact is that blade are long. This helps to increase the efficiency of the turbine. However, the structure behaves as a long spring with low dissipation, thus the aeroelastic behaving can be pronounced on the blades. Ansari and Novinzadeh (2017) showed that using a controller can stabilize a motion of the airplane to an amplitude of $4°$ to an airplane without control.

Additionally, when the blade is straight up it can have a significant difference on wind speeds, according to Eq. 4, and further increase the bending, and twist coupling (MAHMUDDIN et al, 2017).

2.2.6   Wing Tip losses

The flow of airfoil creates a differential pressure, creating the lift. High pressure below and low pressure at the top of the blade. However, at the tip of the blade the gradient of pressure is equalized through a vortex. This vortex makes the wing tip inefficient (PINTO; GONÇALVES, 2017). Fig. 10 shows different turbulent methods on CFD for wing losses to different types of turbulent methods.

**Figure 10 – Different turbulent methods for wingtip losses**
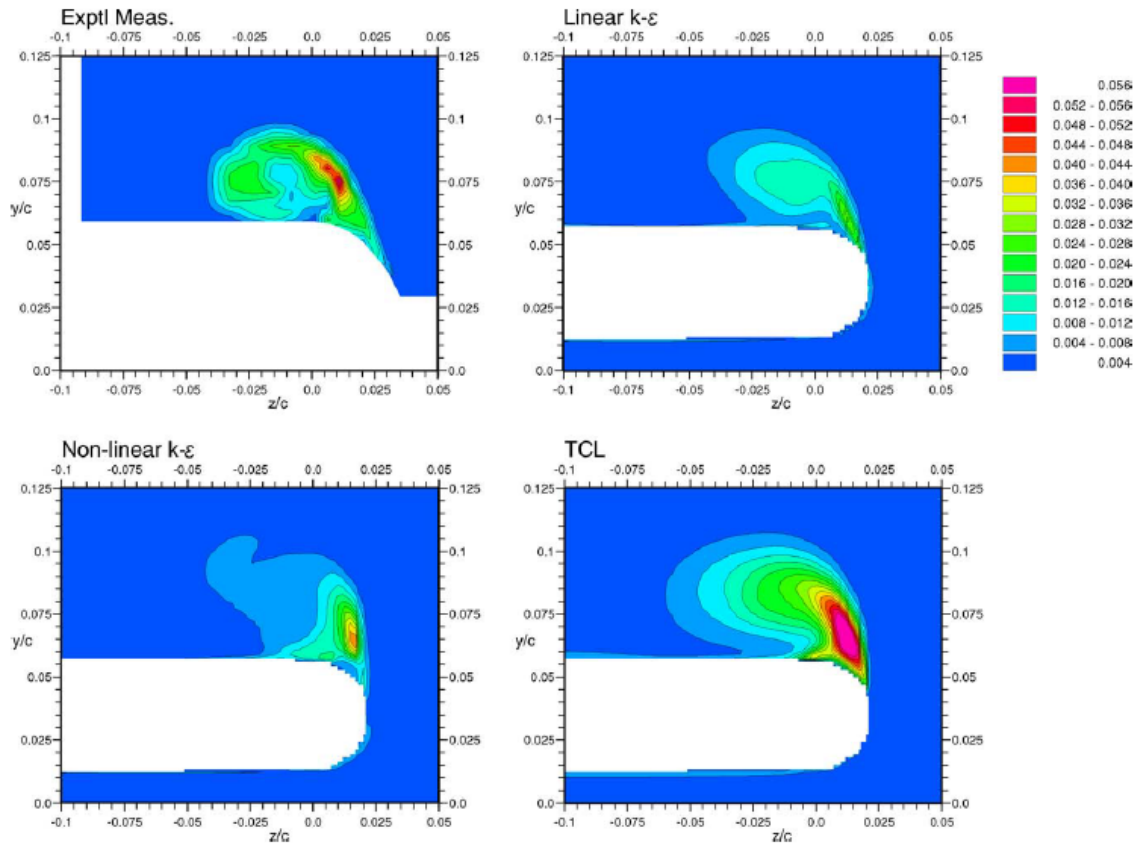
where the red areas means lower pressure areas, and blue represents high pressure area.

The study on wing tip vortex is a special field on aviation, because of the catastrophic result on smaller airplanes. The same approach is used for raked wing tips or fences (FARHAN et al, 2018). The raked wingtip redirect the vortex and alleviate the losses, where the fence prolongs the effective wing and physically reduce the the vortex (FARHAN et al, 2018). On HAWT, a common method is the raked wingtip, and the method used to calculate the inefficient is through the $F$ parameter, from the Prandlt in Eq. 10 (PINTO; GONÇALVES, 2017).

## 2.2.7   Optimization

The optimization process in the blade as discussed before is to obtain the best cost/benefits ratio. Additionally, avoiding structural and design flaws. The main points of optimization is on the airfoil selection, chord size ($c$) and twist angle ($\theta_p$) of the blade.

The airfoil optimization has many criteria to fulfill. Because of the singularity nature of each airfoil, the aerodynamics characteristic shown in Fig. 4 ($C_L/C_D$) depends on the airfoils. Thus, the blade can be dived in three section: structural, low and high speed. First, The structural section it is the root of the blade. It does not require any aerodynamic characteristic, and it only transfers the torque from the blade to the shaft (WOOD, 2010).

Second, the low speed region is the section between the structural and high speed. It is the transition between a high speed and the structural section. These regions must have the lowest drag. Third, the high speed section must be optimized to produce the main torque. This region is the tip of the blade.

Additionally, other factors could be imputed to airfoils selection, such as noise levels, robust against dirt on the surface. For example, Fuglsang and Bak (2004) used a SIMPLEX algorithm to optimize the airfoils to meet the structural and efficiency requirements, along with noise pollution.

According to Fuglsang and Bak (2004) noise and $T_{SR}$ were important factors to HAWT close to urban environments. Because the cinematographic view of wind turbines at 25 miles, can be positive and raise the price of house at this region. However, it diminish the quality of life for residents closer than 25 miles and de-noise techniques must be used to suppress the noise pollution (DRöES; KOSTER, 2016; HUI; CAIN; DABIRI, 2018; JENSEN et al, 2018; DESHMUKH et al, 2019).

Furthermore, the cord size has the function of providing structural support and alleviate the natural rise of Reynolds. By mitigating and controlling the increase of the Reynolds number, it is possible to maintain the same airfoil just adjusting the angle of twist. For example, an optimization comparison is presented on Fig. 5 along with torsion optimization.

**Graph 5 – Sample of optimization fto chord (A) and twist angle (B)**



(A)



(B)
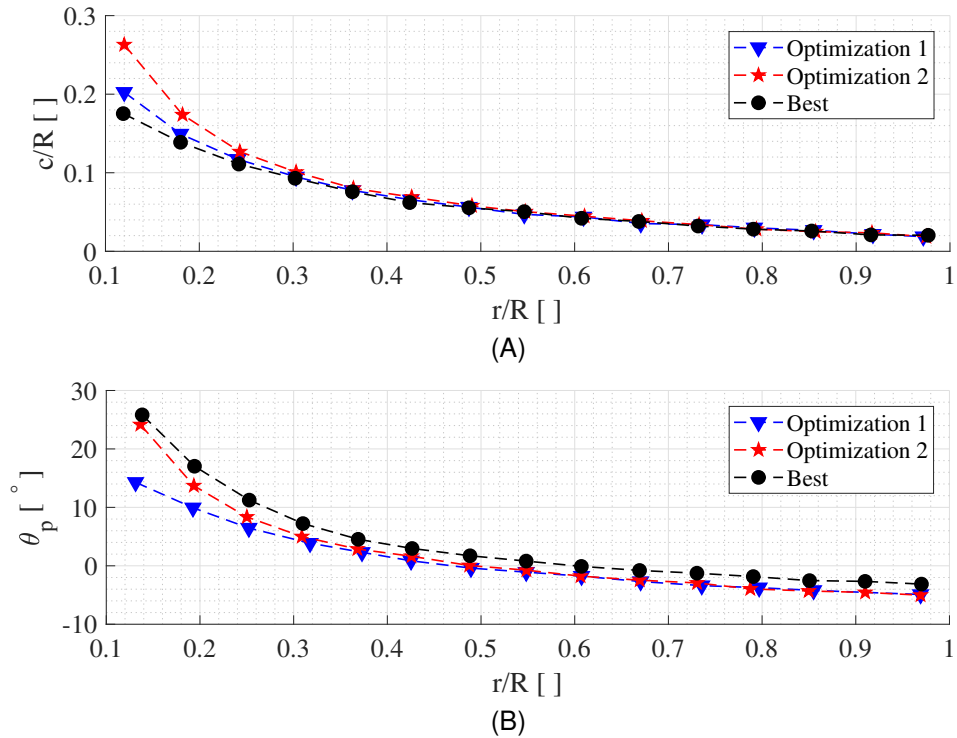
As shown in Graph 5, the triangle and blue, method one by Wood (2010), the star and red ,method two by Wood (2010), and circle and black, method three, without any simplification by Wood (2010). This trend of simplification for optimization method deviate to each method. Additionally, a good optimization will result in the optimum having a few degrees of motion to be at the optimum in neighbor around the $T_{SR}$ (YANG et al, 2016)

### 2.2.8 Rotation Dynamics

Wind turbines rotation dynamics follow the second law of Newton to torque. Fig. 11 shows schematic with the relationship with the rotation and the angle of control $\beta$ .

**Figure 11 – Schematic to wind turbine, where (A) is the front view
and (B) is the side view**
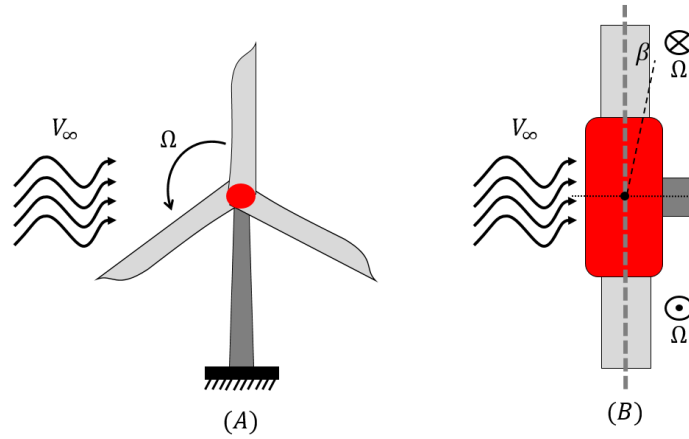


**Source: Adapted from Wood (2010), Lenz et al (2018)**

Thus, it can be expressed as follows:

$$J_0\dot{\Omega} = T_m - T_e - T_{NC} \tag{18}$$

where $T_e$ is the torque of the electric generator, $T_{NC}$ is the torque of the non-conservatives energies such as friction, and inefficiencies, $J_0$ is the sum of moments of Inertia.

As showed in Eq. 15, the $c_P$ is a complex function, dependenting on the $V_\infty$, $T_{SR}$ and $\beta$. However, Luo, Vidal and Acho (2014) simplify this as a function of several variable and constants to base his control on the electric power, Eq. 19.

$$\begin{cases} c_P(T_{SR},\beta) = C_1 \left( \frac{C_2}{\psi_2} + C_3 T_{SR} + C_4 \right) e^{\psi_1} \\ \psi_1 = \frac{C_5}{\psi_2} + C_6 T_{SR} \\ \psi_2 = \left( \frac{1}{T_{SR}+0.08\beta^*} - \frac{0.035}{\beta^{*3}+1} \right)^{-1} \end{cases} \tag{19}$$

where $\beta^*$, $C_7$, $C_1$, $C_2$, $C_3$, $C_4$, $C_5$, $C_6$,$C_7$, are adjusted parameters to fit the $c_P$ database to the desired wind turbine.

For the electrical control this model is valid to project the controller (LUO; VIDAL; ACHO, 2014). However, for some model it does not have a great fitness parameter(LENZ et al, 2019). The dynamic force of an electric generator is investigate in Luo,

Vidal and Acho (2014), Janzen et al (2019), and is presented in Eq. 20 .

$$
\begin{cases}
T_e = k_t i \\
k_b \omega = -Li - R^* i
\end{cases}
\tag{20}
$$

where $R^*$ is the sum of the load and the electric generator resistance, $L$ is the inductance of the engine, $k_t$ and $k_b$ are the equivalent electromechanics, $i$ is the electric current.

The dynamics then can be simplified using Eq. 14 inserted the dynamic will be simply to $T_e + T_{NC} = c_e$. Thus,it is possible to direct establish the coefficient of power for the turbine, with the rotation on Eq.21 .

$$
J_0 \dot{\Omega} = \frac{P_t}{\Omega} - c_e \Omega
\tag{21}
$$

Additionally, Eq. 21 can be rewritten as Eq .22

$$
J_0 \dot{\Omega} = \frac{c_P \pi R^2 \rho_{air} V_\infty^3}{4\Omega} - c_e \Omega
\tag{22}
$$

where $J_0$ is the sum of moments of inertia. Thus, using the Eq. 22 with a large data set or an equation that maps $c_P$ it is possible to analyze the dynamic of rotation the Buhll's methodology.

## 2.3  PARTICLE SWARM OPTIMIZATION

Particle Swarm Optimization (PSO) is a stochastic and base-population method for optimization that mimics the swarm of animals. This method of optimization works by minimizing a function. It is a relative new method and it is attributed to Kennedy and Eberhart (1995) and Shi and Eberhart (1998). Fig. 12 shows the basic behavior of PSO, over interactions until they swarm to the desired output, the star that is the minimum of the function cost.

**Figure 12 – Example of PSO**



$(A)$      (B)      (C)

**Source: Adapted from Dorigo and Birattari (2007)**
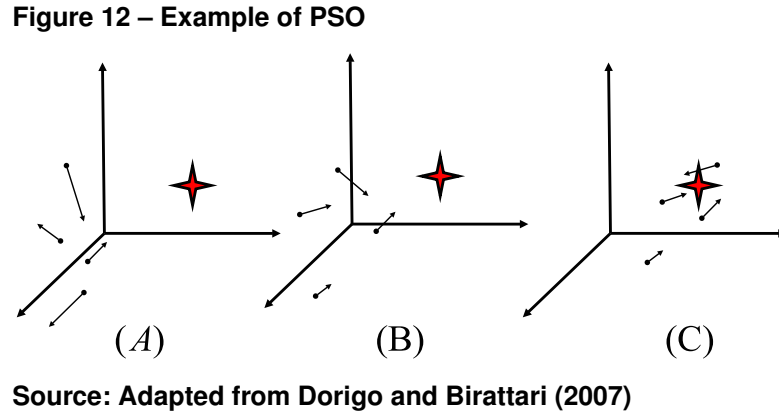
Fig. 12 (A) represents the first iterations, where all the particles at a random start have initial speed, based on the self knowledge and the global knowledge. In 12 (B), the majority of the particles are roughly on the right direction, and with lower speeds. In 12 (C), they swarm around the desired output, with small deviations. This presented behavior is desired and is explained by the speed equation of each particle, shown in Eq. 23 (PARSOPOULOS; VRAHATIS, 2010; KAVEH, 2017).

$$V_p^i = C_0 V_p^{i-1} + C_1 R_1 (X_{lb} - X_p) + C_2 R_2 (X_{pb} - X_p) \tag{23}$$

where $C_0$ is the inertia of the system, $V_p$ is the speed of the particle, , $C_1$ is the self knowledge, $R_1$ and $R_2$ are random values, $X_{lb}$ is the direction for the local best, $X_p$ is the current position, $C_2$ is the group knowledge, $X_{pb}$ is the direction for the group best. All the parameter have a range depending on the type of problem to be optimized, a standard and accepted range of parameters can be found in Erik, Pedersen and Laboratories (2010).

As many optimization methods, it already has many variations and adaptation of the method. Kaveh, Bakhshpoori and Afshari (2014) reviewed the evolution of the PSO algorithm. Such variations usually affect direclty the basic Eq. 23 and the variables (EBERHART; SHI; KENNEDY, 2001; VENTER; SOBIESZCZANSKI-SOBIESKI, 2003; CLERC, 2006).

This method can be employed on many variables, because the particle are driven by the results of the function cost, not the variables. The cost functions is the functions that relates the trade off of all the variables to be optimized. (KARABOGA; BASTURK, 2007; ADACHI et al, 2019)

## 2.4 NEURO FUZZY CONTROLLERS

Neuro fuzzy controllers are an evolution of the classic fuzzy logic, by using methods of training and learning from neural networks on regular fuzzy logic. Thus, making an improvement on the performance of fuzzy controller. This combination takes advantages of the strength of the neural network of being adaptive and the fuzzy set theory of the knowledge representation (JANG; SUN; MIZUTANI, 1997; NAUCK; KLA-WONN; KRUSE, 1997).

It was developed in the 1990, by the vein of Artificial Intelligence (AI) at the time when developing and implementing algorithm that can learn patterns was at the begging . Thus,this methodology of learning was extended to fuzzy logic (JANG; SUN; MIZUTANI, 1997; NAUCK; KLAWONN; KRUSE, 1997).

Comparing the fuzzy controllers with linear controllers, fuzzy controllers can have the same performance that linear controllers have in linear plants. However, when presented with a nonlinear plant, the fuzzy controller outperform the linear controllers. (CHMIELOWSKI, 2016; CHEN; PHAM, 2000).

### 2.4.1 Fuzzy Logic

The fuzzy logic was introduced by Zadeh (1965), where the current modern logic control derive from. The fuzzy logic allowed infinite levels of control, different of on/off logic the trend at the time. In addition, the fuzzy control allows an easy interface with the user, without a precise mathematical modelling of the structure or the plant (TUSSET, 2008).

Differently than most controllers, where the mathematical modeling is a requirement for SDRE and PID (LIBERTY, 1972). Fuzzy control uses the common knowledge of the operator and a set of logic operators to attribute the output. Thus, it can balance contradictory inputs that usually made other controllers misbehave. For example the thermal design of a power plant that usually relies just on the exhaust temperature, where a fuzzy controller can be feed with coal input, air temperature, and humidity of the air to set the right amount air on the burner (KOCAARSLAN; ÇAM; TIRYAKI, 2006).

Linear controllers such PID, account for 90% of the industrial controllers, working in nonlinear and linear plants. To overcome problems with nonlinear problems, self-

tuning mechanics must be implement for different phases of operation or reduced outputs (ZADEH; KLIR; YUAN, 1996; ÅSTRöM; HäGGLUND, 2001; MENDES; OSÓRIO; ARAÚJO, 2017). In comparison, fuzzy controllers can have the same efficiency as linear controllers at linear plants.

However, in nonlinear plants, fuzzy outweigh the linear control on performance because it is more robust on a wide range, easy to understand because of the linguist term (ZADEH; KLIR; YUAN, 1996; REZNIK, 1997). By creating a set of rules and membership functions the inputs and output can be treat by states as that describe the states, such as: "hot", "warm" and "cold"" (MITRA; HAYASHI, 2000; JANG; SUN, 1995). Thus, a variable can be partially from on group and inherent characteristic and behavior this group have.

Differently from the on/off logic, that a variable belong or not belong to that classification. In addition, nonlinear plants have multivariable, multiloop and many times lack of perfect knowledge. Thus, misleading the linear representation of the plant, where as fuzzy control thrives because the linguist representation lead to a better understanding and setup by the operator. Consequently the implementation of fuzzy controller results on better performance (REZNIK, 1997)

## 2.4.2 Fuzzy Set Theory

The fuzzy theory is based on sets, where each set represent a membership or entitle to the same group. In other words, the relationship can be establish by answering question: "is the element the same as the others on this group? How much this elements correlate with this group?" This theory correlate not just a membership, but how much similarity the new element has within the group.

In addition, the classification method is bias toward the evaluator. *e.g.*, one can deem the temperature of the water at 30ºC as hot, and other person can evaluate it is warm. Differently from the Boolean logic, where the threshold is a crisp. There is not a transit state.

The association level can be describe by a membership function, which related the association level with the analyzed member, the input at that sample time. The most common membership function are triangle, and the Gaussian function. Nevertheless some other function, such as quadratic, prismatic and custom function could be use.

The Gaussian function and he triangle function are presented on the Graph 6 (REZNIK, 1997).

This method made the fuzzy logic approachable to users, because made it easy to tune the function to the desire specific situations. It made easy to the operator o translate the common knowledge in to fuzzy logic. The Fig. 6 show a set of membership functions.(JANG; SUN, 1995)

**Graph 6 – Set of Membership functions**
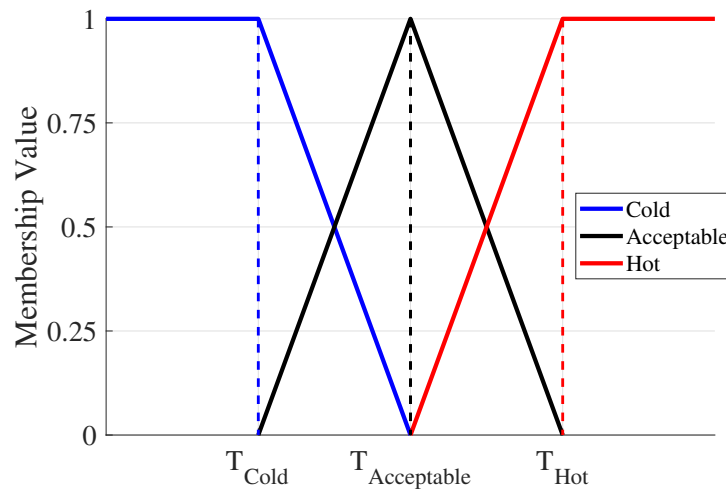
The set of equations that describe the triangle and the trapezium are describe on the Eq. 24.

$$f(x,c_1,c_2,c_3,c_4) = \begin{cases} 0, if \ x \leqslant c_1 \\ \frac{x-c_1}{c_2-c_1}, if \ c_1 \leqslant x \leqslant c_2 \\ 1, if \ c_2 \leqslant x \leqslant c_3 \\ \frac{c_3-x}{c_3-c_2}, if \ c_3 \leqslant x \leqslant c_4 \\ 0, if \ c_4 \leqslant x \end{cases} \tag{24}$$

where $c_1$, $c_2$, $c_3$, $c_4$ are the parameter of the membership function. When $c_2 = c_3$, the trapezium equation is the triangle equation.

As shown on Graph 6, for the operator made easy to set the Values of $T_{cold}$, $T_{Warm}$ and $T_{Hot}$ on the fuzzy controller. In this case this variables saturates, and the warm functions overlaps 50 %, in average can be between 75% to 25%, to assure a smooth transition between activation functions. (TUSSET, 2008).

The activation function can have different shapes, such a function sine , logistic and trapezoidal. The selection of the function can create a saturation such as Cold and Hot on Graph 6. Or have a very sharp definition as Warm. tational power available. To fulfill the whole range, usually is necessary a set of membership function. For example, "cold", "warm" and "hot" to cover an input of water temperature on a pressure cooker. This number of function fluctuates between 3 and 7. Whereas, three membership function are selected for speed without losing significant precision, and seven functions are more selective, with some penalty on processing time. More than seven function usually results on loss of precision and slower processing time (TUSSET, 2008)

For the output, the deffuzyfication process is similar to the fuzzification process. Similarly, many process of disfuzzification were created. It can be divide in main process, Centroid of area, average of maximum, center of maximum, and Sugeno (TUSSET, 2008). Each process modify the output.

Additionally, the fuzzy rules on the output can be divided by Mandani and Sugeno. Mandani was proposed on 1975 by Ebrahim Mamdani, and it is more a linguistic output, where as Sugeno was introduced on 1985 and outputs a function or a constant (MAMDANI; ASSILIAN, 1975; SUGENO, 1985).

The Mandani process consist on interpreting the desire action, i.e. slower, nothing ,accelerate for a cruise control. Thus, it relies on the knowledge of the programmer, and the output range to interpolate between the outputs.

The Sugeno process is more mandarin set of interface system was the first system implement by Mamdani and Assilian (1975), to control a boiler and an engine. This set of interference is based on logic gates to attribute a desire output. Whereas the Sugeno create by Sugeno (1985) type system, only have two output, constant or linear for output. The Mandani and Sugeno desfuzication method works in different ways, sugeno works as a function output shown on Eq. 25.

$$Z = b_1 T_{sr} + b_2 V_{\infty} + b_3 \tag{25}$$

where $Z$ is the output, $b_n$ is a coefficient to tune the fuzzy. Thus, an output can be fine tuned to the desired data set.

## 2.4.3   Neural Network

Neural Networks or machine learning mimic the brain activity of processing information. Despite it being chaotic, the information is processed through a net of brain cells, that have almost random connections and loops. It was first develop by McCulloch and Pitts (1943), and since then, many models improve in different branch. *e.g* image processing, patter recognition, and general regression.

Similar to brain activity, the neural network have layers, and the information passes through this layers and it changes as passes. Each layer is composed by several neurons, and it connection can be determine by the user or by an self-arrangement algorithm. Each layer could have a weight and a bias factor to tune the function into the desired output. The most common activation functions are radial, linear, tanh, convolute and clustering. The Fig. 13 illustrates a neural network with multiple layers and internal loop.

**Figure 13 – Basic Neural Network**
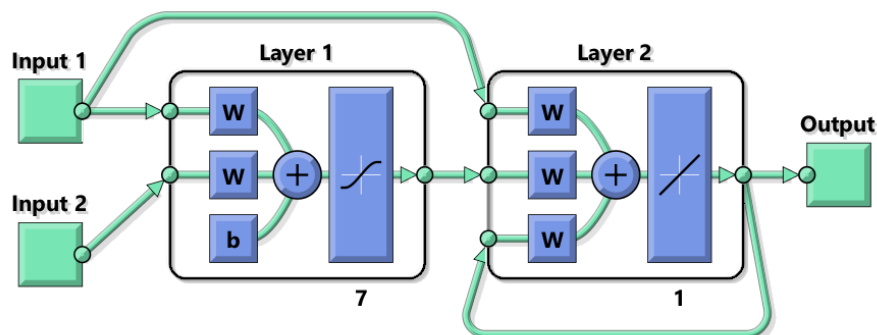


**Source: Self-Authorship**

As shown in the Fig. 13, the neural network in this case have two inputs (Input 1 and Input 2). The Layer 1 have 7 neurons with a bias factor (b). The Layer 2 have 1 neuron, because it is the last layer before the output. Thus it must have the same amount of neurons.

In addition, the Input 1 is connected direct by Layer 2, and it is connected with Layer 1 and Layer 2 via a loop. Thus, the results of Layer 2 is added at the next iteration. Nowadays, there are standard layouts to image processing, regression methods and algorithm. In addition, the training method can change the layout to further improve the results (NAUCK; KLAWONN; KRUSE, 1997; CHEN; PHAM, 2000).

2.4.4   Adaptive Neuro-Fuzzy Inference Systems

The Adaptive Neuro-Fuzzy Inference Systems is a method of converting the learning adaptability to the IF-Then rules of Fuzzy Logic to a variable system. (JANG; SUN, 1995; JANG; SUN, 1995; JANG, 1993) To train or fit each variable it can be done on-line or offline. For on-line the training mechanism will adjust each input to the desire output, using the gradient as a training mechanism. However, this method can be trapped on a local minimal (JANG; SUN, 1995; JANG, 1993). For the off-line training it can combine the gradient and the least square estimate to train the variables. This methods is more robust than the on-line training because avoid the local minimal and learn the behavior, instead of the instantaneous error.

However, the amount of rules increase exponentially the number of variables to be fitted. The Fig. 14 show the diagram for a three rules with two variables.

**Figure 14 – Neuro-fuzzy sub systems**
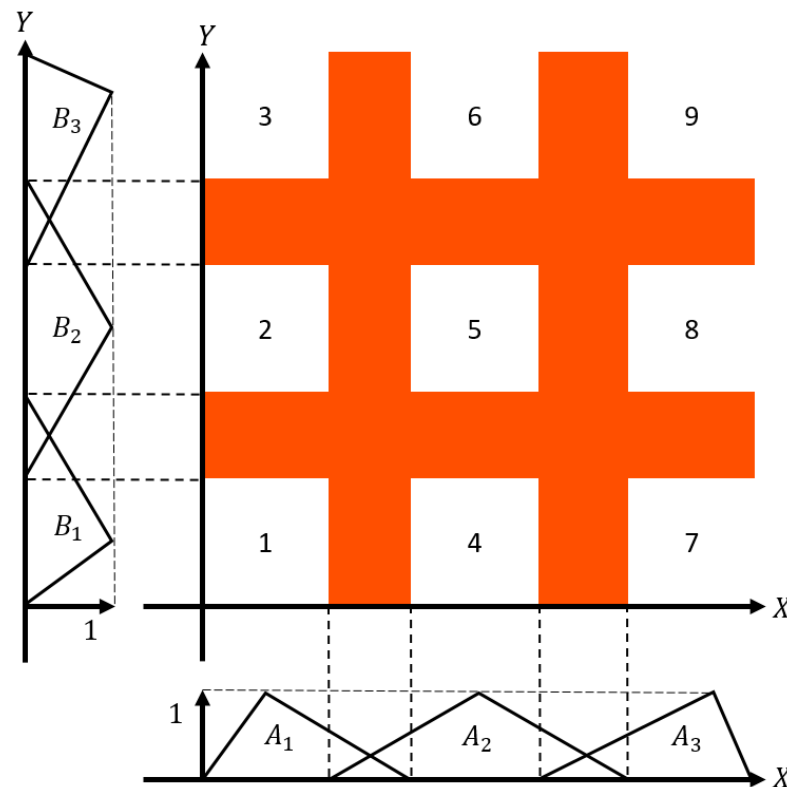


**Source: Adapted from Jang (1993)**

As shown on Fig. 14 shows the rules in one variables $A_1, A_2, A_3$ and for the other variable as $B_1, B_2, B_3$, the subsystems created are 9. In orange is the transition between each rule. Each subsystem has parameters $b_1, b_2, b_3$ associated with Eq. 25.

# 3 METHODOLOGY

In this chapter it will be explain the methodology, the parameters selected and the procedures adapted to achieve the general and specific objectives. Thus, the initial operations were summarized on Fig. 15.

**Figure 15 – Flowchart of operations - Part 1**
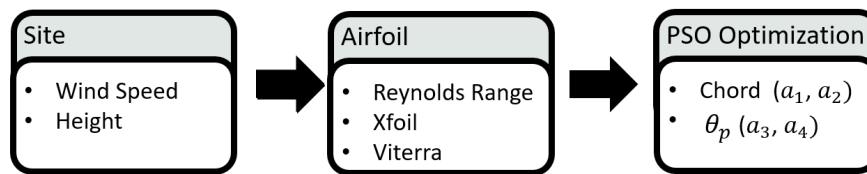


**Source: Self-Authorship**

First, the site parameters were selected based on New World Wind (2018), 4 [m/s] is consider an economic viable site. Thus, a safety height of the hub was selected as 20 [m]. Consequently, the Eq. 4 was utilized to calculate the average wind speed at of 5.5 [m/s] at the safety height.

Second, the airfoil parameter were selected, such as that the PSO will not crash. Thus, the $C_L$ and $C_D$ was obtained by the Xfoil® software (MARTEN et al, 2013). The parameters used on the Xfoil® were 100 interactions with a range from $-10°$ to $20°$ with a step of $0.1°$, filtering 5, Ncrit 9 standard wind tunnel. The complete range was using the Vittera extrapolation until the angle of $-90°$ with a step of $1°$. The airfoil selection were NACA 0012, NACA 0015, NACA 2412, NACA 2415, NACA 4412, NACA4 4415, S821, S822, S823, S833, S834, S835 based on previous paper of wind turbines (MAHMUDDIN et al, 2017).

The range of Reynolds number were the combination of the following set of ranges: from 100k to 1M with a step of 20k, from 1M to 100M with a step of 200k. The lower bound due to simulation limitation was 100k, and the upper limits were just set as a reference value to the transition from laminar to supercrital laminar flow (XU et al, 2018a). This software was integrated with the Matlab ®, allowing the construction of tables from the selected airfoils. Thus, the following operation on the flowchart in Fig.

16

**Figure 16 – Flowchart of operations - Part 2**
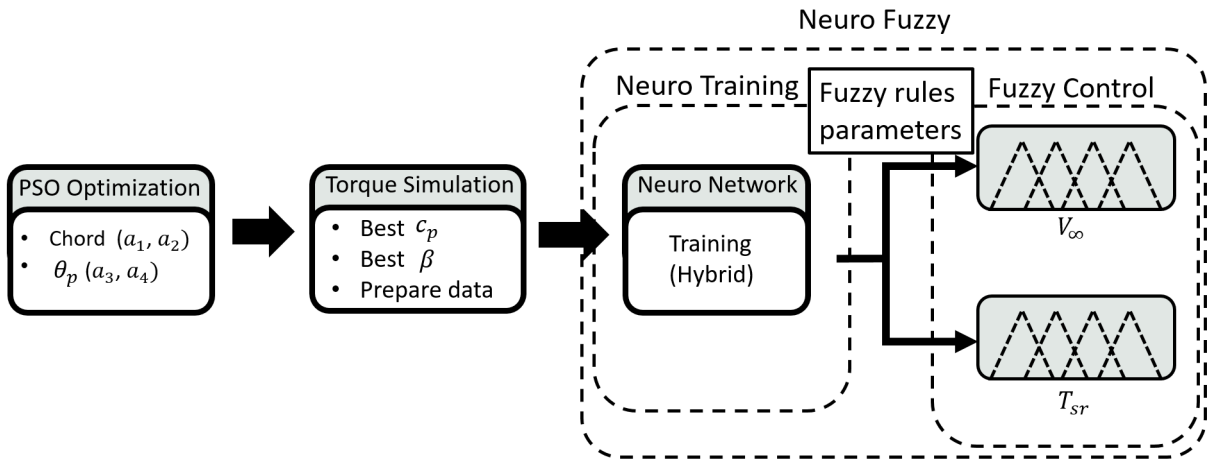


**Source: Self-Authorship**

Thus, a table with $C_L$ and $C_D$ was built and used with the PSO optimization (DRELA, 1989; MORGADO et al, 2016; KUMAR; ALI; AROCKIARAJAN, 2018). The optimization process used the Matlab with the configurations to PSO is on the Tab. 2:

**Table 2 – Parameter of PSO**

| Variable | Value | Variable | value |
|----------|-------|----------|-------|
| Swarm Size | 100 | Function Tolerance | $10^{-5}$ |
| Max Stall Iterations | 35 | Max Iterations | 550 |
| Inertia Range | 0.6 | Self Adjustment Weight | 1 |
| Social Adjustment Weight | 1.49 | Objective Limit | 0 |

**Source: Adapted from Pedersen (2010)**

The parameters to the turbine are presented on Tab. 3

**Table 3 – Parameter of Turbine for PSO**

| Variable | Value | Variable | value |
|----------|-------|----------|-------|
| $T_{sr}$ [  ] | 8 | $V_\infty[m/s]$ | 5.5 |
| $R_{hub}$ [ m ] | 0.1 | $d_x[m]$ | 0.001 |
| $R_{max}$ [ m ] | 4.5 | $\rho_{air}[kg/m^3]$ | 1.2 |
| $\nu_{air}\ [m^2/s]$ | $1.81 \times 10^{-5}$ | | |

**Source: Self-Authorship**

The selected parameter $T_{SR} = 8$ was to situate the HAWT at the lower range recommended to avoid excessive noise due to high speeds (WOOD, 2010). The radius restriction (4.5m) is to have a maximun power of 10kW at the average wind speed. The

the optimization is shown on Eq. 26:

$$\underset{J}{\text{minimize}} \quad J(u_1, u_2, u_3, u_4) = \frac{1}{c_p}$$

$$\text{subject to}$$

$$-10 < u_1 < 0, -10 < u_2 < 0, ,$$

$$20 < u_3 < 150, 0.1 < u_4 < 0.5$$

(26)

The $dx$ is the step in the radial direction using the Buhl's methodology, it was selected to avoid error due to big steps. Thee air proprieties was evaluated at $20°C$. To the wing profile, a function was created based on previous optimized literature (GLAUERT, 1983; WOOD, 2010; SCHAFFARCZYK, 2014; SORENSEN, 2016). The function of the chord was required to have a continuous profile.

$$c(r) = \begin{cases} \left[ \ln \left( \frac{u_3 u_4}{R_{max}} + e \right) \right]^{-1}, & if \ \frac{r}{R_{max}} \leqslant \frac{u_4}{R_{max}} \\ \left[ \ln \left( \frac{u_3 r}{R_{max}} + e \right) \right]^{-1} \end{cases}$$

(27)

where $c$ is chord, $R_{max}$ is the maximun radius of the blade, ,$r$ is the local radius, and $u_3, u_4$ are the parameter to be optimized. The same procedure was adapted for the torsion angle ($\theta_p$), on Eq.28:

$$\theta_p(r) = u_1 \ln \left( \frac{r}{R_{max}} \right) + u_2$$

(28)

where $\theta_p$ is the twist angle, and $u_1, u_2$ are the parameters to be optimized. Thus, the only variables were the limited of the variables $u_n$, and for this variables the following bound were select so the values of $c(r)$ and $\theta_p(r)$ were reasonable. Otherwise, the PSO could increase significantly the values to take advantage of higher Reynolds and making the blade unfeasible for future construction.

**Table 4 – Bound parameters**

| $u_n$ | Lower bound | Upper Bound |
|---|---|---|
| 1 | -10 | 0 |
| 2 | -10 | 0 |
| 3 | 20 | 150 |
| 4 | 0.1 | 0.5 |

**Source: Self-Authorship**

After the PSO result were obtain a range of $c_P$ were calculated using the Buhl's methodology from Eq.12, Eq. 13, to obtain the torque and $c_P$ in Eq. 14 and Eq. 15

respectively. Thus, the range of angles from $-40°$ to $25°$ could be calculated. Thus the efficiency in this range will create the neuro fuzzy rules, following the Eq. 29.

$$P_{T_{sr},V_\infty} \leq 10^4 \begin{cases} c_{pf} = \begin{cases} c_{p(opt)}, else \\ \\ c_{p(10^4)} \end{cases} \\ \\ \beta_p = \begin{cases} \beta_{(opt)}, else \\ \\ \beta_{(10^4)} \end{cases} \end{cases} \tag{29}$$

where $c_{pf}$ is the $c_P$ to be trained on the neuro fuzzy, $c_{p(opt)}$ is the optimum coefficient of power, $c_{p(10^4)}$ is the coefficient of power for $10^4$ [W], $\beta_{pf}$ is the $\beta_P$ to be trained on the neuro fuzzy, $\beta_{p(opt)}$ is the optimum best angle of power, $\beta_{p(10^4)}$ is the $\beta$ angle for $10^4$ [W]. This methodology was based on the following regiments:

1. Protect over power greater than $10^4$ [W];

2. Optimize the angle when (1.) not occurs to yield the maximum power.

Nevertheless, the protections for low wind speeds to prevent wear and tear can not be added without adding a timer. Fig. 17 shows the proposed control fuzzy during a dynamics simulation.

**Figure 17 – Model of Fuzzy control**
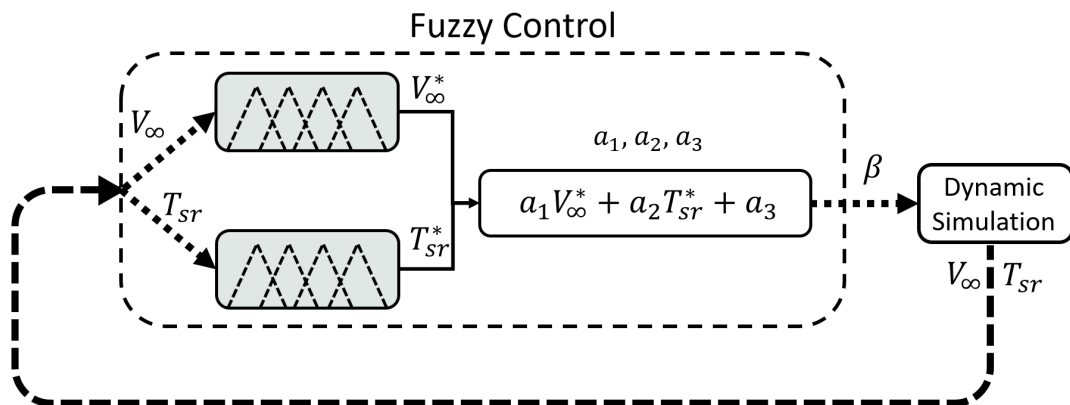


Source: Self-Autorship

where $V_\infty^*$ is the fuzzified value of $V_\infty$, and $^*_{SR}$ is the fuzzified value of $_{SR}$. This methodology was applied to the dynamic simulation, with 49 Sugeno rules. The rules were obtain from the training are presented on Fig. 14.

The dynamic of the electric generator was simplified as a viscous damper, as describe on Eq. 22. The linear damping parameter was taken in to account the torque

produced by the turbine at $T_{SR} = 8$ [ ] and $V_\infty = 5.5$ $[m/s]$, thus $c = 50$ $[Nm/rad]$. The momentum of inertia was based on a solid wing, made of aluminum with density of $2700$ $[kg/m^3]$ , where the area of the airfoil section was used by 2000 points with a step on the radial direction of $10^{-3}$. Thus $J_0 = 3 \times 480.1385$ $[kgm^2]$. As presented on Eq. 22, the power extracted from the turbine is divided by the rotation speed. To avoid errors, the lower rotation speed was set to $10^{-12}$.

To simulate dynamics the following wind profiles were select to compare and contrast the efficiency of the controller, break of inertial and stability of the controller.

$$V_\infty = \begin{cases} \text{constant } speed, case\ 1 \\ 5.5 + 5\sin(2\pi ft), \text{case } 2 \\ \text{Rayleigh distribution with an average of } 5 \text{ [m/s], case } 3 \end{cases} \tag{30}$$

The case 1 was selected to simulate a steady state of wind. This Case is to investigate the efficiency to break the inertial and the capability to limit the max rotation. Because, to test the controller below the max energy the controller should track the $\beta_{(opt)}$ and above this threshold it should track the $\beta_{(10^4)}$, thus regulating the power output, after it passes $10^4$ [W].

The case 2 and the case 3 were select to analyze the behaviour on non static wind speeds. The case 2 investigate a fluctuation on wind speed between the average speed and the speed with most energy with a frequency between 0 and 2 [Hz] with 128 intervals. Because the natural frequecies are below 6 [Hz] (WAIT et al, 2019). This cases was selected because of the variation of wind can cause the wind turbine to extract more than it is possible, and at the lower region it can come to a halt due to drag and power extracted from the generator side. Thus, proving that the controll is a better solution. The case 3 was selected to analyze the behavior with a random wind speeds, thus simulating a very unstable weather, that could be rainy day. The Rayleigh distribution was selected because it is the stander probability in wind turbine design, it also was divide in 128 intervals between 0 and 2 [Hz].

# 4 RESULTS AND DISCUSSION

In this chapter, the results and the main discussion are presented, in the same order as presented on the Chapter 3. First, the wind distribution to the selected site is shown on Graph 7 .

**Graph 7 – Distributions parameter to the selected site (A) Wind Probability (B) Energy Distribution**



(A)

(B)
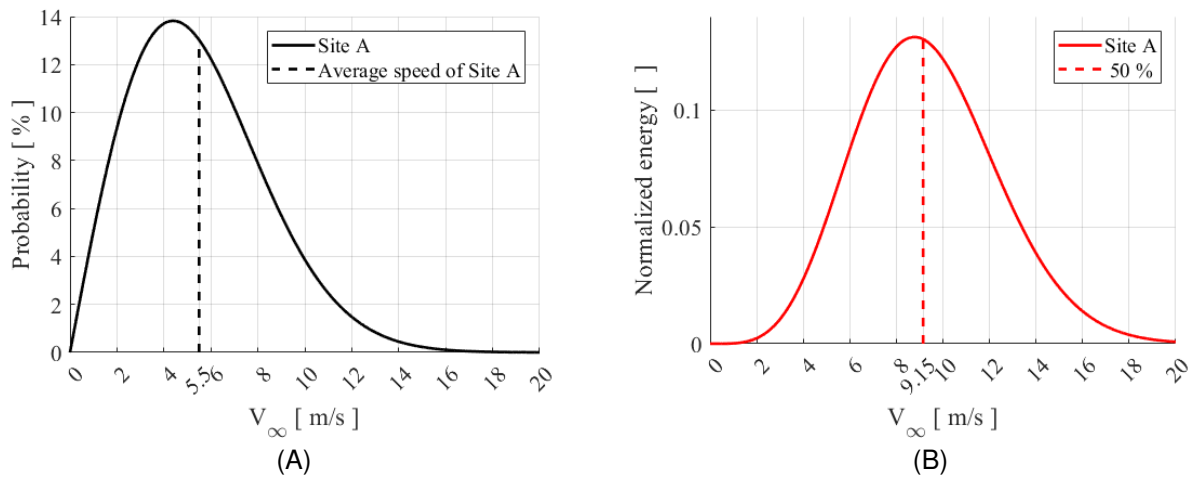
**Source: Self-Authorship**

As presented in Graph 7, the speed of most energy is $9.15\ [m/s]$. Consequently, this energy is included on all the cases to wind profile. Thus, using this wind as an optimization parameter in the PSO.

## 4.1 RESULT OF PSO

Tab. 5 shows the results to the PSO optimization for the average speed and the speed of most energy ($5.5\ [m/s]$).

**Table 5 – Comparison of wind turbine types results for** $5.5\ [m/s]$

| $u_1$ | $u_2$ | $u_3$ | $u_4$ | Interactions | $c_p$ | Airfoil |
|---|---|---|---|---|---|---|
| -3.178 | 0 | 59.185 | 0.498 | 73 | 0.4517 | NACA 0015 |
| -4.596 | 0 | 150.000 | 0.500 | 120 | 0.4501 | NACA 4412 |
| -4.680 | 0 | 135.918 | 0.500 | 82 | 0.4467 | NACA 2412 |
| -4.527 | -1.1109 | 149.917 | 0.499 | 61 | 0.4463 | NACA 2415 |
| -4.313 | 0 | 119.069 | 0.499 | 142 | 0.4432 | S822 |
| -4.243 | 0 | 135.045 | 0.500 | 68 | 0.4398 | S835 |
| -4.416 | -11.740 | 150.000 | 0.500 | 87 | 0.4397 | NACA 4415 |
| -3.736 | -0.003 | 116.781 | 0.436 | 117 | 0.4396 | S833 |
| -2.816 | -0.001 | 86.941 | 0.499 | 86 | 0.4384 | S834 |
| -4.692 | 0 | 150.000 | 0.500 | 65 | 0.4384 | S823 |
| -3.714 | 0 | 81.001 | 0.500 | 80 | 0.4340 | NACA 0012 |
| -3.372 | -0.011 | 136.910 | 0.370 | 125 | 0.4278 | S821 |
| -4.0235 | -1.0687 | 122.5639 | 0.4834 | 92 | 0.4413 | Average |
| 0.6411 | 3.5393 | 31.0502 | 0.0401 | 27 | 0.0068 | Standard deviation |

**Source: Self-Authorship**

In addition, the same optimization was done to speed of maximum Energy $(9.15[m/s])$.

**Table 6 – Comparison of wind turbine types results for** $9.15\ [m/s]$

| $u_1$ | $u_2$ | $u_3$ | $u_4$ | Interactions | $c_p$ | Airfoil |
|---|---|---|---|---|---|---|
| -5.013 | 0 | 30.402 | 0.403 | 24 | 0.4669 | NACA0015 |
| -8.798 | 0 | 44.212 | 0.278 | 20 | 0.4662 | NACA2412 |
| -6.272 | 0 | 26.207 | 0.387 | 26 | 0.4630 | NACA0012 |
| -7.809 | 0 | 37.629 | 0.317 | 16 | 0.4587 | S833 |
| -9.709 | 0 | 25.282 | 0.340 | 35 | 0.4586 | S822 |
| -9.718 | 0 | 80.927 | 0.316 | 46 | 0.4526 | NACA2415 |
| -9.717 | 0 | 81.007 | 0.314 | 40 | 0.4526 | NACA4415 |
| -9.717 | 0 | 81.007 | 0.314 | 40 | 0.4526 | NACA4412 |
| -7.970 | 0 | 36.286 | 0.279 | 31 | 0.4446 | S834 |
| -7.507 | 0 | 48.243 | 0.363 | 17 | 0.4445 | S832 |
| -7.690 | 0 | 71.213 | 0.260 | 32 | 0.4400 | S823 |
| -8.365 | 0 | 38.460 | 0.340 | 34 | 0.4299 | S821 |
| -8.190 | 0 | 50.073 | 0.326 | 30 | 0.4525 | Average |
| 1.489 | 0 | 22.159 | 0.043 | 10 | 0.011 | Standard deviation |

**Source: Self-Authorship**

As shown on Table 5 and Table 6 the results pointed to the same airfoil PSO optimization. Regardless, the selected airfoil the $c_P$ were very close with a different less than $3\%$ on both optimization. This shows the efficiency on optimization of the PSO technique, given the constrain imposed by the variation on each Airfoil to achieve the $\frac{C_L}{C_D}$ at different $\alpha$.

In addition, the result showed lower standard deviation to the parameter $u_1$, $u_2$, $u_4$ , $c_P$. The deviation on $a_3$ can be explain because of different angles of stall,as discuss above.

### 4.1.1 Coefficient of Power Results

The best profile was NACA 0015, it was selected the optimization to $5.5\ [m/s]$. These parameters were used on different wind speeds to create a data base of the relationship of wind speed ($V_\infty$) and $T_{sr}$ to build the data set to the neuro fuzzy controller. The various results can be seen on Chapter A. The average $c_P$ is shown on Graph 8.

**Graph 8 – $c_P$ for the average: where A is the surface view and B is the contour view**



(A)                                                                  (B)
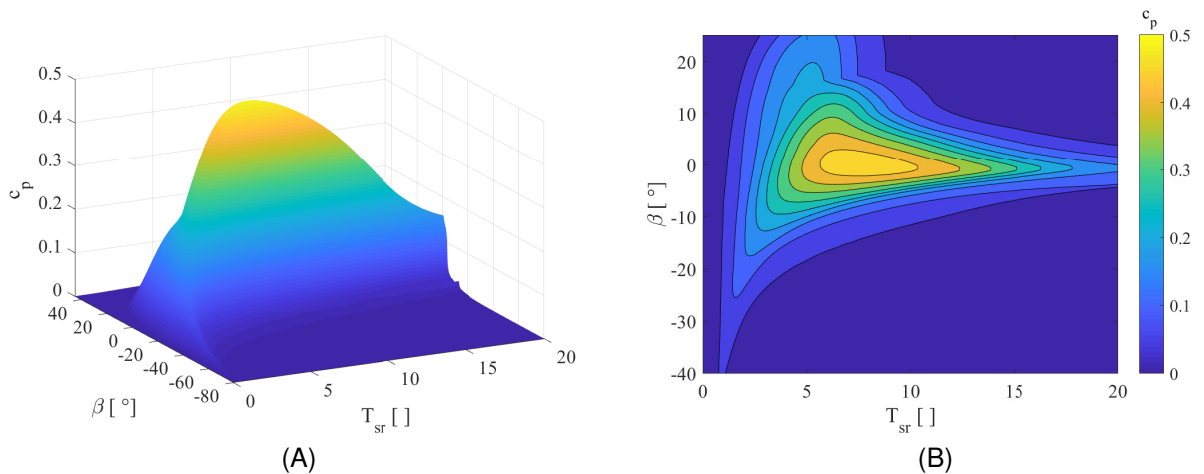
**Source: Self-Authorship**

Extracting the best $\beta$ by searching the max $c_P$ for each $T_{SR}$

**Graph 9 – All of best, where A is the best $\beta$ angle and B is the best $c_P$ for each wind speed**



(A)                                                                  (B)
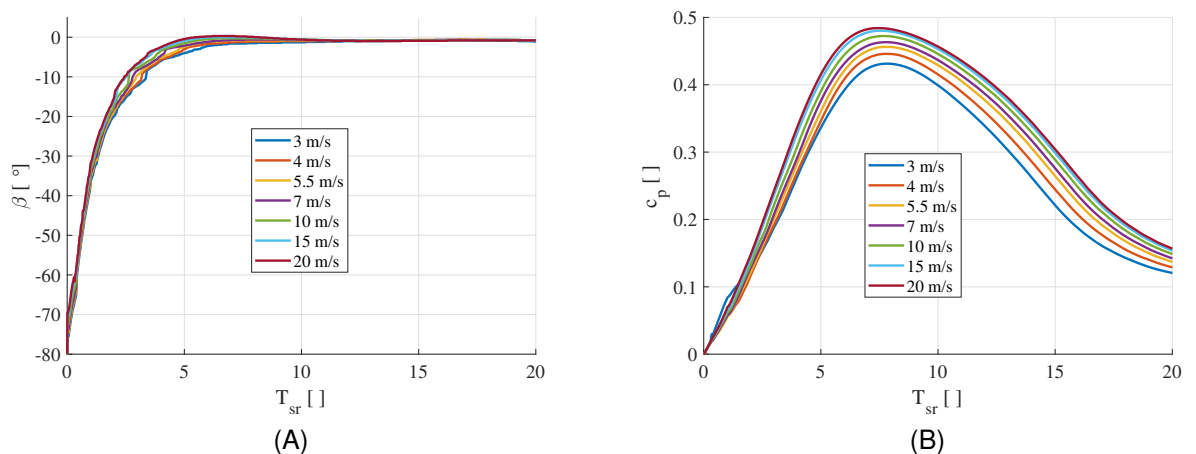
**Source: Self-Authorship**

The results of the best $\beta$ for each $V_\infty$ presented similar behaviour. However, due to better flow the $\frac{C_L}{C_D}$ are higher, increasing the efficiency. The wind turbine is more efficient. In addition, Yang et al (2016) argued the result of good optimization must be

with a limited range in the neighborhood of the desire $T_{SR}$, as presented in Fig. 9. Thus, showing a good optimization. For the remaining dynamic analyzes, to simplify the dynamics the average of Fig. 9 will be used and it was presented in Fig. 10.

**Graph 10 – Average of best, where A is the average of the best $\beta$ angle and B is the best $c_P$ for each $T_{SR}$**



(A)                                         (B)
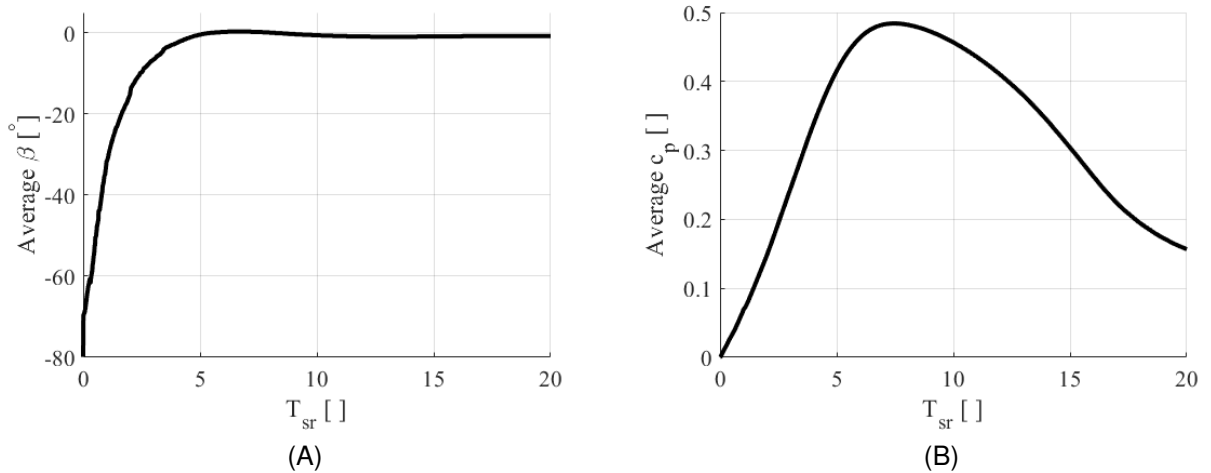
**Source: Self-Authorship**

After using the averaging $c_P$ with wind probability, and frequency. It was calculated the available power and energy, to this site the results are in Graph 11.

**Graph 11 – Using optimized turbine, in A the Power available and B the energy available**



(A)                                         (B)
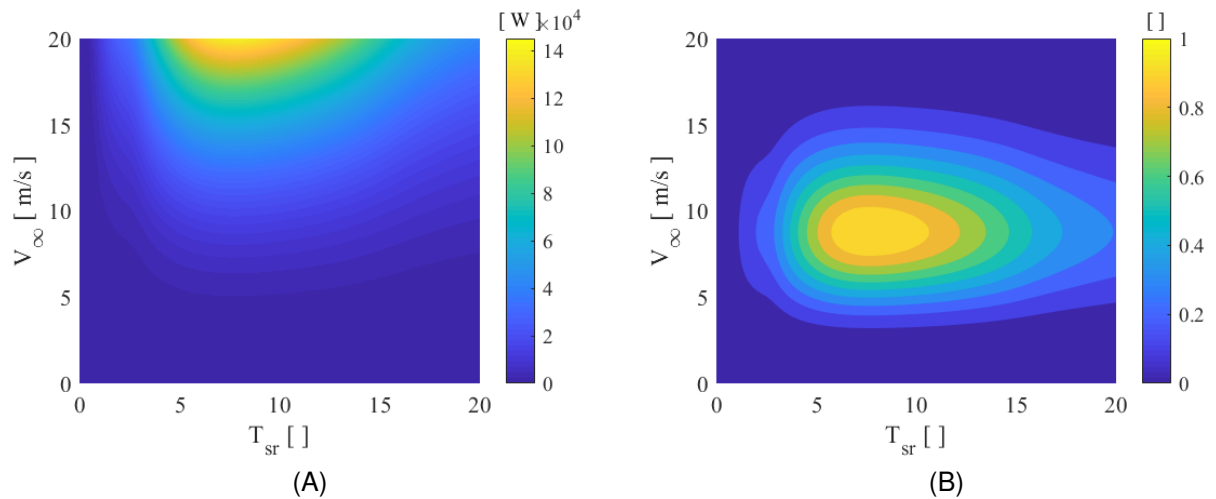
**Source: Self-Authorship**

Analyzing Graph 10, it is clear that bulk of the energy is in the region of $V_\infty = 9 \ [m/s]$ and $T_{SR} = 8$.

## 4.2   CONTROL RESULTS

Frist, the control rule on Eq. 29 was adopted with the help of the result on Graph 11. Following the Eq. 29, it is possible to built a database of $c_P$.

**Graph 12 – $c_{pf}$ angle limited to power,in (A) the surface and (B) is the contour**



(A)                                           (B)
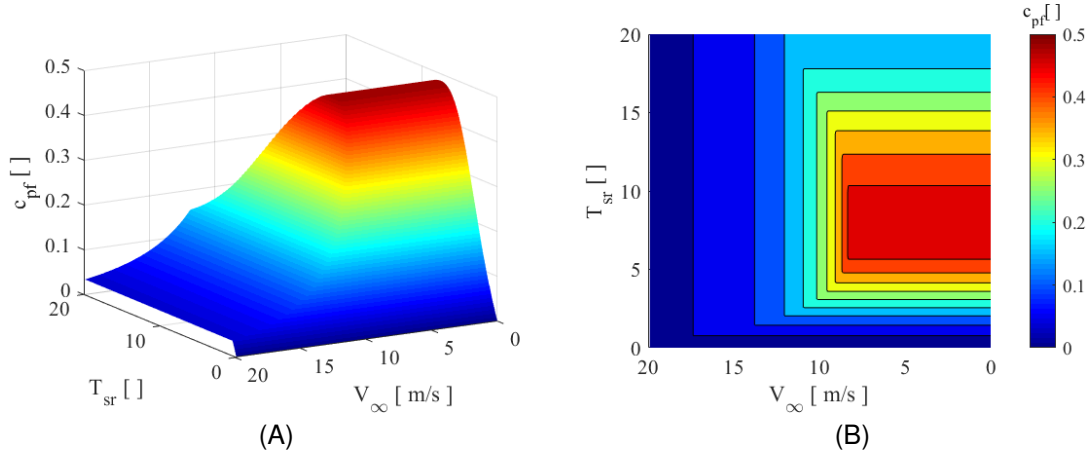
**Source: Self-Authorship**

Converting the $c_P$ to $\beta$, it is obtain Graph 13.

**Graph 13 – $\beta_f$ angle limited to power,in (A) the surface and (B) is the contour**



(A)                                           (B)
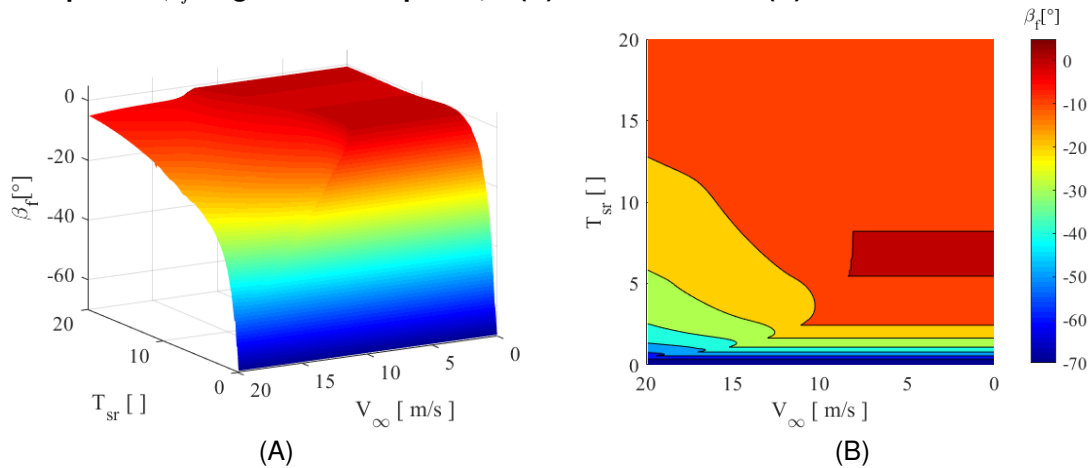
**Source: Self-Authorship**

As expected on Graph 13, before the power threshold the angle remains at the optimum. After that the angle is reduced to an inefficient level to extract the maximum allowed by the generator. The results of the rules obtained after the training is shown on Graph 14.

**Graph 14 – Input rules for fuzzy control,in (A) for the $T_{sr}$ and (B) is for $V_\infty$**



(A)



(B)
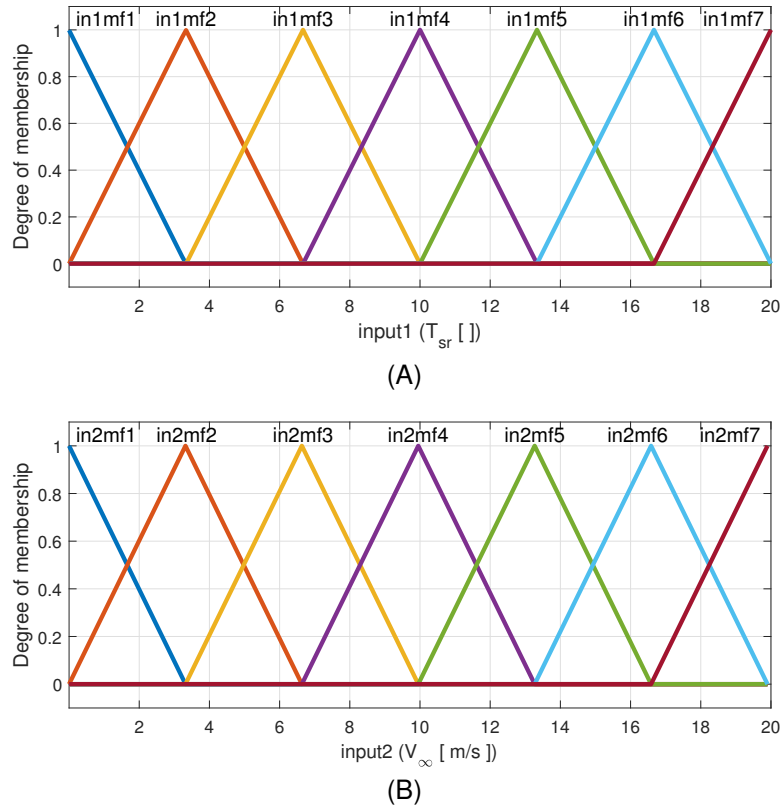
**Source: Self-Authorship**

Table 7 shows the relationship between the inputs and the coefficient on Table 8.

**Table 7 – Relationship for the input rules and the coefficients**

| Input 1 $T_{sr}$ | Input 2 $V_\infty$ MF1 | Input 2 $V_\infty$ MF2 | Input 2 $V_\infty$ MF3 | Input 2 $V_\infty$ MF4 | Input 2 $V_\infty$ MF5 | Input 2 $V_\infty$ MF6 | Input 2 $V_\infty$ MF7 |
|---|---|---|---|---|---|---|---|
| MF1 | | | | | | | |
| MF2 | MF8 | MF9 | MF10 | MF11 | MF12 | MF13 | MF14 |
| MF3 | MF15 | MF16 | MF17 | MF18 | MF19 | MF20 | MF21 |
| MF4 | MF22 | MF23 | MF24 | MF25 | MF26 | MF27 | MF28 |
| MF5 | MF29 | MF30 | MF31 | MF32 | MF33 | MF34 | MF35 |
| MF6 | MF36 | MF37 | MF38 | MF39 | MF40 | MF41 | MF42 |
| MF7 | MF43 | MF44 | MF45 | MF46 | MF47 | MF48 | MF49 |

**Source: Self-Authorship**

Thus, each parameters was obtained by the training are presented on Tab. 8.

**Table 8 – Value of variables to the fuzzy controller**

| MF | $b_1$ | $b_2$ | $b_3$ | MF | $b_1$ | $b_2$ | $b_3$ |
|---|---|---|---|---|---|---|---|
| MF1 | 209.5421 | -11.8275 | -71.3524 | MF26 | 360.7708 | -215.6002 | -754.2534 |
| MF2 | 210.9077 | -11.7962 | -32.5122 | MF27 | 204.5275 | -215.7973 | 1522.8474 |
| MF3 | 246.5002 | -11.6292 | 6.3580 | MF28 | 124.3731 | -215.7315 | 3035.9750 |
| MF4 | 131.7435 | -10.4485 | 31.8517 | MF29 | 182.8899 | -127.9472 | -2439.4192 |
| MF5 | 392.5962 | -11.8927 | 85.8663 | MF30 | 184.2302 | -127.9879 | -2032.8042 |
| MF6 | 224.1827 | -12.3879 | 137.7985 | MF31 | 219.8116 | -128.1504 | -2081.8127 |
| MF7 | 140.5114 | -12.5309 | 180.9589 | MF32 | 105.7098 | -129.3643 | -124.8053 |
| MF8 | 185.7659 | 2.1595 | -624.6992 | MF33 | 360.7561 | -129.4366 | -3097.7329 |
| MF9 | 186.7650 | 2.0962 | -635.0041 | MF34 | 204.6186 | -129.0912 | -595.1393 |
| MF10 | 223.1672 | 1.7675 | -761.3604 | MF35 | 124.0818 | -129.1142 | 905.6686 |
| MF11 | 105.5388 | -0.5600 | -354.3971 | MF36 | 182.9245 | -168.0603 | -3049.3832 |
| MF12 | 363.7759 | 1.0055 | -1244.3634 | MF37 | 184.2699 | -168.0751 | -2514.3604 |
| MF13 | 206.2198 | 1.1327 | -727.9533 | MF38 | 219.8516 | -168.0885 | -2549.8146 |
| MF14 | 126.1277 | 1.3344 | -473.7770 | MF39 | 105.6490 | -167.9909 | -89.8300 |
| MF15 | 182.8298 | -236.8756 | -1218.4627 | MF40 | 360.7780 | -168.0723 | -3787.0037 |
| MF16 | 184.1390 | -236.8376 | -441.4987 | MF41 | 204.5253 | -167.5107 | -636.1563 |
| MF17 | 219.7026 | -236.5516 | 104.9654 | MF42 | 123.8475 | -167.5549 | 1263.6894 |
| MF18 | 105.6862 | -239.3749 | 1669.5282 | MF43 | 182.9329 | -242.0681 | -3659.2211 |
| MF19 | 360.9084 | -240.2945 | 771.7242 | MF44 | 184.2677 | -242.0953 | -2882.9779 |
| MF20 | 204.7426 | -240.3754 | 2607.0711 | MF45 | 219.8902 | -242.1444 | -2792.1300 |
| MF21 | 124.4230 | -240.4031 | 3935.3071 | MF46 | 105.5320 | -242.3030 | 299.4925 |
| MF22 | 182.7427 | -214.0856 | -1827.8288 | MF47 | 360.7347 | -244.0768 | -3980.2208 |
| MF23 | 184.0712 | -214.0816 | -1131.0858 | MF48 | 204.4709 | -244.1344 | -44.7182 |
| MF24 | 219.6532 | -213.9801 | -777.3067 | MF49 | 123.6558 | -244.2840 | 2383.1995 |
| MF25 | 105.7150 | -215.1136 | 1078.7766 | | | | |

**Source: Self-Authorship**

This set up has a fitness $R^2$ of 0.9961, with the desired dataset of $\beta_f$. Analyzing the error of the desire $\beta_f$ and the fuzzy-controller, it is possible to obtain Fig. 15.

**Graph 15 – Error of the desired and the fuzzy , in (A) the surface and (B) is the contour**



(A)                    (B)
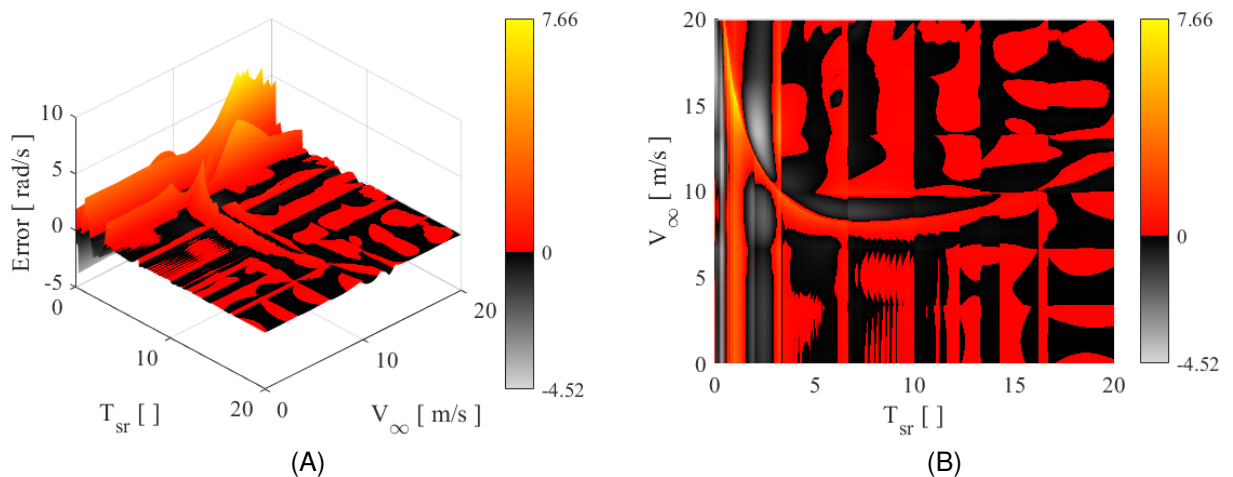
**Source: Self-Authorship**

Where the negative error in black to white means a higher angle than the optimum and could means an increase rotation speed and extracted power. Thus, burning

the generator. On the other hand, red to yellow a positive error means a smaller angle than the required an it is energy without being extracted or wasted.

## 4.2.1  Results of Applied Control

Analyzing the dynamics through the Eq. 22, it is possible to obtain the $\Omega_{max}$ to different time samples. The selected samples were 5, 10, 50 and 250 to illustrate and analyze the break of inertia, and the reduction of power extracted after the $10^4$ was reached to $V_\infty$ to case 1.

**Graph 16 – Maximum rotation for different time samples to case 1 (A) to t=5s, (B) to t=10s, (C) to t=50s, (D) to t=250s**
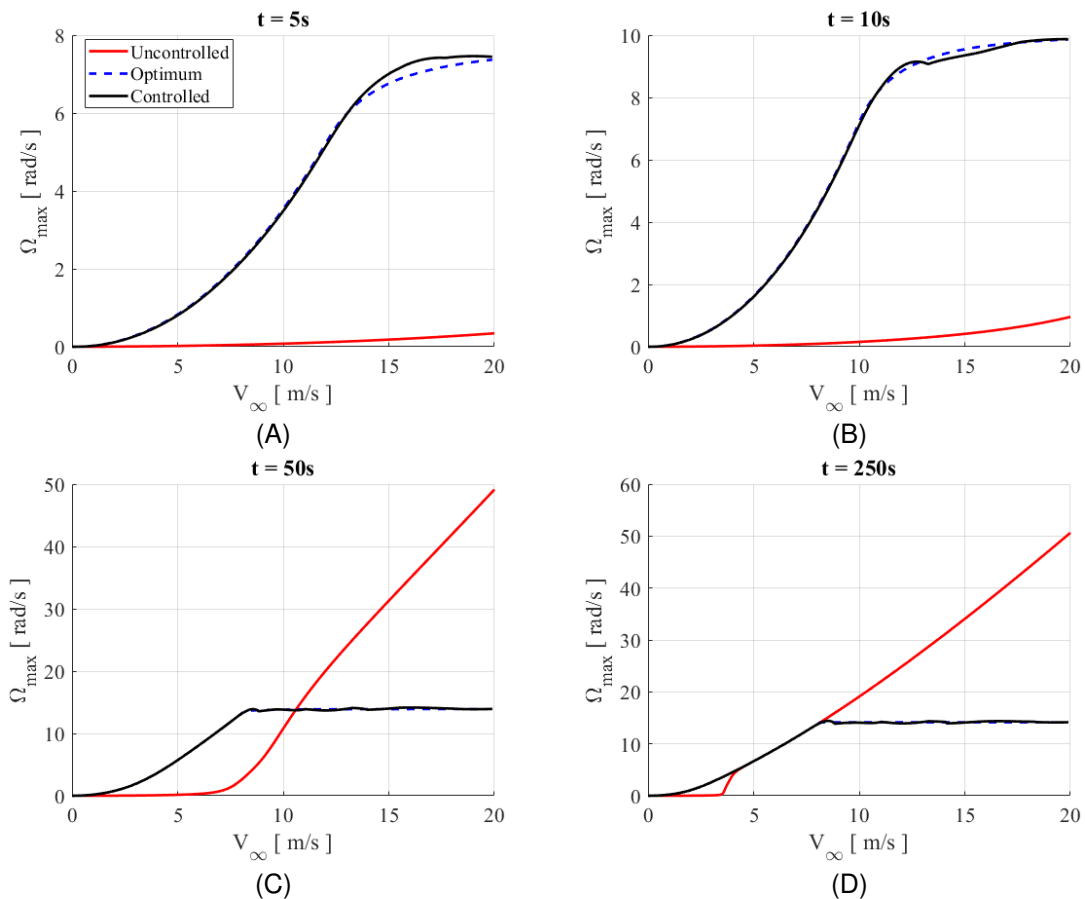


**Source: Self-Authorship**

As expected, the controlled turbine had a higher rotation speed in the beginning. Thus, breaking the inertia quicker than the uncontrolled turbine. Comparing Graph 16 (D) with Graph 2, it is possible to see the similar behavior and the limitation of the rotation. The constant rotation speed in only achieve because the extracted power grows exponential, thus it is possible to stabilizes the rotation due to excess of

power, on red the uncontrolled turbine, shows the exponential grow of extracted power. Transforming the rotation in power extracted, as shown on Graph 17

**Graph 17 – Maximum power for different time samples to case 1 (A) to t=5s,(B) to t=10s,(C) to t=50s,(D) to t=250s**



(A)

(B)

(C)

(D)
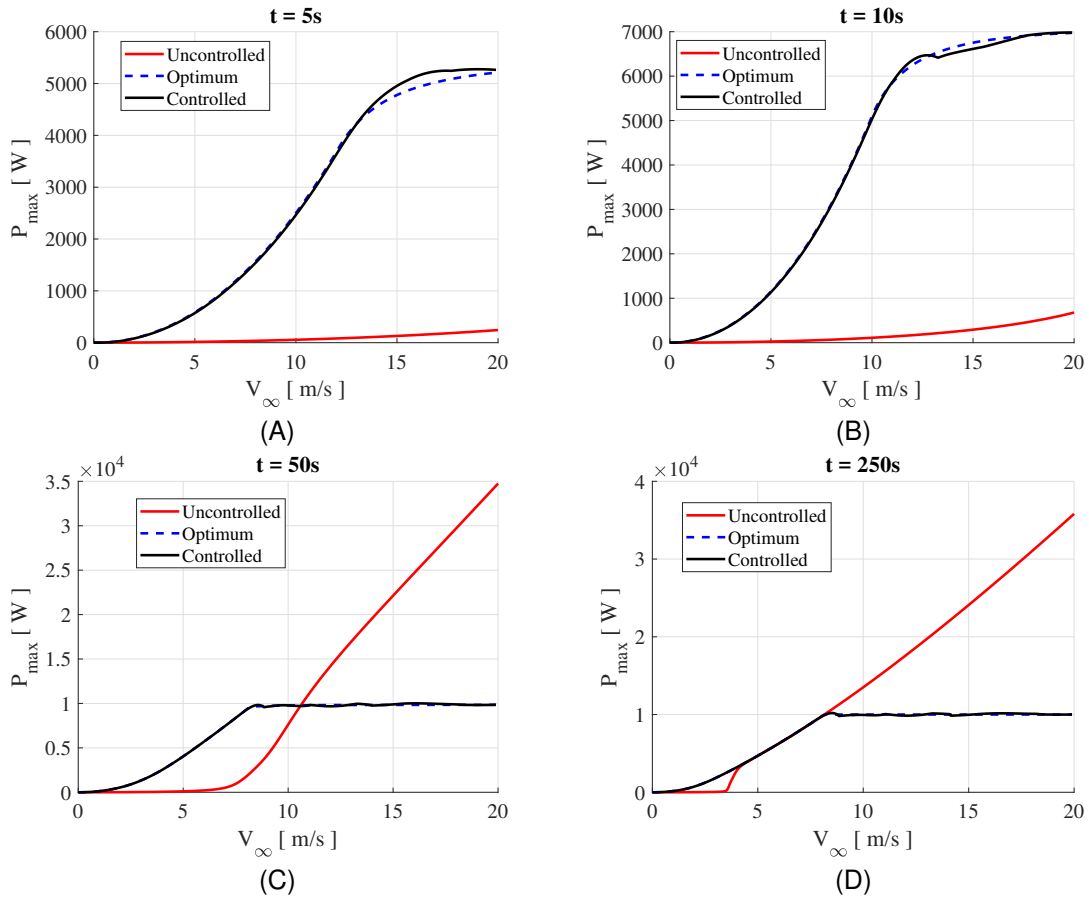
**Source: Self-Authorship**

As expected, the power extracted stabilized after 10 $[m/s]$ , avoiding burning the generator. The same analysis was made in case 2, Graph 18, instead the Rms of rotation was used due to the oscillation behaviour.

**Graph 18 – Rms Ω to different time samples to case 2 (A) for t = 5s,(B) to t = 10s,(C) to t = 50s,(D) to t = 250s**
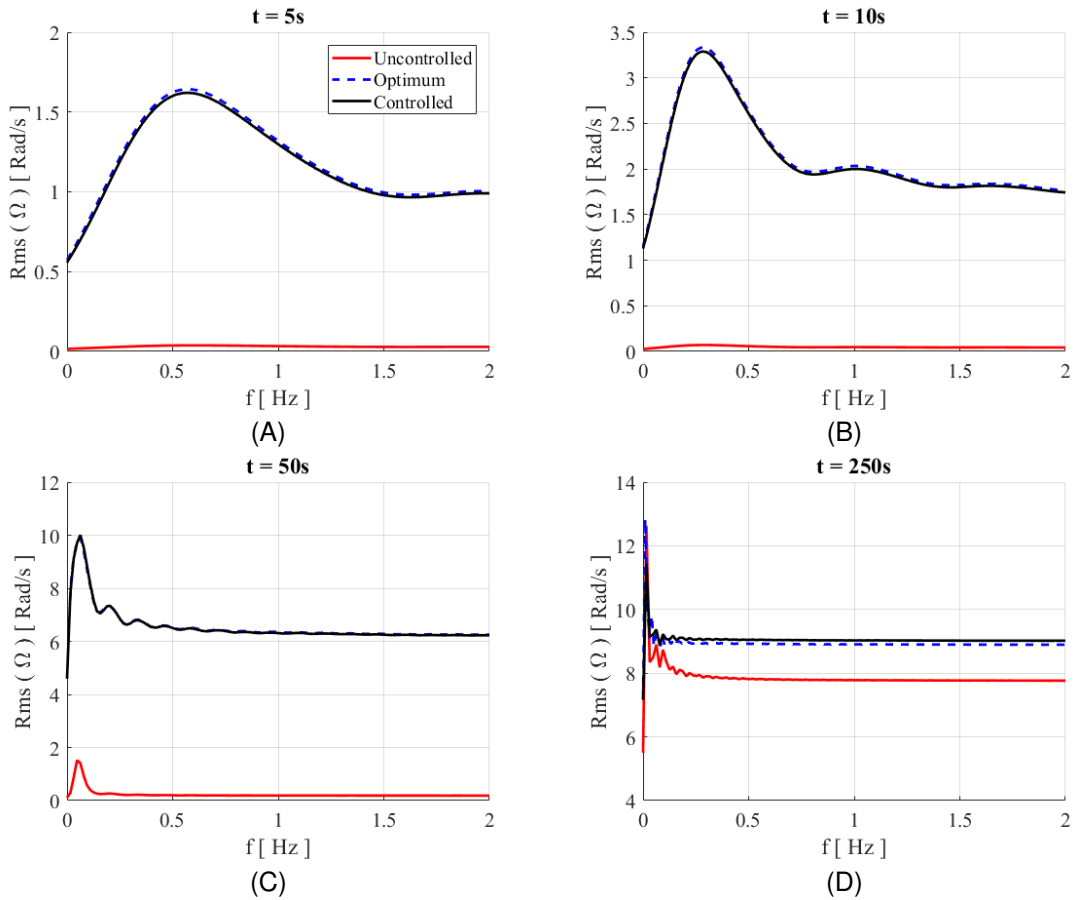


**Source: Self-authorship**

The same behavior on case 1, where the controlled turbine presented a better performance, breaking the inertia and achieving higher rotation speeds during the time simulated. Graph 18 (A), (B) and (C) show lower rotation speeds, until break the inertia in (D).

**Graph 19 – Rms Ω for different time sample to case 3 (A) to t = 5s,(B) to t = 10s,(C) to t = 50s,(D) to t = 250s**



(A)

(B)

(C)

(D)
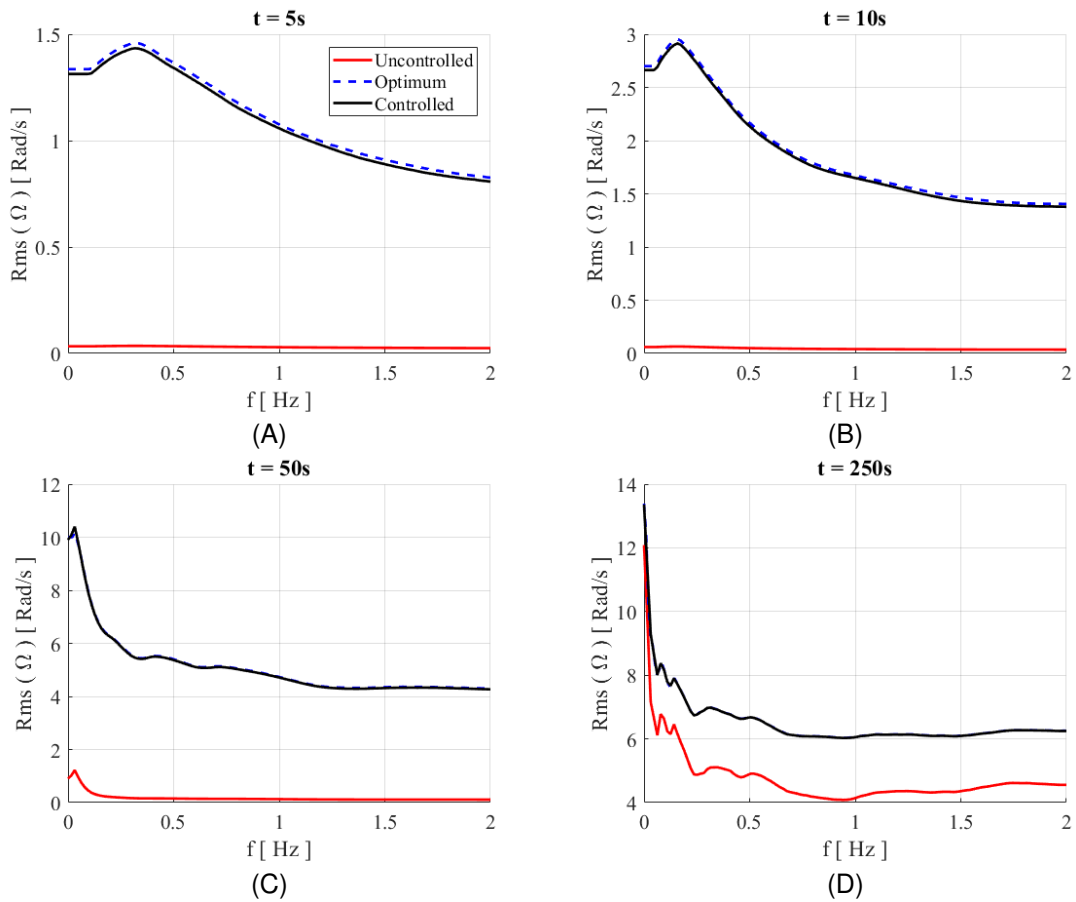
**Source: Self-authorship**

The same behavior was observed on case 1 and 2, where the controlled turbine presented a better performance, breaking the inertial and maintaining higher rotation speeds during the simulated time.

### 4.2.2 Error of Control

To evaluate the performance of the neuro-fuzzy controller, the same simulation was made with the dataset. Thus, the dynamic error can be evaluated on Graph 20 .

**Graph 20 – Error between the Optimum and the fuzzy control for case 1: (A) in absolute [rad/s] ,(B) in relative [%]**



(A)



(B)
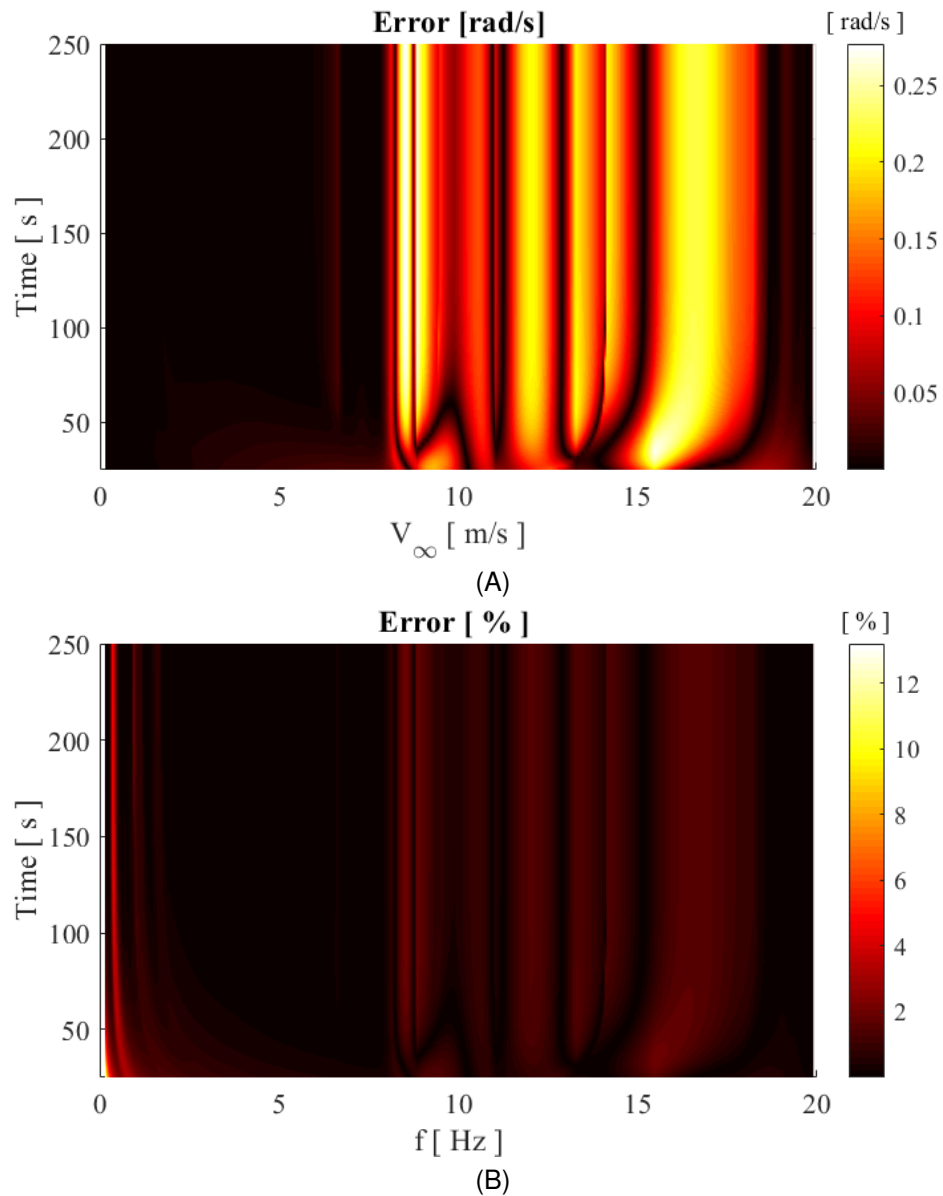
**Source: Self-authorship**

The standard deviation was analyzed to each error in time series, to evaluate the fluctuation on the error, the results are presented in Graph 21 .

**Graph 21 – Standard deviation for case 1**
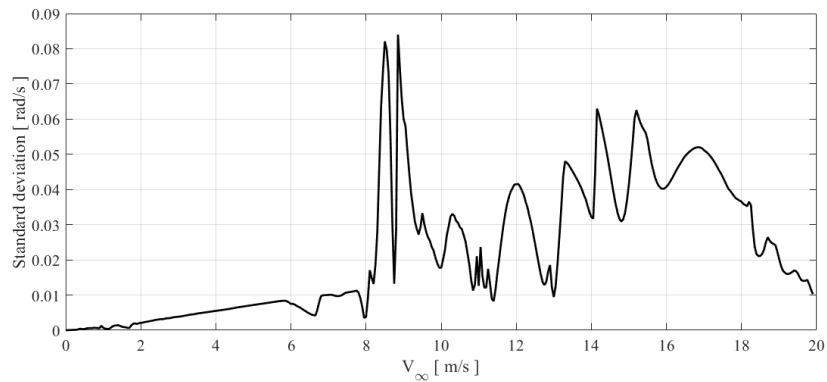
As presented on Graph 21 , Graph 20 the absolute error was 0.32 [rad/s] and the only relative error was high at very lower rotation due to the magnitude of the measurement. Thus, the controller was efficient in all wind speed simulated. The same analyses was made for case 2, presented on Graph 22, Graph 23.

**Graph 22 – Error between the optimum and the fuzzy control for case 2: (A) in absolute [rad/s] ,(B) in relative [%]**



(A)



(B)

**Source: Self-authorship**

The standard deviation was analyzed for each error in time series, to evaluate the fluctuation on the error, the result is presented on Graph 23.

**Graph 23 – Standard deviation for case 2**

The results on Graph 22, Fig. 23, shows a higher error at lower frequency, and a constant standard deviation. Thus, the controller remain efficient at the ranged simulated. Regardless of the high wind speeds at lower frequencies, or the lower part of the sine wave. Applying the same methodology for the case 3.

**Graph 24 – Error between the optimum and the fuzzy control for case 3: (A) in absolute [rad/s] ,(B) in relative [%]**
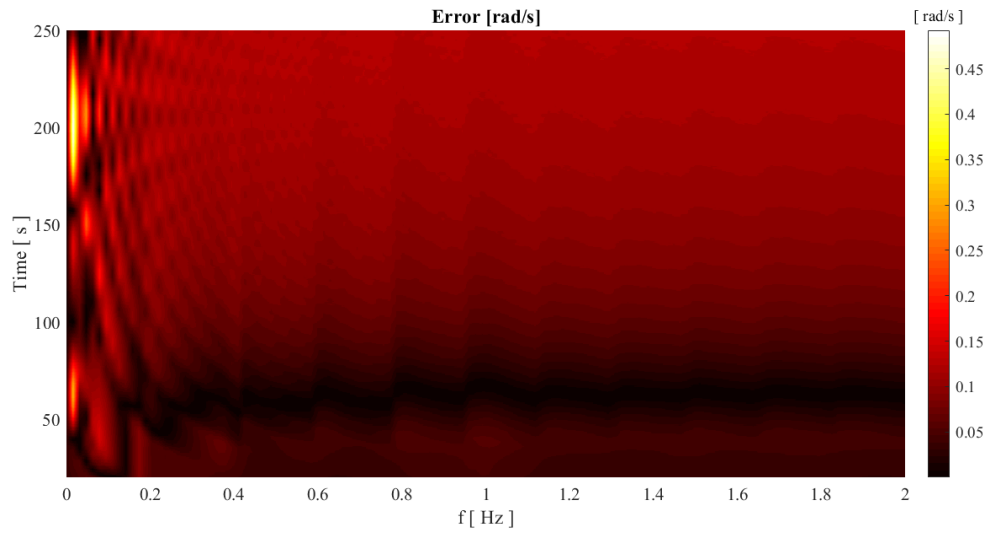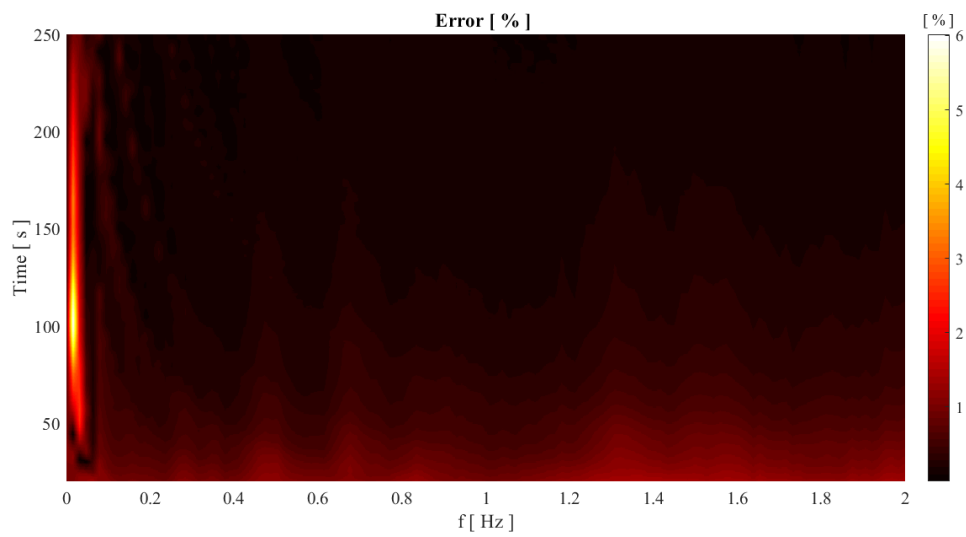


(A)



(B)

**Source: Self-authorship**

The standard deviation was analyzed for each error in time series, to evaluate the fluctuation on the error, the result are presented on Graph 25 .
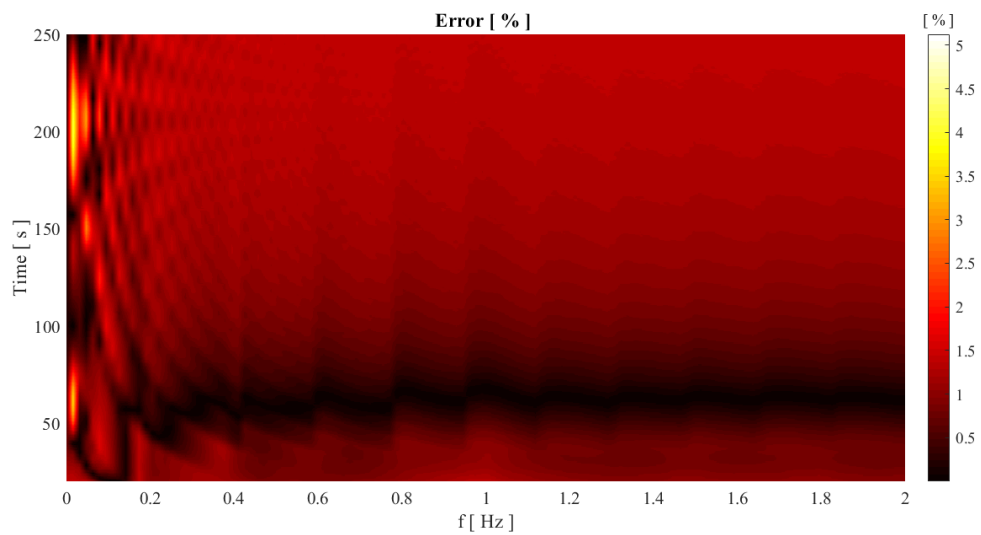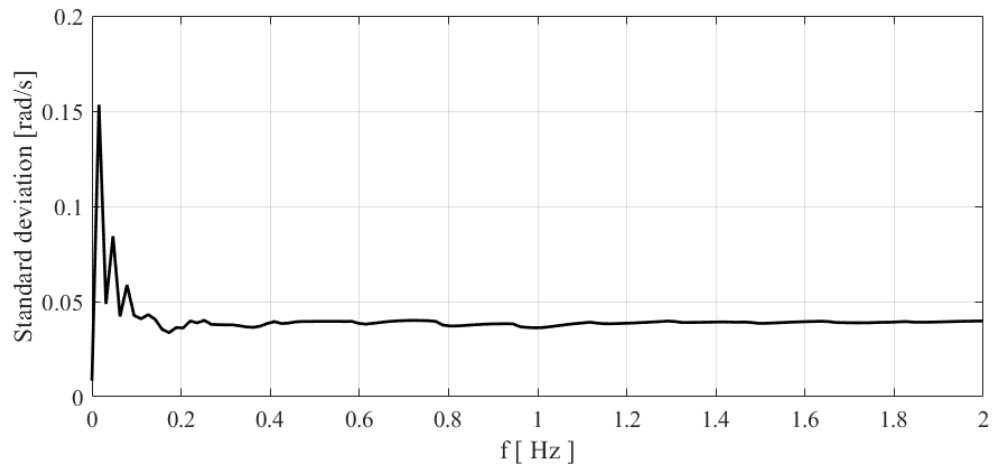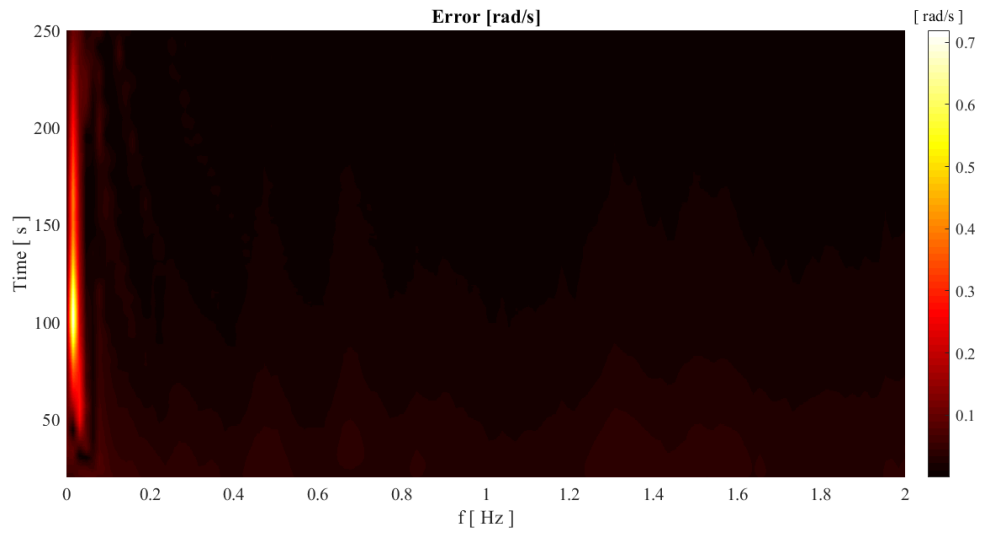
**Graph 25 – Standard deviation for case 3**
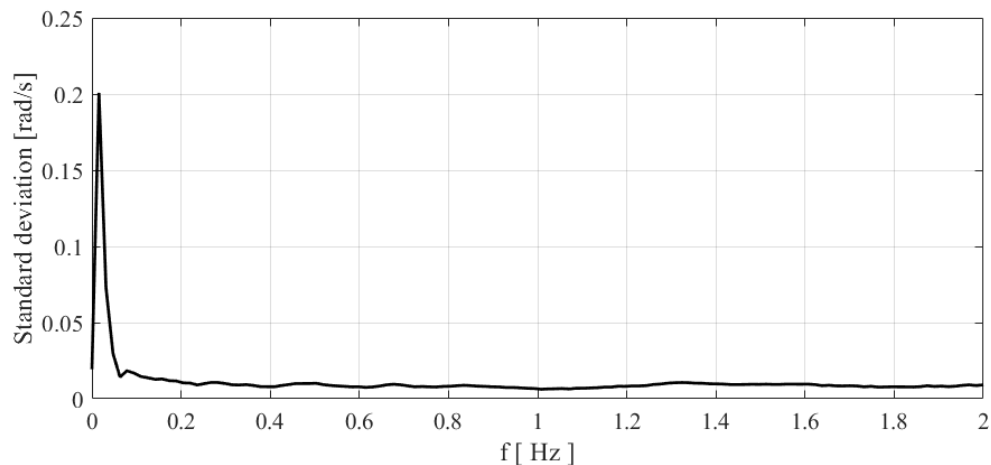
The results on Graph 24, Graph 25, shows a higher error at lower frequency, and a constant standard deviation. It was applied the same methodology for the case 3.Thus, the controller remain stable and efficient at a vast range of constant wind speed and at a vast range of frequencies. Comparing the max rotation over time on Graph 26.

**Graph 26 – Comparison between the fuzzy controlled and uncontrolled for case 1: (A) The max $\Omega$ for controlled [rad/s] ,(B) The max $\Omega$ for uncontrolled turbine[%]**



(A)                                         (B)
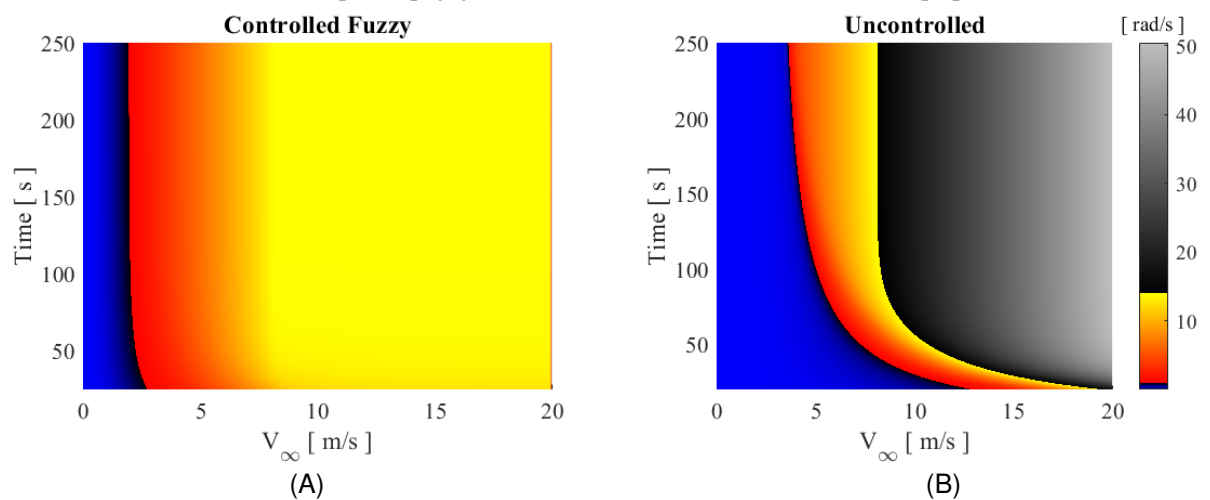
As shown on Graph 26, on blue is the region below $\Omega$ 1 rad/s, as an illustrating point for the efficiency of the wind turbine. Thus showing the bigger range of wind accelerate quicker than the uncontrolled. From red to yellow the range of the controlled turbine, and from black to white the rotation speed bigger than the required for the controlled wind turbine. Thus, showing that the uncontrolled turbine quicker burns the generator. Calculating the difference between the controlled and the uncontrolled turbine, Graph 5 shows this difference.

**Graph 27 – Difference between the fuzzy controlled and uncontrolled for case 1: (A) in absolute [rad/s] ,(B) in relative [rad/s]**



(A)



(B)
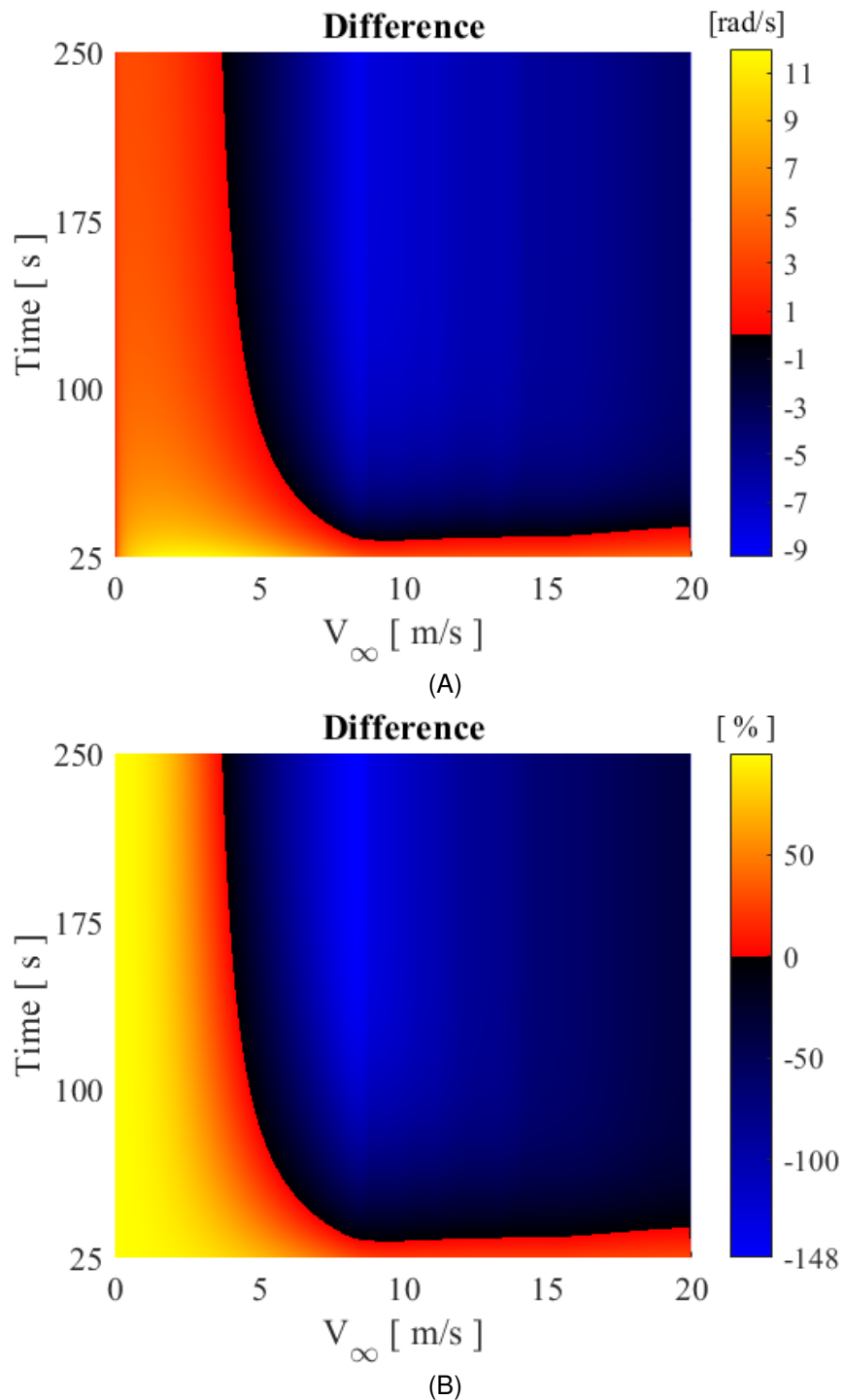
As shown on Graph 5 the controller increasing the rotation. However, as the time and the $V_\infty$ increase, the controller starts to throttle the rotation and the energy to not overpower the generator. The same methodology was used on case 2 and case 3.

**Graph 28 – Difference between the fuzzy controlled and uncontrolled for case 2: (A) in absolute [rad/s] ,(B) in relative [%]**



(A)



(B)
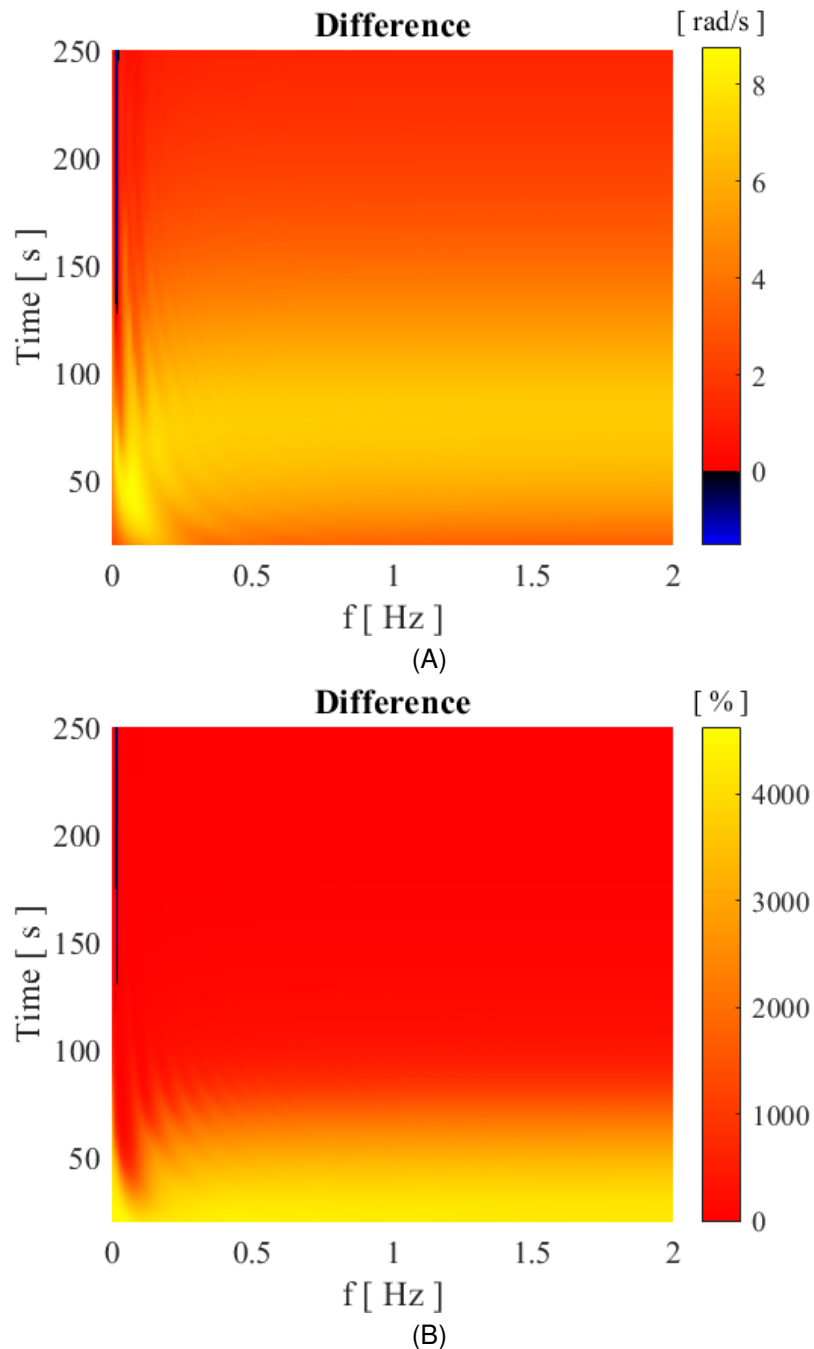
As shown in Graph 28, at lower frequencies, the simulation has the positive part of the sine wave, thus breaking the inertia quickly. However, when the frequency increases there is no notable change. Despite of the relative difference increase, the absolute difference remains the same, around 2 [rad/s]. Only to lower frequencies, the uncontrolled turbine is faster, this means that the controller reduces the extracted power. For case 3 the results are presented on Graph 29.

**Graph 29 – Difference between the fuzzy controlled and uncontrolled for case 3:(A) in absolute [rad/s] ,(B) in relative [%]**



(A)



(B)
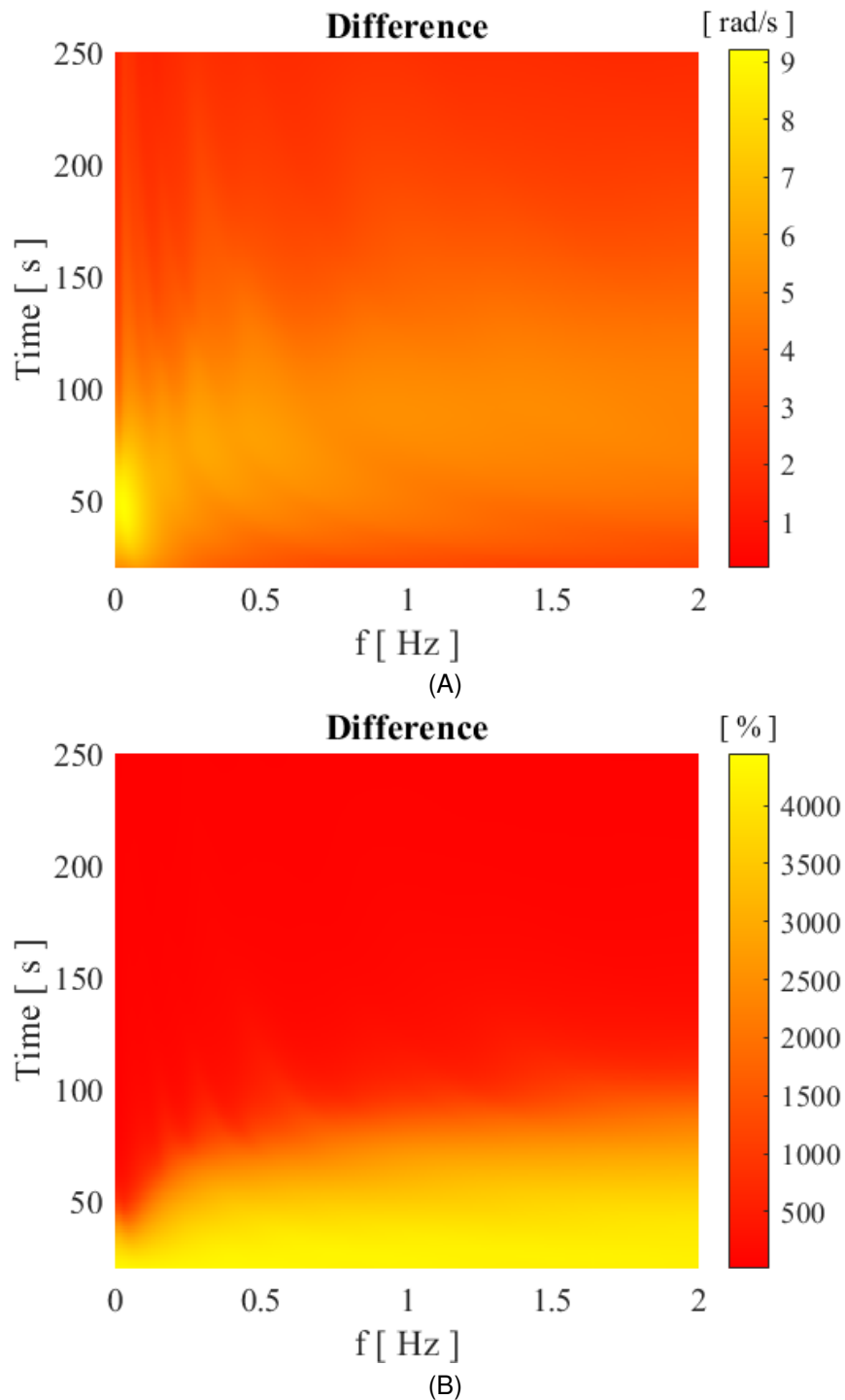
**Source: Self-authorship**

As shown in Graph 28, and Graph 29, the relative difference is high. Nevertheless, the absolute difference is low. Showing the uncontrolled wind turbine requires longer amount of time to break the inertia compared to the neuro fuzzy. The important contrast is expressed on the Tab. 5.

**Table 9 – Summary of main results**

| | Error [$rad/s$] | | Error [%] | | Difference [$rad/s$] | | Difference [%] | |
|---|---|---|---|---|---|---|---|---|
| | Max | Min | Max | Min | Max | Min | Max | Min |
| Case 1 | 0.27 | 3.68E-09 | 13.20 | 2.83E-08 | 11.99 | -9.31 | 100 | -148.13 |
| Case 2 | 0.49 | 1.73E-05 | 5.12 | 2.42E-04 | 8.77 | -1.51 | 4.63E+03 | -11.06 |
| Case 3 | 0.71 | 2.34E-05 | 6.01 | 2.57E-04 | 9.22 | 0.20 | 4.45E+03 | 10.53 |

**Source: Self-Authorship**

As shown on Tab. 5, and on Graph 16 to Graph 29, the error between the desired rotation from the table and neuro fuzzy was low to a steady wind speed $0.27[rad/s]$, and the difference between show at the maximum it was $11.99[rad/s]$ and minimum it was $-9.31[rad/s]$. Thus, increasing the power generation in $11.99[rad/s]$ and avoiding the burn generator in $9.31[rad/s]$.

The same analyses can be done for case 2 and case 3, where the wind speed is not steady. The max deviation from the desired was $0.71[rad/s]$. Comparing the controlled with the uncontrolled it shows that it improves in $9.22[rad/s]$ and reduce the rotation in cases of over speed with $1.51[rad/s]$.

# 5 CONCLUSION AND REMARKS

Comparing with CFD softwares, the Xfoil software was a good choice, because it can quickly build tables of $C_L$ and $C_D$. Despite the last update has been from 2000. Because it runs on C, it can resolve the lift and drag coefficient to a 2D shape quicker than other solutions from CFD. Despite of the lower bound of 100k on $R_E$. Nevertheless, lift and drag coefficient from wind tunnel can be used on a further work to compare the results.

The Buhl's methodology was efficient in representing the HAWT dynamics. Despite being a complex and recursive method that increases the time with the condition on the $a$ variable. The use of function for chord and for $\theta_p$ made the optimization easy code, with consistent results.

The PSO optimization demonstrated to be a good tool. The selection of airfoil shows similar performance to all airfoils. Thus, it shows that the method extracted the most of each profile. However, the optimization function did not take into account the noise generation and mitigation option on the optimization process. This requirement is important from the stakeholders. Other equations could be proposed to $\theta_p$ and $c$, or instead of a function a selection of points could be used with the interpolation function.

The comparison between various $V_\infty$ on the $c_p$ analyses showed that due to higher Re number the $c_p$ becomes a function of the $V_\infty$. This fact is due to better flow over the profile, increasing the $\frac{C_L}{C_D}$. Thus, proving that the model of Luo, Vidal and Acho (2014) is a simplified model, that could be a good starting point for electrical generator design.

The neuro fuzzy control showed to be a very stable and reliable option of controlling given restrictions imposed. Because it was not possible to establish a linear or non linear plant. The modeled did not fit on the (LUO; VIDAL; ACHO, 2014) with sufficient correlation coefficient. In addition the use of PID needed to be tuned and the power processing time to be increased significantly.

The result of the controller showed a good potential to avoid overpower and reduce the time required to break the inertia. The protection from low speed to avoid unnecessary wear and tear could be accomplished by a timer comparing the average wind speed. The neuro fuzzy tool allows to train the controller and even further manual

tuning if necessary. This tool made the construction of the rules easy by supplying the data set after the rules of control being defined.

Averaging the $c_p$ was the solution to overcome using a neuro network to the $c_p$ to study the dynamics. Otherwise, the require processing power will increase significantly. The 3 selected wind profiles mimicked the environment and yielded good results. It showed that the controlled prevails over the uncontrolled turbine. It breaks the inertial quicker and maintain the rotation over different conditions. In addition, the selection of this wind profile showed that the optimization was good. Because, after a long time the uncontrolled turbine has a similar efficiency. However, it also extracted more power than the generator could cope. This is backed up by the results presented in shown on Tab. 5, and on Graph 16 to Graph 29.

Comparing the results with the Menezes, Araújo and Silva (2018), the neuro fuzzy was better than the optimal torque control, because it can maps the non-linear behavior due to increase of speed that increase the efficiency. It also perfomer better than Ashrafi, Ghaderi and Sedaghat (2015) that uses the instantaneous average of optimum angles does not protect the generator. Nevertheless, this method is a good starting point for passive controller such as springs. Because it can directly relate the rotation with the angle (stiffness of torsional spring).

However, this Master's thesis did not analyzed the control and electrical integration that any modern wind turbine and generator already have integrated. When it is compared with modern control that takes in account each blade position with aeroelastic analyses the neurofuzzy presented in this Master's thesis was inferior. Nevertheless, this methodology could also be implemented if the number of input variables does not increase significantly. Comparing the results with Jonkman (2007), both controller work to break the inertia quickly, and avoid the burning of the generator at speed higher than $15[m/s]$ by changing the pitch. However, Jonkman (2007) considers the influence of ocean wave in changes on the pitch. Despite of being a more robust controller the mathematical model was based on the Classical Glauret's model, based on FAST ™.

From the environmental point of view, the addition of neuro fuzzy controller imposes better performance for the same resources. As shown on Graph and Tab. , for the same parameters on wind the controlled wind turbine quickly accelerate to start production and avoid burning the generator, as it can be seen from black to white region. Thus, avoid unnecessary maintenance stops to replace. Additionally, the gen-

erator could be designed for $10^4[W]$, instead of over sizing the generator to take into account the excess of generation, and wasting resources.

## 5.1   FUTURE RESEARCH

The following items can be explored as future research

- Similiar generalized model proposed by: Luo, Vidal and Acho (2014) to facilitated the control.

- Coupling the generator equations and investigated the dynamic using the generator with a controller to stabilized the electrical signal;

- Replace the rigid structure with a flexible structure to avoid flutter;

- To investigate the influence of sharklets, wing fences and raked wingtip on the efficiency, and mathematical modeling;

- To analyze the possible use of spring as passive actuator;

- To add the noise characteristic to the optimization process and optimization function;

- To further research using other CFD tools to generate the $C_l$ and $C_d$ tables such as OpenFOAM®;

- To analyze the Darrieus (VAWT) with the same Buhl's Methodology;

- To design and analyze of the Helix turbine similar to A400;

# BIBLIOGRAPHY

ADACHI, D. et al. Search for common minima in joint optimization of multiple cost functions. **Computer Physics Communications**, Elsevier BV, feb 2019.

AERONAUTICS, National; NASA, Space Administration. **NACA Airfoils**. 2018. Available from Internet: <https://www.nasa.gov/image-feature/langley/100/naca-airfoils>.

AGHBALOU, N. et al. A probabilistic assessment approach for wind turbine-site matching. **International Journal of Electrical Power & Energy Systems**, Elsevier BV, v. 103, p. 497–510, dec 2018.

ANDERSON, D. **Computational Fluid Mechanics and Heat Transfer (Series in Computational and Physical Processes in Mechanics and Thermal Sciences)**. [S.l.]: CRC Press, 2011.

ANEEL, Agência Nacional de Energia Elétrica. **Informações Gerenciais**. 2018. Available from Internet: <http://www.aneel.gov.br/informacoes-gerenciais>.

ANSARI, A. R.; NOVINZADEH, A. R. B. Designing a control system for an airplane wing flutter employing gas actuators. **International Journal of Aerospace Engineering**, Hindawi Limited, v. 2017, p. 1–9, 2017.

ASHRAFI, Z. N.; GHADERI, M.; SEDAGHAT, A. Parametric study on off-design aerodynamic performance of a horizontal axis wind turbine blade and proposed pitch control. **Energy Conversion and Management**, Elsevier BV, v. 93, p. 349–356, mar 2015.

ASSOCIATION, New Zealand Wind Energy. **TARARUA WIND FARM**. 2018. Available from Internet: <http://www.windenergy.org.nz/tararua-wind-farm>.

ÅSTRöM, K.J.; HäGGLUND, T. The future of PID control. **Control Engineering Practice**, Elsevier BV, v. 9, n. 11, p. 1163–1175, nov 2001.

AUER, B. R. How does Germany's green energy policy affect electricity market volatility? An application of conditional autoregressive range models. **Energy Policy**, v. 98, p. 621–628, 2016.

BAI, C.J.; WANG, W.C. Review of computational and experimental approaches to analysis of aerodynamic performance in horizontal-axis wind turbines (HAWTs). **Renewable and Sustainable Energy Reviews**, Elsevier BV, v. 63, p. 506–519, sep 2016.

BAKIRCI, M.; YILMAZ, S. Theoretical and computational investigations of the optimal tip-speed ratio of horizontal-axis wind turbines. **Engineering Science and Technology, an International Journal**, Elsevier BV, aug 2018.

BIANCHI, F. D.; MANTZ, R. J.; BATTISTA, H. **Wind Turbine Control Systems**. [S.l.]: Springer London, 2007.

BILIR, L. et al. An investigation on wind energy potential and small scale wind turbine performance at incek region – ankara, turkey. **Energy Conversion and Management**, Elsevier BV, v. 103, p. 910–923, oct 2015.

BUNDESVERBAND WINDENERGIE E.V. **Facts and figures**. 2018. Available from Internet: <https://www.wind-energie.de/themen/zahlen-und-fakten/>.

CHANG, B.; STARCHER, K. Evaluation of wind and solar energy investments in texas. **Renewable Energy**, Elsevier BV, v. 132, p. 1348–1359, mar 2019.

CHEHOURI, A. et al. Review of performance optimization techniques applied to wind turbines. **Applied Energy**, Elsevier BV, v. 142, p. 361–388, mar 2015.

CHEN, G.; PHAM, T.T. **Introduction to Fuzzy Sets, Fuzzy Logic, and Fuzzy Control Systems**. [S.l.]: CRC Press, 2000.

CHEN, G.Q.; WU, X.F. Energy overview for globalized world economy: Source, supply chain and sink. **Renewable and Sustainable Energy Reviews**, Elsevier BV, v. 69, p. 735–749, mar 2017.

CHMIELOWSKI, W. Z. **Fuzzy Control in Environmental Engineering**. [S.l.]: Springer International Publishing, 2016.

CLERC, M. **Particle Swarm Optimization**. [S.l.]: Wiley-ISTE, 2006.

COUNIHAN, J. Adiabatic atmospheric boundary layers: A review and analysis of data from the period 1880â€"1972. **Atmospheric Environment (1967)**, v. 9, n. 10, p. 871 – 905, 1975. ISSN 0004-6981.

CRAFT, T.J. et al. A computational study of the near-field generation and decay of wingtip vortices. **International Journal of Heat and Fluid Flow**, Elsevier BV, v. 27, n. 4, p. 684–695, aug 2006.

DESHMUKH, S. et al. Wind turbine noise and its mitigation techniques: A review. **Energy Procedia**, v. 160, p. 633 – 640, 2019. ISSN 1876-6102. 2nd International Conference on Energy and Power, ICEP2018, 13â€"15 December 2018, Sydney, Australia.

DIVEUX, T. et al. Horizontal axis wind turbine systems: optimization using genetic algorithms. **Wind Energy**, Wiley, v. 4, n. 4, p. 151–171, oct 2001.

DORIGO, M.; BIRATTARI, M. Swarm intelligence. **Scholarpedia**, Scholarpedia, v. 2, n. 9, p. 1462, 2007.

DRELA, M. Xfoil: An analysis and design system for low reynolds number airfoils. In: MUELLER, Thomas J. (Ed.). **Low Reynolds Number Aerodynamics**. Berlin, Heidelberg: Springer Berlin Heidelberg, 1989. p. 1–12.

DRöES, M. I.; KOSTER, H. R.A. Renewable energy and negative externalities: The effect of wind turbines on house prices. **Journal of Urban Economics**, Elsevier BV, v. 96, p. 121–141, nov 2016.

EBERHART, R. C.; SHI, Y.; KENNEDY, J. **Swarm Intelligence (The Morgan Kaufmann Series in Evolutionary Computation)**. [S.l.]: Morgan Kaufmann, 2001.

ELTAYEB, S. **Renewable Energy Potential in New Zealand -By The Numbers**. 2013. Dissertation (Master) — Massey University, New Zealand, 2013.

ENDO, M. **Wind Turbine Airfoil Optimization by Particle Swarm Method**. 2010. Thesis (Ph.D.), 2010.

ERIK, M.; PEDERSEN, H.; LABORATORIES, H. **Good Parameters for Particle Swarm Optimization By**. 2010.

FARHAN, A. et al. Numerical study of effect of winglet planform and airfoil on a horizontal axis wind turbine performance. **Renewable Energy**, Elsevier BV, aug 2018.

FREITAS, S.; SANTOS, T.; BRITO, M. C. Impact of large scale PV deployment in the sizing of urban distribution transformers. **Renewable Energy**, Elsevier BV, v. 119, p. 767–776, abr. 2018.

FUGLSANG, P.; BAK, C. Development of the risø wind turbine airfoils. **Wind Energy**, Wiley, v. 7, n. 2, p. 145–162, apr 2004.

GENERAL ELECTRIC. **HALIADE-X OFFSHORE WIND TURBINE PLATFORM**. 2018. Available from Internet: <https://www.ge.com/renewableenergy/wind-energy/turbines/haliade-x-offshore-turbine>.

GERHART, P. M. **Munson, Young and Okiishi's Fundamentals of Fluid Mechanics, Binder Ready Version**. [S.l.]: Wiley, 2016.

GHASEMIAN, M.; ASHRAFI, Z. Na.; SEDAGHAT, A. A review on computational fluid dynamic simulation techniques for darrieus vertical axis wind turbines. **Energy Conversion and Management**, Elsevier BV, v. 149, p. 87–100, oct 2017.

GLAUERT, H. **The Elements of Aerofoil and Airscrew Theory**. [S.l.]: Cambridge University Press, 1983.

GOLNARY, F.; MORADI, H. Dynamic modelling and design of various robust sliding mode controls for the wind turbine with estimation of wind speed. **Applied Mathematical Modelling**, Elsevier BV, v. 65, p. 566–585, jan 2019.

GOUPEE, A. J.; KIMBALL, R. W.; DAGHER, H. J. Experimental observations of active blade pitch and generator control influence on floating wind turbine response. **Renewable Energy**, Elsevier BV, v. 104, p. 9–19, apr 2017.

GRIFFIN, D. A. **NREL Advanced Research Turbine (ART) Aerodynamic Design of ART-2B Rotor Blades**. [S.l.], 2000. Available from Internet: <https://www.nrel.gov/docs/fy00osti/28473.pdf>.

HANSEN, M. O. L. **Aerodynamics of Wind Turbines: second edition**. 2. ed. [S.l.]: Earthscan, 2008.

HAYAT, K.r et al. Flutter performance of bend–twist coupled large-scale wind turbine blades. **Journal of Sound and Vibration**, Elsevier BV, v. 370, p. 149–162, may 2016.

HEIER, S. **Grid integration of wind energy**. Chichester, West Sussex, United Kingdom: John Wiley & Sons Inc, 2014.

HOLTON, J. R.; HAKIM, G. J. **An Introduction to Dynamic Meteorology, Volume 88 (International Geophysics)**. [S.l.]: Academic Press, 2012.

HSU, S. A.; MEINDL, Eric A.; GILHOUSEN, David B. Determining the power-law wind-profile exponent under near-neutral stability conditions at sea. **Journal of Applied Meteorology**, American Meteorological Society, v. 33, n. 6, p. 757–765, jun 1994.

HUI, I.; CAIN, B. E.; DABIRI, J. O. Public receptiveness of vertical axis wind turbines. **Energy Policy**, Elsevier BV, v. 112, p. 258–271, jan 2018.

JANG, J. R.; SUN, C. Neuro-fuzzy modeling and control. In: **PROCEEDINGS OF THE IEEE**. [S.l.: s.n.], 1995. p. 378–406.

JANG, J. R.; SUN, C.; MIZUTANI, E. **Neuro-Fuzzy and Soft Computing: A Computational Approach to Learning and Machine Intelligence**. [S.l.]: Pearson, 1997.

JANG, J.-S.R. ANFIS: adaptive-network-based fuzzy inference system. **IEEE Transactions on Systems, Man, and Cybernetics**, Institute of Electrical and Electronics Engineers (IEEE), v. 23, n. 3, p. 665–685, 1993.

JANG, J.-S.R.; SUN, C. Neuro-fuzzy modeling and control. **Proceedings of the IEEE**, Institute of Electrical and Electronics Engineers (IEEE), v. 83, n. 3, p. 378–406, mar 1995.

JANZEN, F. C. et al. Offshore energy harvesting of a marine floating pendulum platform model. **Latin American Journal of Solids and Structures**, FapUNIFESP (SciELO), v. 16, n. 1, feb 2019.

JENSEN, C. U. et al. The impact of on-shore and off-shore wind turbine farms on property prices. **Energy Policy**, Elsevier BV, v. 116, p. 50–59, may 2018.

JIANG, H. et al. Comparison of numerical methods and metaheuristic optimization algorithms for estimating parameters for wind energy potential assessment in low wind regions. **Renewable and Sustainable Energy Reviews**, Elsevier BV, v. 69, p. 1199–1217, mar 2017.

JONKMAN, J.M. **Dynamics Modeling and Loads Analysis of an Offshore Floating Wind Turbine**. [S.l.], 2007.

JONKMAN S. BUTTERFIELD, W. Musial J.; SCOT, G. **Definition of a 5-MW Reference Wind Turbine for Offshore System Development**. [S.l.], 2009.

JUNG, C.; SCHINDLER, D.; GRAU, L. Achieving germany's wind energy expansion target with an improved wind turbine siting approach. **Energy Conversion and Management**, Elsevier BV, v. 173, p. 383–398, oct 2018.

KARABOGA, D.; BASTURK, Bahriye. A powerful and efficient algorithm for numerical function optimization: artificial bee colony (abc) algorithm. **Journal of Global Optimization**, v. 39, n. 3, p. 459–471, Nov 2007. ISSN 1573-2916.

KARIMI, M. et al. Photovoltaic penetration issues and impacts in distribution network – a review. **Renewable and Sustainable Energy Reviews**, Elsevier BV, v. 53, p. 594–605, jan. 2016.

KAVEH, A. **Advances in Metaheuristic Algorithms for Optimal Design of Structures**. [S.l.]: Springer International Publishing, 2017.

KAVEH, A.; BAKHSHPOORI, T.; AFSHARI, E. An efficient hybrid particle swarm and swallow swarm optimization algorithm. **Computers & Structures**, Elsevier BV, v. 143, p. 40–59, sep 2014.

KENNEDY, J.; EBERHART, R. Particle swarm optimization. In: . [S.l.: s.n.], 1995. v. 4, p. 1942–1948 vol.4.

KIKUMOTO, H. et al. Observational study of power-law approximation of wind profiles within an urban boundary layer for various wind conditions. **Journal of Wind Engineering and Industrial Aerodynamics**, v. 164, p. 13 – 21, 2017. ISSN 0167-6105.

KOCAARSLAN, I.; ÇAM, E.; TIRYAKI, H. A fuzzy logic controller application for thermal power plants. **Energy Conversion and Management**, Elsevier BV, v. 47, n. 4, p. 442–458, mar 2006.

KOOTEN, G.C. van; VRIES, F.P. de. Carbon offsets. In: **Encyclopedia of Energy, Natural Resource, and Environmental Economics**. [S.l.]: Elsevier, 2013. p. 6–8.

KUMAR, D.; ALI, S. Faruque; AROCKIARAJAN, A. Structural and aerodynamics studies on various wing configurations for morphing. **IFAC-PapersOnLine**, v. 51, n. 1, p. 498 – 503, 2018. 5th IFAC Conference on Advances in Control and Optimization of Dynamical Systems ACODS 2018.

LACAL-ARÁNTEGUI, R. Globalization in the wind energy industry: contribution and economic impact of european companies. **Renewable Energy**, Elsevier BV, v. 134, p. 612–628, apr 2019.

LENZ, W. B. et al. Particle swarm optimization for small horizontal axis wind turbine. **Mathematics in Engineering, Science and Aerospace (MESA)**, v. 10, n. 1, p. 201–213, 7 2019.

____. Genetic algorithm optimization for horizontal axis wind turbine. ABCM, Salvador/Bahia, 2018.

LIAO, C.C.; ZHAO, X.L.; XU, J.Z. Blade layers optimization of wind turbines using FAST and improved PSO algorithm. **Renewable Energy**, Elsevier BV, v. 42, p. 227–233, jun 2012.

LIBERTY, S. Modern control engineering. **IEEE Transactions on Automatic Control**, Institute of Electrical and Electronics Engineers (IEEE), v. 17, n. 3, p. 419–419, jun 1972.

LORENZON, A. S. et al. Itaipu royalties: The role of the hydroelectric sector in water resource management. **Journal of Environmental Management**, Elsevier BV, v. 187, p. 482–489, feb 2017.

LOUDIYI, K.; BERRADA, A. Experimental validation of gravity energy storage hydraulic modeling. **Energy Procedia**, Elsevier BV, v. 134, p. 845–854, oct 2017.

LUO, N.; VIDAL, Y.; ACHO, L. **Wind Turbine Control and Monitoring (Advances in Industrial Control)**. [S.l.]: Springer, 2014.

MA, K. **Power Electronics for the Next Generation Wind Turbine System**. [S.l.]: Springer International Publishing, 2015.

MA, K. et al. Appliances scheduling via cooperative multi-swarm PSO under day-ahead prices and photovoltaic generation. **Applied Soft Computing**, Elsevier BV, v. 62, p. 504–513, jan 2018.

MAHMUDDIN, F. et al. Airfoil lift and drag extrapolation with viterna and montgomerie methods. **Energy Procedia**, Elsevier BV, v. 105, p. 811–816, may 2017.

MAMDANI, E.H.; ASSILIAN, S. An experiment in linguistic synthesis with a fuzzy logic controller. **International Journal of Man-Machine Studies**, Elsevier BV, v. 7, n. 1, p. 1–13, jan 1975.

MARTEN, D. et al. Qblade: An open source tool for design and simulation of horizontal and vertical axis wind turbines. v. 3, p. 264–269, 03 2013.

MCCULLOCH, W. S.; PITTS, W. A logical calculus of the ideas immanent in nervous activity. **The Bulletin of Mathematical Biophysics**, Springer Nature, v. 5, n. 4, p. 115–133, dec 1943.

MENDES, J.; OSÓRIO, L.; ARAÚJO, R. Self-tuning PID controllers in pursuit of plug and play capacity. **Control Engineering Practice**, Elsevier BV, v. 69, p. 73–84, dec 2017.

MENEZES, E. J. N.; ARAÚJO, A. M.; SILVA, N. S. B. A review on wind turbine control and its associated methods. **Journal of Cleaner Production**, Elsevier BV, v. 174, p. 945–953, feb 2018.

MICHOS, A.; BERGELES, G.; ATHANASSIADIS, N. Aerodynamic characteristics of naca 0012 airfoil in relation to wind generators. v. 7, p. 247–262, 01 1983.

MITHRARATNE, N. Roof-top wind turbines for microgeneration in urban houses in new zealand. **Energy and Buildings**, Elsevier BV, v. 41, n. 10, p. 1013–1018, oct 2009.

MITRA, S.; HAYASHI, Y. Neuro-fuzzy rule generation: survey in soft computing framework. **IEEE Transactions on Neural Networks**, Institute of Electrical and Electronics Engineers (IEEE), v. 11, n. 3, p. 748–768, may 2000.

MITTAL, P.; MITRA, K.; KULKARNI, K. Optimizing the number and locations of turbines in a wind farm addressing energy-noise trade-off: A hybrid approach. **Energy Conversion and Management**, Elsevier BV, v. 132, p. 147–160, jan 2017.

MORGADO, J. et al. Xfoil vs cfd performance predictions for high lift low reynolds number airfoils. **Aerospace Science and Technology**, v. 52, p. 207 – 214, 2016. ISSN 1270-9638.

MURRAY, R. L.; HOLBERT, K. E. The history of nuclear energy. In: **Nuclear Energy**. [S.l.]: Elsevier, 2015. p. 109–121.

NAGAI, B. M.; AMEKU, K.; ROY, J. N. Performance of a 3kw wind turbine generator with variable pitch control system. **Applied Energy**, Elsevier BV, v. 86, n. 9, p. 1774–1782, sep 2009.

National Oceanic and Atmospheric Administration. **Surface and Planetary Boundary Layer Processes**. 2018. Available from Internet: <https://www.esrl.noaa.gov/research/themes/pbl/>.

NAUCK, D.; KLAWONN, F.; KRUSE, R. **Foundations of Neuro-Fuzzy Systems**. New York, NY, USA: John Wiley & Sons, Inc., 1997.

New World Wind. **The Wind Tree**. 2018. Available from Internet: <http://www.newwind.fr/en>.

OLIVEIRA, T.; VARUM, C.; BOTELHO, A. Wind power and CO2 emissions in the irish market. **Energy Economics**, Elsevier BV, v. 80, p. 48–58, may 2019.

OSTOWARI, C.; NAIK, D. Post stall studies of untwisted varying aspect ratio blades with an naca 4415 airfoil section - part i. **Wind Engineering**, Sage Publications, Ltd., v. 8, n. 3, p. 176–194, 1984.

OUDAH, A.; I.MOHD, I.; HAMEED, A. Wind turbines control: Features and trends. **Modern Applied Science**, Canadian Center of Science and Education, v. 8, n. 6, nov 2014.

PARSOPOULOS, K. E.; VRAHATIS, M. N. **Particle Swarm Optimization and Intelligence**. [S.l.]: IGI Global, 2010.

PEDERSEN, M. E. H. Good parameters for particle swarm optimization. **Hvass Lab., Copenhagen, Denmark, Tech. Rep. HL1001**, 2010.

PETROVIĆ, V.; JELAVIĆ, M.; BAOTIĆ, M. Advanced control algorithms for reduction of wind turbine structural loads. **Renewable Energy**, Elsevier BV, v. 76, p. 418–431, apr 2015.

PINTO, R. L. U. F.; GONÇALVES, B. P. F. A revised theoretical analysis of aerodynamic optimization of horizontal-axis wind turbines based on BEM theory. **Renewable Energy**, Elsevier BV, v. 105, p. 625–636, may 2017.

PRATUMNOPHARAT, P.; LEUNG, P.S. Validation of various windmill brake state models used by blade element momentum calculation. **Renewable Energy**, Elsevier BV, v. 36, n. 11, p. 3222–3227, nov 2011.

PRITCHARD, P. J. **Fox and McDonald's Introduction to Fluid Mechanics**. [S.l.]: Wiley, 2011.

REHMAN, S.; AL-HADHRAMI, L. M.; ALAM, Md. M. Pumped hydro energy storage system: A technological review. **Renewable and Sustainable Energy Reviews**, Elsevier BV, v. 44, p. 586–598, apr 2015.

REZNIK, L. Fuzzy sets, logic and control. In: **Fuzzy Controllers Handbook**. [S.l.]: Elsevier, 1997. p. 3–18.

RICHTER, M. Business model innovation for sustainable energy: German utilities and renewable energy. **Energy Policy**, Elsevier BV, v. 62, p. 1226–1237, nov 2013.

RUFFATO-FERREIRA, V. et al. A foundation for the strategic long-term planning of the renewable energy sector in brazil: Hydroelectricity and wind energy in the face of climate change scenarios. **Renewable and Sustainable Energy Reviews**, v. 72, p. 1124 – 1137, 2017.

SAQIB, M. A.; SALEEM, Ali Z. Power-quality issues and the need for reactive-power compensation in the grid integration of wind power. **Renewable and Sustainable Energy Reviews**, Elsevier BV, v. 43, p. 51–64, mar 2015.

SCHAFFARCZYK, A. P. **Introduction to Wind Turbine Aerodynamics**. [S.l.]: Springer Berlin Heidelberg, 2014.

SELIG, M. S.; MCGRANAHAN, B. D. **Wind Tunnel Aerodynamic Tests of Six Airfoils for Use on Small Wind Turbines** . [S.l.], 2004. Available from Internet: <https://www.nrel.gov/docs/fy00osti/28473.pdf>.

SEMSP, Secretaria de Energia e Mineraçâo. **Hidroeletricidade**. 2018. Available from Internet: <http://www.energia.sp.gov.br/energias-renovaveis/hidroeletricidade/>.

SHAKYA, P.; SUNNY, M. R.; MAITI, D. K. A parametric study of flutter behavior of a composite wind turbine blade with bend-twist coupling. **Composite Structures**, Elsevier BV, v. 207, p. 764–775, jan 2019.

SHI, Y.; EBERHART, R. A modified particle swarm optimizer. In: . [S.l.: s.n.], 1998. p. 69–73.

SIMÓN-MARTÍN, M. et al. Wind energy planning for a sustainable transition to a decarbonized generation scenario based on the opportunity cost of the wind energy: Spanish iberian peninsula as case study. **Energy Procedia**, Elsevier BV, v. 157, p. 1144–1163, jan 2019.

SOMMERS, D.M. **The S819, S820, and S821 Airfoils**. [S.l.], 2005. Available from Internet: <https://www.nrel.gov/docs/fy06osti/39797.pdf>.

SØRENSEN, J. N. Aerodynamic aspects of wind energy conversion. **Annual Review of Fluid Mechanics**, Annual Reviews, v. 43, n. 1, p. 427–448, jan 2011.

SORENSEN, J. N. **General Momentum Theory for Horizontal Axis Wind Turbines**. [S.l.]: Springer International Publishing, 2016.

STEPHENSON, J. et al. Smart grid research in New Zealand – A review from the GREEN Grid research programme. **Renewable and Sustainable Energy Reviews**, 2017.

SUGENO, M. **Industrial Applications of Fuzzy Control**. [S.l.]: Elsevier Science Ltd, 1985.

SURESH, C.; RAMESH, K.; PARAMAGURU, V. Aerodynamic performance analysis of a non-planar c-wing using CFD. **Aerospace Science and Technology**, Elsevier BV, v. 40, p. 56–61, jan 2015.

TALAVERA, M.; SHU, F. Experimental study of turbulence intensity influence on wind turbine performance and wake recovery in a low-speed wind tunnel. **Renewable Energy**, Elsevier BV, v. 109, p. 363–371, aug 2017.

TANGLER, J.L.; SOMERS, D.M. **NREL Airfoil Families for HAWTs**. [S.l.], 1995. Available from Internet: <https://www.nrel.gov/docs/fy06osti/39797.pdf>.

TIAN, W. et al. Shape optimization of a savonius wind rotor with different convex and concave sides. **Renewable Energy**, Elsevier BV, v. 117, p. 287–299, mar 2018.

TJIU, W. et al. Darrieus vertical axis wind turbine for power generation II: Challenges in HAWT and the opportunity of multi-megawatt darrieus VAWT development. **Renewable Energy**, Elsevier BV, v. 75, p. 560–571, mar 2015.

TUSSET, A. M. **Application of optimal control in model of nonlinear vehicular suspension controlled through magneto-rheological damper**. 11 2008. Thesis (Ph.D.) — UFRGS, Porto Alegre, 11 2008.

VAZ, J. R.P.; WOOD, D. H. Performance analysis of wind turbines at low tip-speed ratio using the betz-goldstein model. **Energy Conversion and Management**, Elsevier BV, v. 126, p. 662–672, oct 2016.

VAZ, J. R. P.; PINHO, J. T.; MESQUITA, A. L. A. An extension of BEM method applied to horizontal-axis wind turbine design. **Renewable Energy**, Elsevier BV, v. 36, n. 6, p. 1734–1740, jun 2011.

VENTER, G.; SOBIESZCZANSKI-SOBIESKI, J. Particle swarm optimization. **AIAA Journal**, American Institute of Aeronautics and Astronautics (AIAA), v. 41, n. 8, p. 1583–1589, aug 2003.

WAGNER, H.; MATHUR, J. **Introduction to Hydro Energy Systems**. [S.l.]: Springer Berlin Heidelberg, 2011.

WAGNER, H.-J. Introduction to wind energy systems. **EPJ Web of Conferences**, EDP Sciences, v. 54, p. 01011, 2013.

WAHYUDI, B.; SOEPARMAN, S.; HOEIJMAKERS, H.W.M. Optimization design of savonius diffuser blade with moving deflector for hydrokınetıc cross flow turbıne rotor. **Energy Procedia**, Elsevier BV, v. 68, p. 244–253, apr 2015.

WAIT, I. et al. Wind-induced instabilities and monitoring of wind turbine. **Earthquake Engineering and Engineering Vibration**, Springer Nature, v. 18, n. 2, p. 475–485, abr. 2019.

WALMSLEY, T. G.; WALMSLEY, M. R.W.; ATKINS, M. J. Energy return on energy and carbon investment of wind energy farms: A case study of new zealand. **Journal of Cleaner Production**, Elsevier BV, v. 167, p. 885–895, nov 2017.

WANG, L.; WANG, T.; LUO, Y. Improved non-dominated sorting genetic algorithm (NSGA)-II in multi-objective optimization studies of wind turbine blades. **Applied Mathematics and Mechanics**, Springer Nature, v. 32, n. 6, p. 739–748, jun 2011.

WANG, S.; WANG, S.; LIU, J. Life-cycle green-house gas emissions of onshore and offshore wind turbines. **Journal of Cleaner Production**, v. 210, p. 804 – 810, 2019. ISSN 0959-6526. Available from Internet: <http://www.sciencedirect.com/science/article/pii/S0959652618334310>.

WEBER, G.; C., Ignazio. The transition of Germany's energy production, green economy, low-carbon economy, socio-environmental conflicts, and equitable society. **Journal of Cleaner Production**, v. 167, p. 1222–1231, 2018.

WHITE, L. V.; WAKES, S. J. Permitting best use of wind resource for small wind-turbines in rural New Zealand: A micro-scale CFD examination. **Energy for Sustainable Development**, v. 21, n. 1, p. 1–6, 2014.

WOOD, D. Small wind turbines for remote power and distributed generation. **Wind Engineering**, SAGE Publications, v. 34, n. 3, p. 241–254, may 2010.

WOOD, D. (Ed.). **Small Wind Turbines**: Analysis, design, and application. London: Springer, 2011. 211 p.

XU, J. et al. Study of boundary layer transition on supercritical natural laminar flow wing at high reynolds number through wind tunnel experiment. **Aerospace Science and Technology**, v. 80, p. 221 – 231, 2018. ISSN 1270-9638.

XU, Y. et al. Global status of recycling waste solar panels: A review. **Waste Management**, Elsevier BV, v. 75, p. 450–458, may 2018.

YANG, Y. et al. A multi-objective optimization for HAWT blades design by considering structural strength. **Journal of Mechanical Science and Technology**, Springer Nature, v. 30, n. 8, p. 3693–3703, aug 2016.

ZADEH, L.A. Fuzzy sets. **Information and Control**, Elsevier BV, v. 8, n. 3, p. 338–353, jun 1965.

ZADEH, L. A; KLIR, G. J.; YUAN, B. **Fuzzy Sets, Fuzzy Logic, and Fuzzy Systems**. [S.l.]: WORLD SCIENTIFIC, 1996.


ZHANG, Z.; CHEN, B.; NIELSEN, R.K. Coupled-mode flutter of wind turbines and its suppression using torsional viscous damper. **Procedia Engineering**, v. 199, p. 3254 – 3259, 2017. ISSN 1877-7058. X International Conference on Structural Dynamics, EURODYN 2017.


ZIEGLER, L. et al. Lifetime extension of onshore wind turbines: A review covering germany, spain, denmark, and the UK. **Renewable and Sustainable Energy Reviews**, Elsevier BV, v. 82, p. 1261–1271, feb 2018.

**APPENDIX  A  –  DATABASE**

To build the average $c_P$, a data-set of points were build. Thus, Fig. 30 shows the results to $c_P$ for $V_\infty = 3\,[m/s]$ .
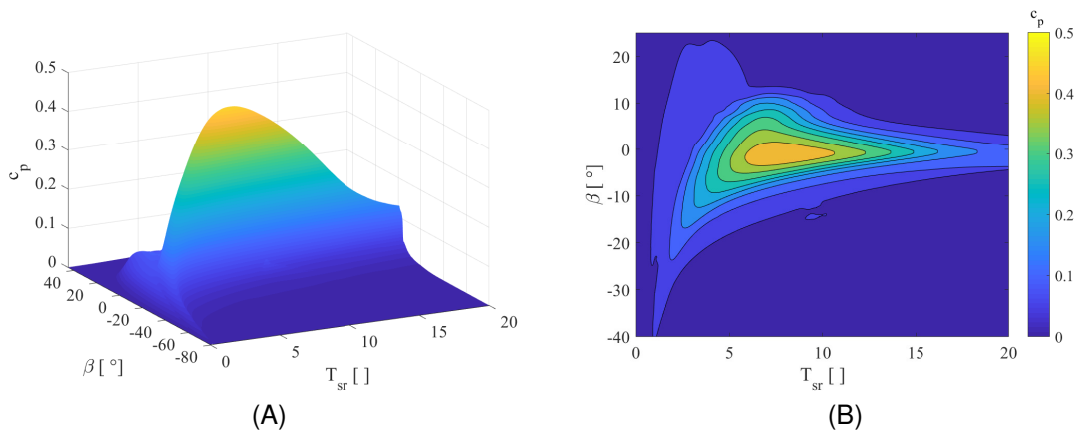
**Graph 30 – Results for $c_P$ for $V_\infty = 3\,[m/s]$ (A) is the surface view and (B) is the Contour view**



(A)                                                    (B)
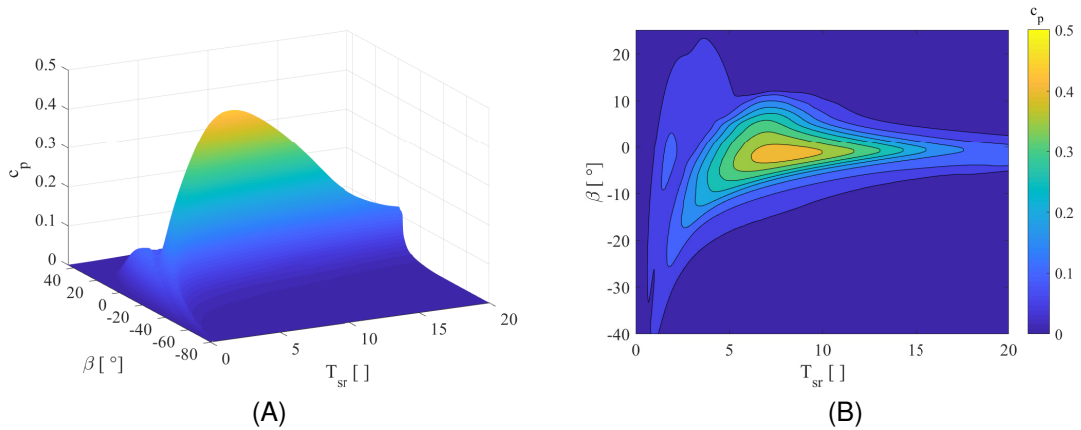
**Source: Self-Authorship**
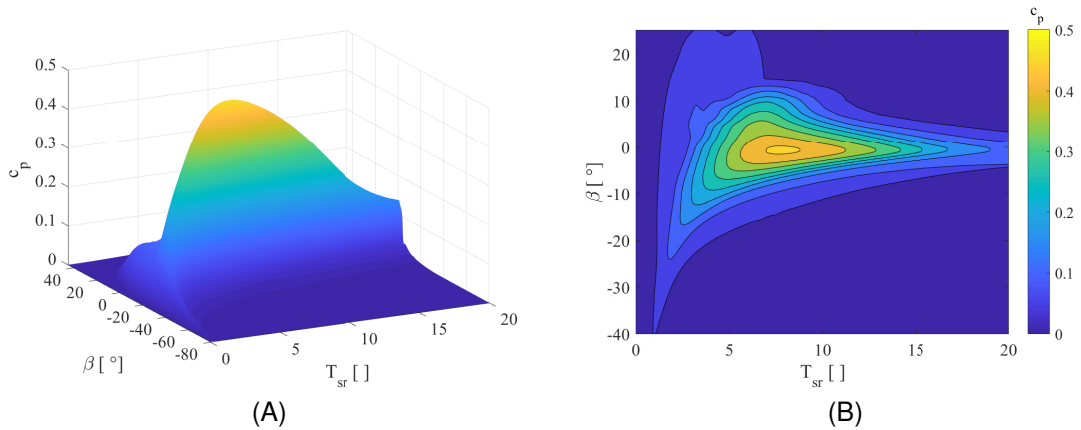
Graph 31 shows the results to $c_P$ for $V_\infty = 4\,[m/s]$ .

**Graph 31 – Results for $c_P$ for $V_\infty = 4\,[m/s]$ (A) is the surface view and (B) is the Contour view**



(A)                                                    (B)

**Source: Self-Authorship**

graph 32 shows the results to $c_P$ for $V_\infty = 5\,[m/s]$.

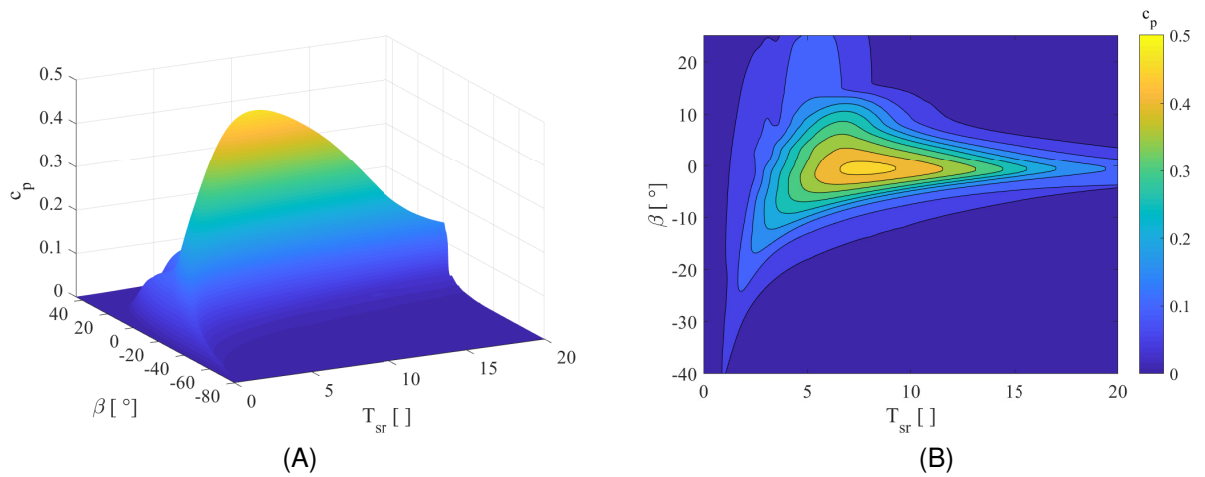**Graph 32 – Results for $c_P$ for $V_\infty = 5\ [m/s]$ (A) is the surface view and (B) is the Contour view**



(A)                                                                                    (B)
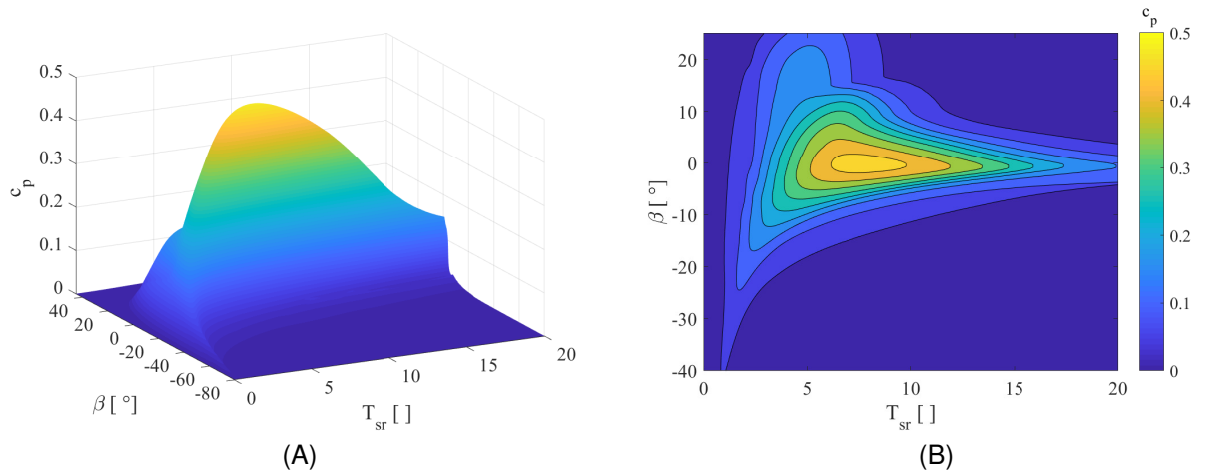
**Source: Self-Authorship**

Graph 33 shows the results to $c_P$ for $V_\infty = 7\ [m/s]$ .

**Graph 33 – Results for $c_P$ for $V_\infty = 7\ [m/s]$ (A) is the surface view and (B) is the Contour view**



(A)                                                                                    (B)
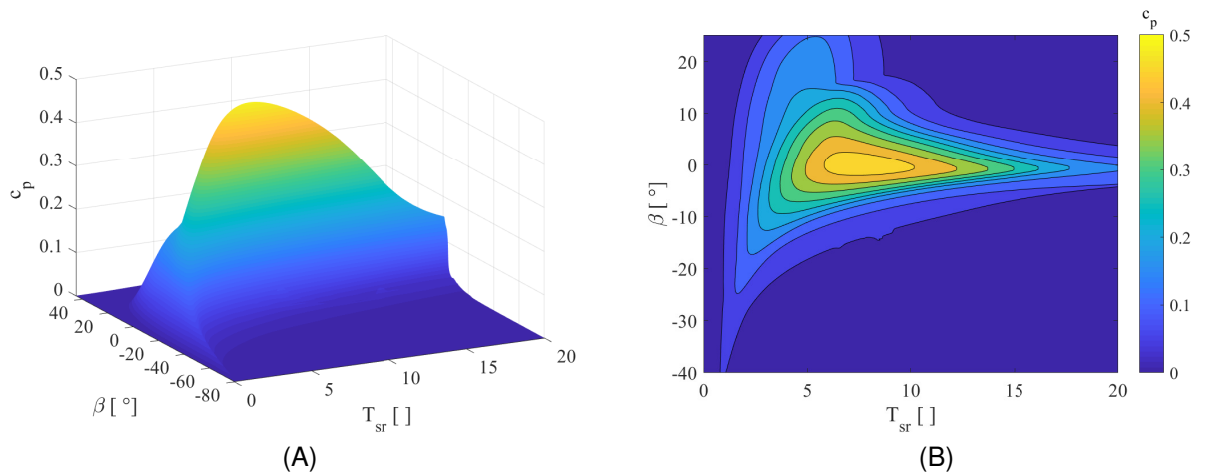
**Source: Self-Authorship**

Graph 34 shows the results to $c_P$ for $V_\infty = 10\ [m/s]$ .

**Graph 34 – $c_P$ for $V_\infty = \ 10 \ [m/s]$: where (A) is the surface view and (B) is the contour view**



(A)                                    (B)

**Source: Self-Authorship**

Graph 35 shows the results to $c_P$ for $V_\infty = \ 15 \ [m/s]$ .

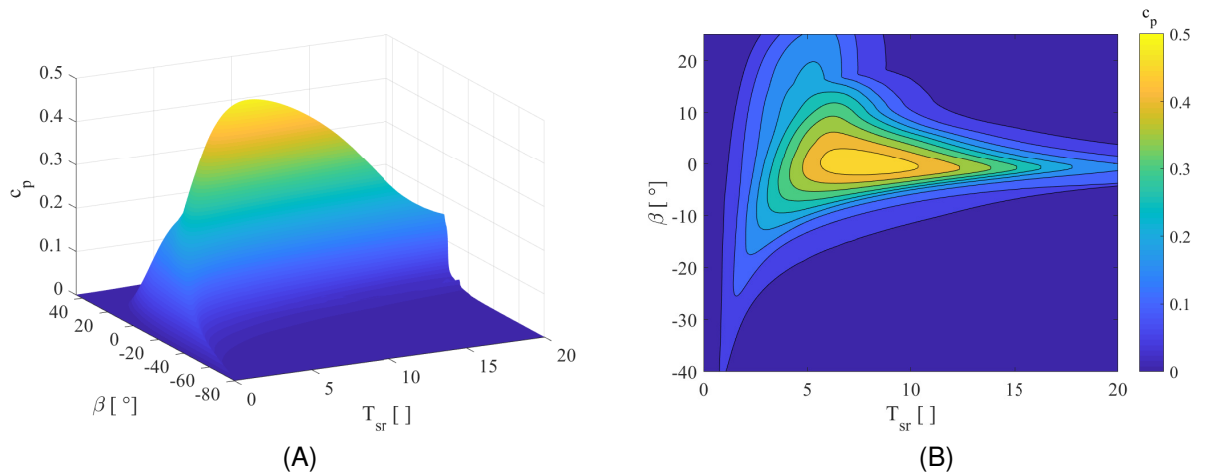**Graph 35 – $c_P$ for $V_\infty = \ 15 \ [m/s]$: where (A) is the surface view and (B) is the contour view**



(A)                                    (B)

**Source: Self-Authorship**

Graph 36 shows the results for $c_P$ for $V_\infty$ $20 m/s$ .

**Graph 36 – $c_P$ for $V_\infty$ $20m/s$: where (A) is the surface view and (B) is the contour view**



(A)

(B)

**Source: Self-Authorship**

This database was used build Graph 9.

# APPENDIX B – PUBLISHED PAPERS

This dissertation originated the following papers, directly or indirectly:

LENZ, W. B. et al. Particle swarm optimization for small horizontal axis wind turbine. **Mathematics in Engineering, Science and Aerospace (MESA)**, v. 10, n. 1, p. 201–213, 7 2019.

LENZ, W. B. et al. Genetic algorithm optimization for horizontal axis wind turbine. ABCM, Salvador/Bahia, 2018.